FT-IR STUDY OF THE H_2O CRYSTALLINE ICE SURFACE

By

JAMES BRADLY ROWLAND

Bachelor of Science

Southeastern Oklahoma State University

Durant, Oklahoma

1990

Submitted to the Faculty of the
Graduate College of the
Oklahoma State University
in partial fulfillment of
the requirements for
the Degree of
DOCTOR OF PHILOSOPHY
December, 1995

FT-IR STUDY OF THE H_2O CRYSTALLINE ICE SURFACE

Thesis Approved:

J Paul Devlin
Thesis Advisor

Donald L. Thompson

James P. Wiebstad

Lionel M. Raff

Thomas C. Collins
Dean of the Graduate College

PREFACE

The ice surface of H_2O crystalline ice is composed of three distinct groups of surface-sites. These sites have localized vibrational modes that are observed in the IR spectrum of an ice surface. By using various sampling techniques, the IR spectrum of the ice surface is obtained for nanocrystalline particles (small particles of ice that are approximately 25-70 nm in diameter) that are formed at ~70 K, and allows the assignment of the exposed IR surface bands to specific groups of surface sites. Therefore, the IR surface spectrum of crystalline ice is composed of IR bands that corresponds to specific groups of surface-sites. This site-specific view of the ice surface is useful in studying the interactions of adsorbing molecules (such as N_2 and CO) with the ice surface. Information such as the heat of adsorption or preferential adsorption of an adsorbate onto specific surface-sites is also be obtained and presented in this thesis.

I sincerely thank God, my wife (Suzette Rowland), and my family for their unwavering support and love. I especially thank my doctoral committee--Dr. Devlin for his personal guidance and support as my advisor, Dr. Thompson for his lessons in professionalism, Dr. Raff for his lessons in presentation and professional countenance, and Dr. Wicksted for his patients, kindness, and availability. I also thank Dr. Mains for his assistance in learning and obtaining MOPAC and GAUSSIAN programs, and Dr. Victoria Buch for her computational guidance in interpreting the IR surface spectra of crystalline ice. I would like to thank Lance Delziet and Mark Fisher for their many discussions with me regarding the data presented in this thesis. Finally, I thank the American taxpayers for their financial support of my research.

TABLE OF CONTENTS

LIST OF TABLES

LIST OF FIGURES

Figure Page

Figure Page

Figure | Page

I. Introduction

I.1. General

This thesis describes the spectroscopic studies of the crystalline ice surface and of adsorbates on the surface. Large volumes of literature exist on H_2O in its gas, liquid, glass, and ice phases. On earth, H_2O is commonly found in the gas, liquid, and crystalline phases, and is an important molecule in terrestrial life. However, most of the H_2O molecules in the universe are in the ice phase, and are commonly found in interstellar dust particles and comets.[1,2] Small ice particles are also found in the stratosphere, and participate in atmospheric chemistry.[3,4] With the abundance of small H_2O particles in our universe and our planet, many disciplines of science would benefit from a detailed understanding of the ice surfaces. Although information about the H_2O ice surface would benefit science in general, atmospheric chemists, astrophysics, and astrochemists would have immediate applications for such knowledge.

Examples that are of interest to atmospheric chemists are the roles that surfaces of small ice particles play in ozone depletion and cloud electrification.[5] Molina and coworkers have determined that the uptake of HCl on the surface of H_2O, nitric acid trihydrate, and sulfuric acid trihydrate particles is an important step in the process of ozone depletion.[3,4] The ice surface catalyzes the reactions that release Cl_2 from $ClNO_2$. Ultraviolet radiation promotes the formation of Cl radicals that react with O_3 to form ClO and O_2. ClO molecules can react with NO_2 to form $ClONO_2$ molecules that will react with the ice surface to produce more Cl radicals that further destroy O_3 molecules.

Another interesting prospect for future ice particle research is to study the charge transfer between ice particles that are involved in cloud electrification.[5] Up drafts and down drafts are common within clouds and cause charge separation in clouds by collisional charge-transfer between ice particles. The ice particles in the down draft

collide with water droplets and smaller ice particles in the up draft. This mechanism causes the cloud to become positively charged at the bottom and negatively charged at the top. Again, we intend that our research will aid in understanding cloud electrification and ozone depletion on a molecular level.

Astrophysicists are concerned with reactions within and on the surface of interstellar dust particles. Dust particles of H_2O ice are usually contaminated by contain other molecules such as CO and are found in comets and in interstellar clouds.[1,2,6] Interstellar dust particles are formed when H_2O and other molecules condense or are produced (by chemical reactions) on the surface of a silicate core. The ice portion of the dust particles gives an indication to their history. For example, if the ice of the dust particles are amorphous, the interstellar dust particles were formed in interstellar space at low temperatures. However, if crystalline ice is present, the particles must have encountered a heat source.

The surfaces of the icy interstellar dust particles are thought to play a role in ionization and radical processes that occur in comets and interstellar clouds.[6-9] Icy analogs of cometary ice show that cosmic ray bombardment causes the formation of organic molecules, such as H_2CO, CO_2, C_2O, C_3O, and H_2CO_3, from H_2O+CO and H_2O+CO_2 icy mixtures.[6] Organic molecules, such as C_2H_3OH, H_2CO, CH_4, CO, and CO_2, are formed from a 1 μm thick layer of CH_3OH+H_2O mixture that is bombarded with cosmic rays. Similar results are observed for UV (ultraviolet) photolysis of icy interstellar dust analogs.[2] Although the reactions above occur within the mantel of an icy analog, they do indicate that carbon bearing molecules could condense (adsorb) on the surface of an icy dust particle, and could polymerize to form larger organic molecules. These surface reactions may be significant in determining the abundance, history, and distribution of organic molecules throughout the universe.[7]

Information about interactions of adsorbates with the amorphous ice surface has already been useful in debating the origin of H_2 frozen on the surface of interstellar dust

particles in interstellar clouds.[45] Previous theories suggested that H_2 molecules are formed by irradiating H_2O molecules with UV light. The H_2 molecules would remain trapped in the mantels of the dust particles or drift onto surface sites.[8] However, knowledge about the adsorption of H_2 on the surface of amorphous ice is used to predict another mechanism for H_2 molecules frozen on the surface of interstellar dust particles. This method is that free H_2 molecules adsorb on an icy surface upon contact with the icy interstellar particles.[9]

Obviously, these examples are not the only application for the knowledge gained about crystalline ice surfaces. They are meant only to illustrate some potential uses of our research. Our model of the ice surface could be useful in understanding and evaluating other surfaces. However, this thesis will focus only on the identification and source of the surface-defect vibrational modes on the crystalline ice surface, as well as the adsorbate interactions with the ice surface.

I.2. The Ice Surface

I.2.1. History

The history of the identification of surface-defect sites and adsorption of small molecules on the crystalline ice surface is brief. The earliest scientific results that are correspond to the crystalline ice surface are reported for a matrix-isolated H_2O dimer study that was published in 1957.[10] This study was the first of many matrix-isolation studies on H_2O dimers. These studies determined the proper geometry for the dimer, and assigned the infrared absorption frequencies of the vibrational modes for the dimer.[11,12] Molecular beam infrared predissociational spectroscopy[13] and *ab initio* calculations[14] are also used to assign the dimer structure and the vibrational frequencies of the dimer. The similarity between the H_2O dimer and an H_2O ice surface is that the frequency

assignment for the antisymmetric stretch vibrational mode of the proton-donor molecule in the dimer (see Fig. 1A) is used to justify the assignment of a surface-defect vibrational mode that is first reported for the FT-IR (Fourier Transform Infrared) study of amorphous ice.[15] Also, the shifts in the dimer vibrational frequencies upon a change in matrices (Ar, N_2, and Xe)[13] correspond to the observed shifts in the surface-defect vibrational frequencies caused by the adsorption of molecules on an ice surface.[46]

Figure 1A shows the H_2O dimer geometry. The only correspondence between the dimer and the crystalline ice surface is the vibrational frequency of the antisymmetric proton donor H_2O stretch of the dimer. One hydrogen of the H_2O proton donor molecule is hydrogen bonded to the proton-acceptor H_2O molecule, and the remaining hydrogen is free of hydrogen bonding. The IR vibrational frequency of the antisymmetric proton-donor stretch is located at ~3730 cm^{-1}.[13] This frequency aids in assigning the first surface-defect vibrational mode observed for amorphous ice in 1975.[15]

In an infrared spectroscopy study of amorphous ice, Ritzhaupt et al.[15] observed an IR adsorption band at 3697 cm^{-1}. They assigned the band to the surface-defect vibrational mode of the dangling-H (d-H) group (see Fig 1B) that forms when H_2O surface molecules lack the four hydrogen bonds that the internal H_2O molecules possess. The defect in the hydrogen bonding leaves one hydrogen free of hydrogen bonding with the other hydrogen bond to the oxygen of an "internal" H_2O molecule. There are three hydrogen bonds around the oxygens of the dangling-H molecules, which accounts for the shift in the d-H IR frequency to a value than is lower that the antisymmetric proton-donor dimer frequency.

Observations of icy interstellar dust particles motivated various research groups to create laboratory analogs that could be used to reproduce the infrared spectra of the interstellar dust particles.[16] Success was achieved by slowly depositing mixtures of H_2O with other molecules (such as CO and NH_3) on an infrared transparent window at a temperature of ~10K. This formed amorphous ice with various impurities. Ritzhaupt et

A

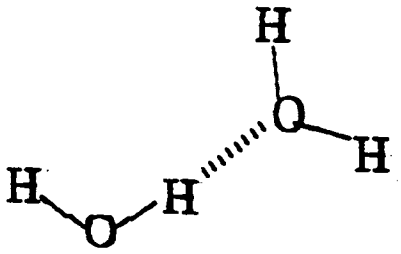

B

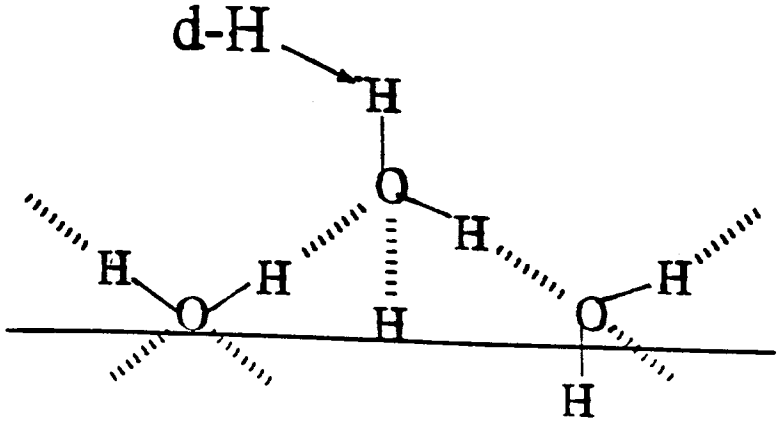

Figure 1. The geometries of the H_2O dimer (A) and the d-H (B)

al. and Tielens et al. discovered that the infrared absorption band at 3700 cm^{-1} increases intensity as the dilution of H_2O increases.[15,17] Tielens et al. correctly surmised that the 3700 cm^{-1} band is due to incomplete hydrogen bonding of the H_2O network due to the increase in impurities, and they effectively assigned the 3700 cm^{-1} band to the d-H. Tielens et al. did not report that the d-H is an inherent feature of the amorphous ice surface. However, they did add additional proof to the existence and frequency assignment of the d-H.

The d-H was also observed by Page et al. in 1987.[18] They observed a high frequency band at 3715 cm^{-1} in the infrared predissociation spectra of $(H_2O)_6$ and $(H_2O)_{19}$ clusters, which was attributed to the "free" O-H stretch. The "free" O-H stretch is later shown to be equivalent to the d-H. Their work on $(H_2O)_n$ (n=6 and 19) clusters is discussed at length later in this thesis.

The literature information that is relevant to our study of the crystalline ice surface and that was reported before 1991 has been summarized above. The d-H surface-defect vibrational mode for the crystalline ice surface is first reported in 1991.[19] Since then, the d-H vibrational mode has been observed in zeolites, silicates, and monolayers of H_2O deposited on a Ni surface.[20-23] A complete model of the crystalline ice surface has been developed and is presented in this thesis. Also, the d-H is only out of three distinct surface-defect groups.

I.2.2. Localization of Surface-Sites

It is advantageous when a seemingly complicated observation can be understood by breaking it down into simple notions; especially if these simple notions are rooted in obvious conclusions. This is the case for the spectra of the crystalline ice surface. The IR spectrum in Figure 2A indicates a complex view of the surface. If the IR spectrum for the bulk vibrational modes can be eliminated from the total (bulk + surface) spectrum,

the surface spectrum would be revealed, and composed of bands that are due to the surface-defect vibrational modes. Figure 2B is an IR spectrum of the crystalline H_2O ice surface obtained by an annealing scheme. However, the difficulty of interpreting this spectrum is reduced by using a simple model to identify specific structures of molecules on the crystalline ice surface.

The annealing scheme that was used to expose the IR surface spectrum in Figure 2B will be discussed later in great detail. A simple description is that annealing causes small nanocrystals with large surface areas and less bulk become larger nanocrystals with smaller surface areas and more bulk. The IR spectrum of the surface shown in Figure 2B is composed of the positive bands that result from subtracting the small nanocrystal spectrum by the large nanocrystal spectrum. The negative bands are attributed to the IR spectrum of the interior H_2O molecules. The experimental chapter outlines the actual procedures employed to produce the spectra that are presented in Figure 2.

In the interior of crystalline ice, there are 4-coordinated H_2O molecules (each H_2O molecule is surrounded by four hydrogen bonds) at every position in the crystalline lattice. This repeating 4-coordinate (4-coord) structure comes to its logical end at the surface. The end of the repeating 4-coord molecules is considered to be a defect in the 4-coord structure, hence the term surface-defect. These defects are seen in Figure 3, and are the 3-coord dangling-H (d-H or d-D for the dangling-D), 3-coord dangling-O (d-O), and surface 4-coord (S-4). In amorphous ice, the 2-coord d-H molecules are also observed.[19] The 3-coord d-H molecule is formed by two hydrogen bonds with the oxygen, and one hydrogen-bond with the hydrogen of the d-H molecule. A surface H_2O molecule that has one hydrogen-bond with the oxygen and two hydrogen-bonds with the hydrogens will form the 3-coord d-O. The S-4 molecules are 4-coordinate molecules that experience tetrahedral distortion due to the surface. This model of the crystalline ice surface is identical for crystalline cubic ice and crystalline hexagonal ice.[24]

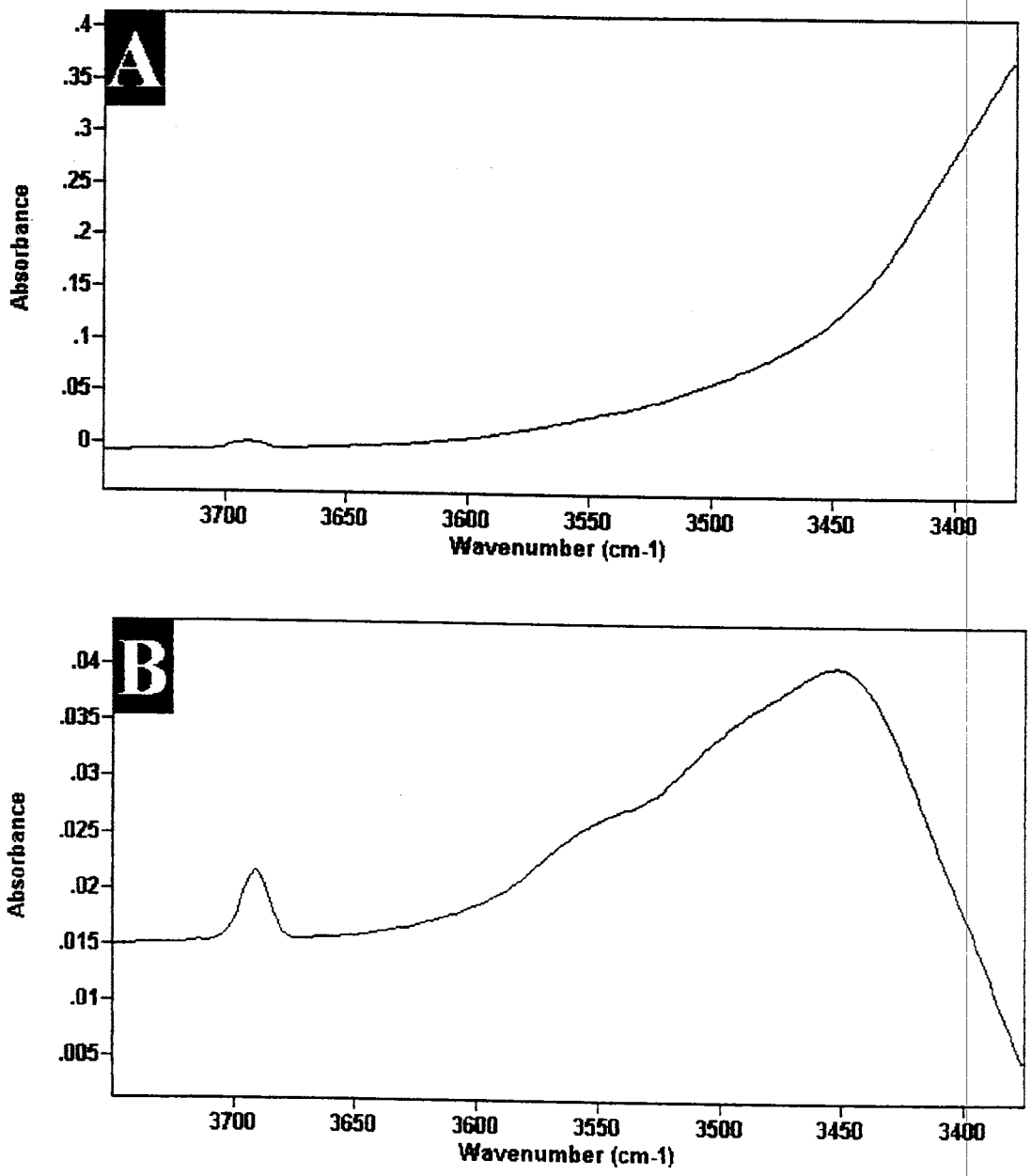

Figure 2. The H_2O IR spectrum of the surface + bulk (A) , and the surface (B)

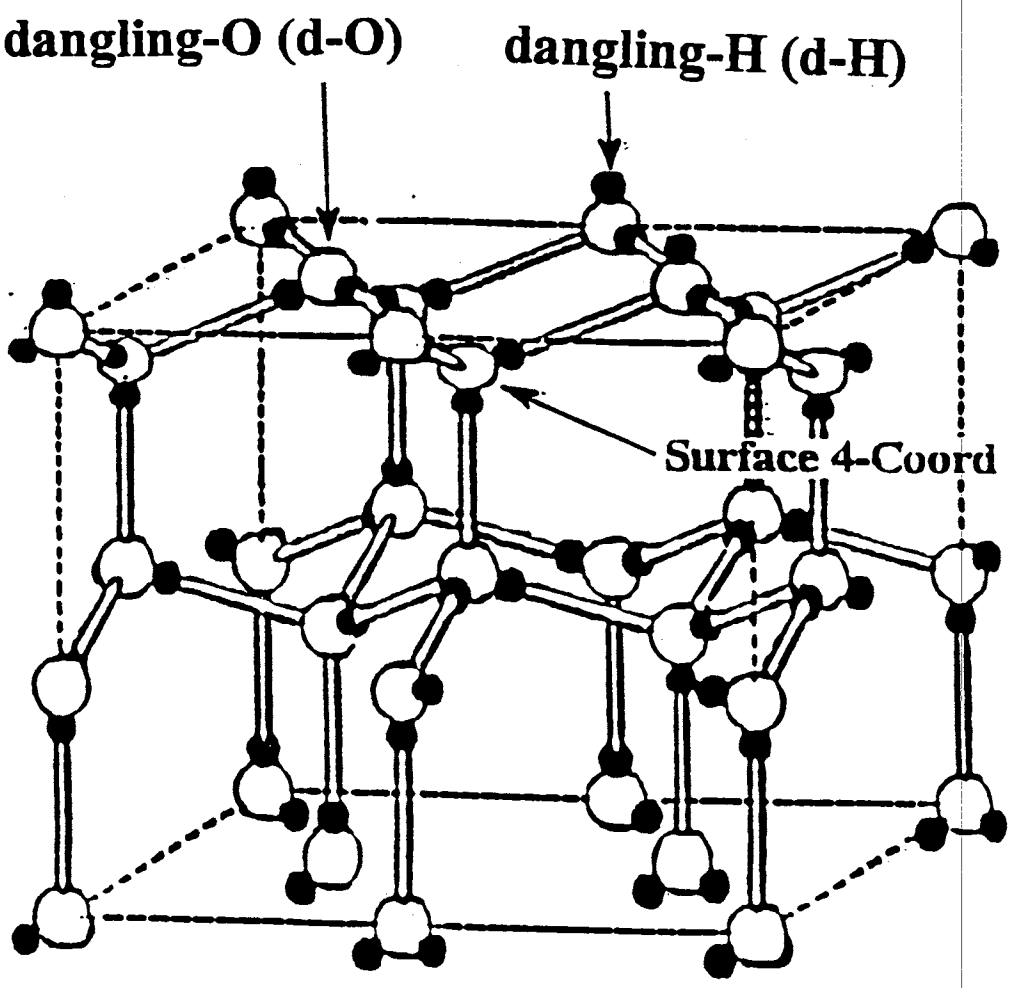

Figure 3. The crystalline ice surface

Recognition of the d-H, d-O, and S-4 surface-defect sites not only simplifies the interpretation of the surface IR spectra, and simplifies the spectral interpretation for other systems such as the Page et al. IR spectrum for the $(H_2O)_{19}$ clusters (see Fig. 4). Notice the qualitative one-to-one correspondence between the $(H_2O)_{19}$ spectrum and our surface spectrum (see Fig. 2B). This demonstrates that the consideration of the hydrogen bonding around H_2O molecules is extremely important to the spectra produced. Spectra produced in different systems are directly related to the coordination of the H_2O molecules within that system. Obviously, the coordination of the molecules involved in producing the surface spectrum are analogous with the coordination of H_2O molecules in the $(H_2O)_{19}$ clusters.

I.2.2.1. $(H_2O)_{20}$

Page et al. created water clusters in a molecular beam and obtained the infrared spectra by using IR predissociational spectroscopy.[18] Predissociation spectra are obtained by crossing a tunable IR laser with the molecular beam. The $(H_2O)_{19}$ clusters that are formed by an expansion dissociate when the laser frequency matches a vibrational mode of the H_2O molecules in the cluster. The vibrationally excited H_2O molecules in the clusters cause the clusters to dissociate. Therefore, spectra are taken by observing the loss of mass from the molecular beam as a function of IR frequency. However, the traditional bolometer that is used as a detector cannot discriminate between clusters of different masses. This makes it difficult to obtain IR spectra for particular $(H_2O)_n$ cluster sizes. Page et al. solved this problem by using a quadrapole mass spectrometer to determine the intensity for specific masses in the exit beam. This allowed IR spectra for $(H_2O)_6$ and $(H_2O)_{19}$ clusters to be obtained. A diagram of their experimental setup is presented in Figure 5.

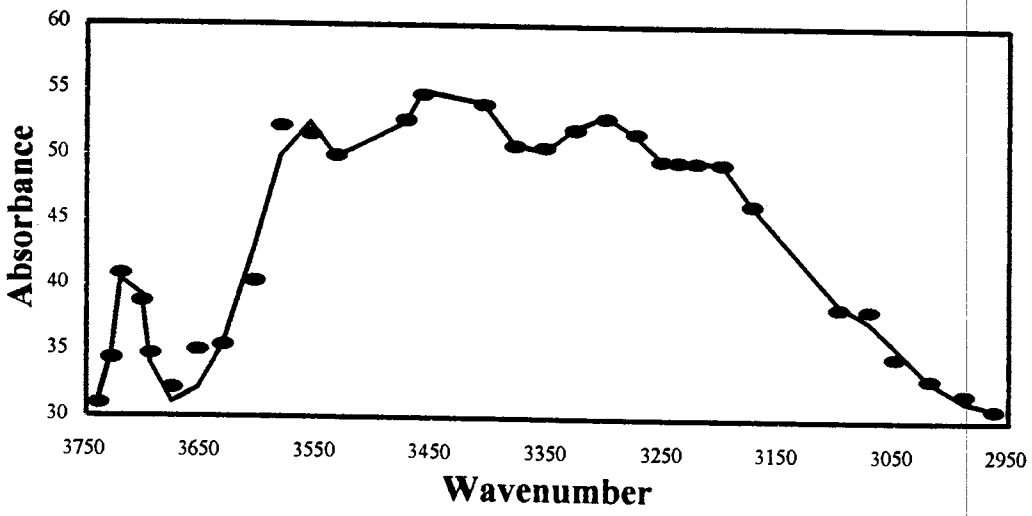

Figure 4. Page et al. predissociational IR spectrum of $(H_2O)_{19}$

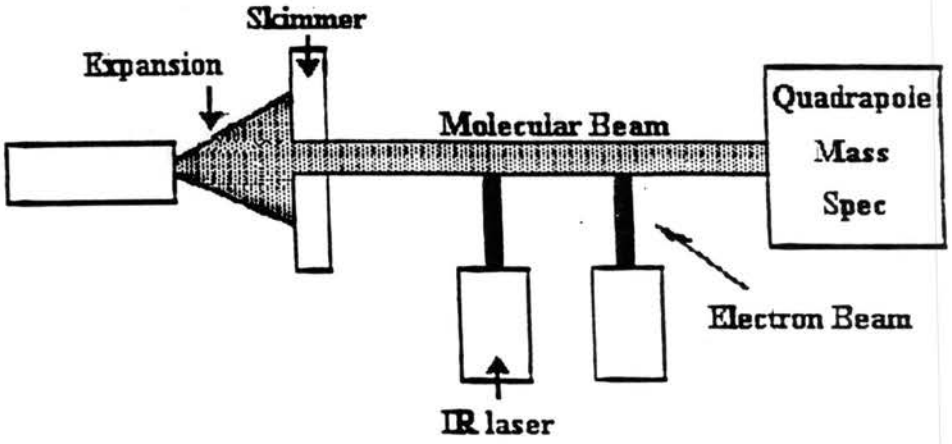

Figure 5. Page et al. experimental diagram

No frequency assignments were reported by Page et al. for the spectra, except the d-H mode at 3700 cm^{-1}. The main thrust of their work was to determine whether these clusters are liquid or crystalline as a function of size. Insights into the frequency assignments of the $(H_2O)_{19}$ spectrum are given by evaluating $(H_2O)_{20}$ structures that are theoretically determined by Buffey and Brown[25] and Jordan and Tsai.[26]

The most stable structures from Buffey et al. and Jordan et al. calculations are presented in Figures 6A and 6B, respectively. Both groups agree that the most stable structures of the $(H_2O)_{20}$ clusters are composed of 3-coordinate d-H and d-O molecules, but Jordan et al. structure also consist of very distorted S-4 H_2O molecules. Buffey and Brown fitted the intermolecular AFHF (analytical fit to the Hartree-Fock sampling) potential to over 230 Hartree-Fock calculated dimers of H_2O, and the H_2O monomers are defined as rigid molecules using experimental data.[25] Jordan et al. used the TIP4P potential[26] to model the intermolecular interactions.

The $(H_2O)_{20}$ structure in Figure 6A is composed of 3-coord d-H and d-O molecules that parallel d-H and d-O surface-defect groups on the crystalline ice surface (see Fig. 3). However, the $(H_2O)_{20}$ structure in Figure 6B is composed of 3-coord d-H and d-O, and S-4 molecules. The difference between the molecules in the $(H_2O)_{20}$ structure in Figure 6B and molecules in the crystalline ice surface is the amount of distortion in the S-4 molecules. The IR spectra of $(H_2O)_{20}$ and of the crystalline ice surface are expected and observed to be qualitatively similar (see the spectra presented in Figures 2B and 4). The conclusion that can be made from the preceding observations is that the spectra of ice surfaces and small $(H_2O)_n$ clusters are viewed as being constructed from the vibrational modes of d-H, d-O, and S-4 groups.

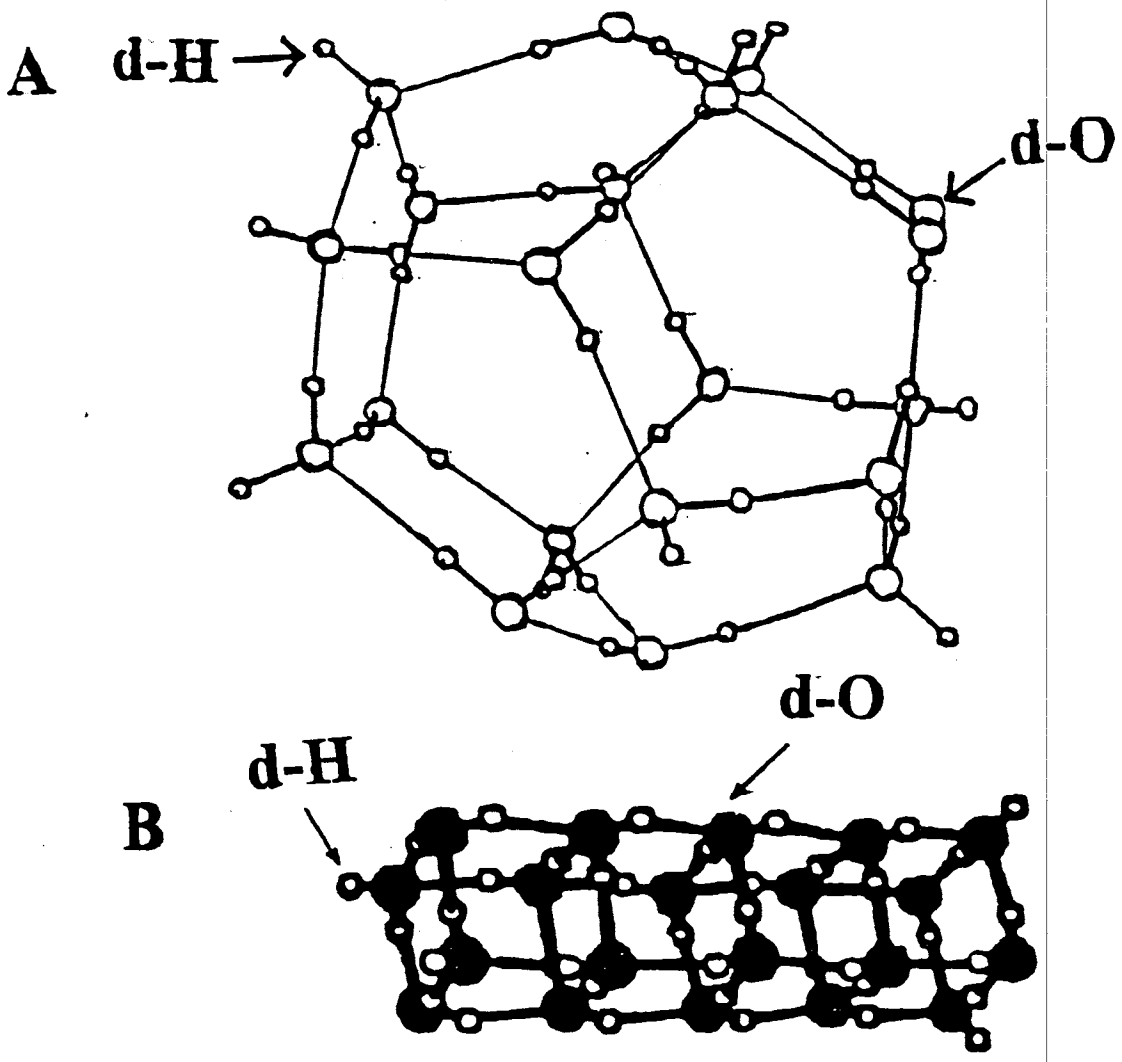

Figure 6. The $(H_2O)_{20}$ icosahedral structure of Buffey et al. (A), and the cubic structure of Jordan et al. (B)

I.2.2.2. The Ice Surface

Further information on the ice surface-defect groups is obtained by analyzing the binding and potential energies in the theoretical publications for $(H_2O)_{20}$ clusters and H_2O ice surfaces.[25-27] This aids in developing a picture of the ice surface by examining stability of the surface-defect groups on the ice surface. The publications of Buffey and Brown[25] as well as Jordan and Tsai[26] offer binding energies for generic H_2O molecules in the $(H_2O)_{20}$ cluster. The reason that binding energies are calculated for generic $(H_2O)_{20}$ molecules is that the $(H_2O)_{20}$ structure is not separated into d-H, d-O, and S-4 sub-structures.[25,26] However, Buch's classical simulation of the H_2O ice surface yield potential energy values for the d-H, d-O, and S-4 surface-defect groups.[27]

Buch created an amorphous $(H_2O)_{450}$ cluster by simulating condensation of $H_2O(g)$ molecules with classical trajectory calculations.[27] The intermolecular potential is described by a TIPS2 potential, and the intramolecular potential for an individual H_2O molecule is described by a customized potential[27] that accounts for the O-H and H-H interactions. The trajectories were carried out for the temperature range of 10 to 27 K, and yielded a structure that has 1-, 2-, 3-, 4-, and 5-coordinate H_2O molecules. The $(H_2O)_{450}$ cluster is displayed in Figure 7, and the number of 1-, 2-, 3-, 4-, and 5-coordinate H_2O molecules in the 450 molecule cluster is listed in Figure 7. Most of the $(H_2O)_{450}$ molecules are located on the surface. Therefore, the potential energies determined for molecules on the 3-coord and 4-coord cluster molecules correspond to potential energies for molecules on the crystalline surface, because the 3-coord and 4-coord structures of the cluster correspond to the structure on the ice surface.

Buffey et al.[25] and Jordan et al.[26] calculated the binding energies to be ~ 7 Kcal/mol and 10 Kcal/mol for the molecules in the $(H_2O)_{20}$ cluster. These binding energies are for generic H_2O molecules, and cannot be separated into 3-coord d-H, d-O, and S-4 binding energies. Also, the binding energies for the $(H_2O)_{20}$ molecules are

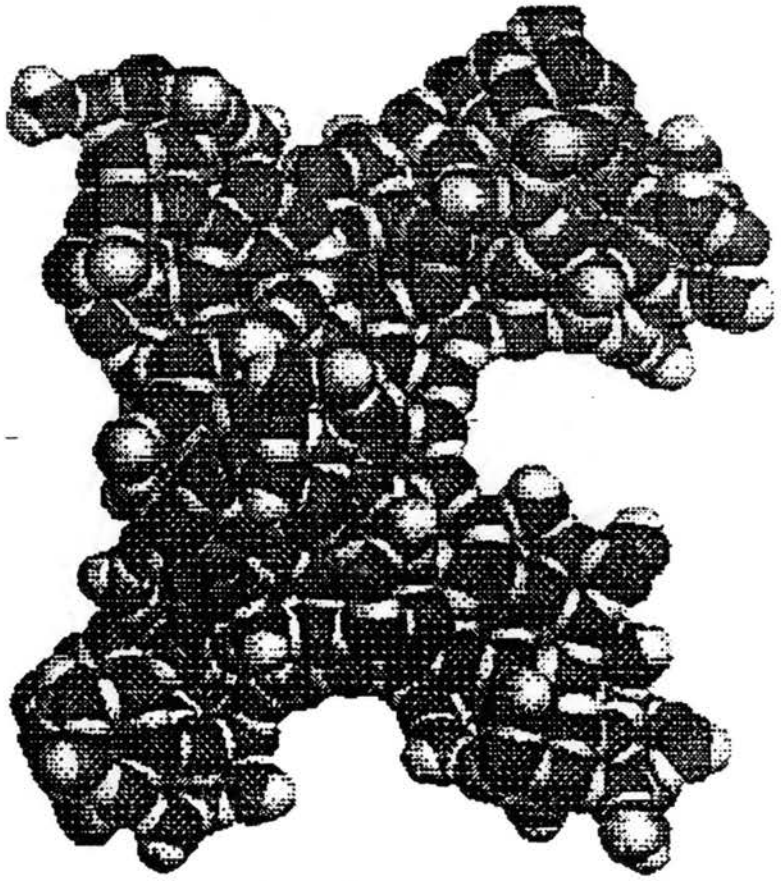

1-coord	2
2-coord	30
3-coord (d-D)	30
3-coord (d-O)	59
4-coord	302
5-coord	27

Figure 7. Buch's $(H_2O)_{450}$ cluster, and the number of differently coordinated H_2O molecules in the $(H_2O)_{450}$ cluster

greater than the H_2O dimer binding energy of 5.44 Kcal/mol (experimentally determined). The increased stability of the $(H_2O)_{20}$ molecules is due to the increase in the number of hydrogen bonds.

Accurate calculations for potential energies of the surface-defect groups were achieved by Buch.[27] The intermolecular potential energies for the d-H, d-O, and S-4 groups are -19.0, -17.7, and -23.3 Kcal/mol, respectively. Advantages of Buch's model over the others are that the 3-coordinate H_2O surface molecules are separated into d-H and d-O sites, and the surface 4-coord molecules are accounted for. The surface molecules of ice are more stable than the $(H_2O)_{20}$ molecules, which are more stable than the dimer.

II. Experimental

II.1. General

The objective of the experimental design is to create sufficient ice surface to be observed by using infrared spectroscopy. Techniques that have been successfully used to do this are vapor deposited amorphous ice[19], monolayer of H_2O molecules on a metal substrate[23], and suspended or deposited nanocrystals (small crystalline H_2O ice clusters that are ~25 nm in diameter).[19,46] The data reported in this thesis were obtained by using nanocrystals.

The experimental chapter is divided into three separate sections that describe the experimental equipment, procedures, and band fitting. This division into three different sections allows greater clarity about the means by which the data are obtained and analyzed. The experimental equipment section provides a detailed list of the equipment as well as the assembly of the experimental apparatus. The procedure section contains topics such as sample preparation, data evaluation, and other procedural tasks. A discussion of the spectral information, which is used to obtain values for the average size of the nanocrystals for the surface-defect vibrational mode assignments and for adsorbate isotherms, is included in the band-fitting section.

II.2. Experimental Equipment

II.2.1. Vacuum Line

The vacuum arrangement that was used to obtain the data is shown in Figure 8, and a description of all the corresponding components is listed in Table 1. The vacuum assembly eliminates thermal transport from the cooled static cluster cell to the

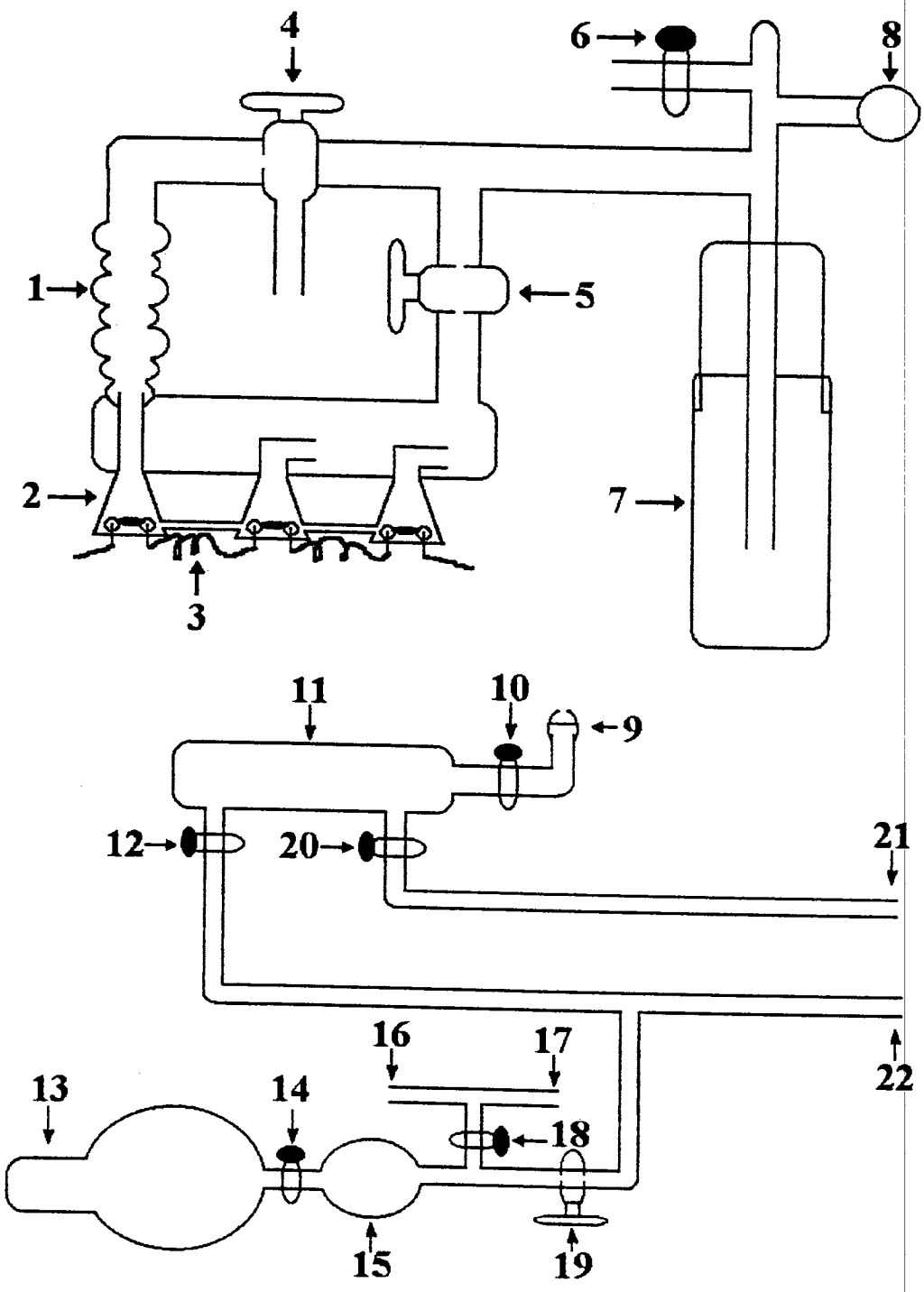

Figure 8. The vacuum line assembly

Table 1.
A list of equipment for vacuum line and diffusion pump

I.D. number	Representation; Function
1	Diffusion Column; cools the oil at the upper tip and condenses it.
2	Oil reservoirs.
3	Heater connection wires; heat the oil.
4	(0-10)mm orifice stopcock; connects vacuum line to mechanical floor pump.
5	(0-10)mm orifice stopcock; connects the vacuum line to the oil diffusion pump.
6	(0-3)mm orifice Teflon vacuum valve; connect vacuum line to the Hastiings DV-5M vacuum gauge.
7	Liquid N_2 trap; traps impurities when dipped in liquid N_2
8	Female glass end; connects the vacuum part of the vacuum line to a vacuum manifold.
9	O-ring sealed male glass end; connects the vacuum manifold of the vacuum line.
10	(0-3)mm orifice Teflon vacuum valve; connects the vacuum manifold to the vacuum line.
11	Vacuum Manifold; connects the vacuum line to the sample portion of the thermos portion to the total vacuum assembly.
12	(0-3)mm orifice Teflon vacuum valve; connects the sample loading section of the vacuum assembly to the manifold.
13	5L sample bulb; reservoir for gaseous samples used.
14	(0-3)mm orifice Teflon vacuum valve; connects the 5L sample bulb to the 1 L charging bulb.
15	1 L charging bulb; connects the sample bulb to the (0-10)mm orifice stopcock and pressure gauges. Used to provide consistent sampling by loading to a specific pressure from the sample bulb.
16	Inlet to a Validine gauge.
17	Inlet to a Validine gauge.
18	(0-3)mm orifice Teflon vacuum valve; connects inlets 16 and 17 to the charging bulb.
19	(0-10)mm orifice stopcock; connect the 1L charging bulb to the vacuum line.
20	(0-3)mm orifice Teflon vacuum valve; connects the vacuum manifold to the inlet that serves to eliminate thermal transport.
21	Inlet to the outer portion of the cluster cell that eliminates thermal transport.
22	Inlet to the inner portion of the cluster cell.

surroundings, and provides a way for loading gas phase H_2O/N_2 samples into the cell. The vacuum line #21, which is connected to the vacuum through inlet #20, provides the necessary vacuum that eliminates thermal transport within the cryogenic equipment assembly. The sample handling region of the vacuum assembly occurs past inlet #19. It is connected to the cluster cell assembly through vacuum line #22. This part of the assembly has several components, such as the sample bulb (#13), charging bulb (#15), and stopcock (#19), that will be discussed in detail.

The vacuum in the line is achieved by using a Welch Duo-Seal model 1402 roughing pump, as well as an oil diffusion pump. The minimal pressure observed is $\sim 10^{-4}$ torr. A Teledyne Hastings-Raydist DV-5M gauge is used to determine the minimal pressure of the vacuum, and is connected to the vacuum assembly through inlet #6. Pressures, which range from 0.01 to 150.0 torr and 0.1 to 1000 torr, are accurately measured by using Validine gauge models AP10-32 and AP10-42, respectively. The AP10-32 gauge is connected by vacuum line #16, and the AP10-42 gauge is connected by vacuum line #17. Both vacuum line #16 and line #17 are connected to the vacuum through inlet #18.

The vacuum apparatus used to load samples into the sample bulb (#13) resembles the vacuum assembly depicted in Figure 8. The differences are that the vacuum line #21 does not exist and that the vacuum line assembly past inlet #12 is removed (e.g., vacuum line #22, and stopcock #19). The sample bulb (#13) is attached to inlet #12, and either the carrier gas, liquid H_2O sample bulb, or lecture bottles can be connected through inlet #20.

II.2.2. The Cryogenic Cluster Cell

The experimental assembly of the cryogenic cluster cell is divided into two parts. The components of the outer portion of the cryogenic cluster cell assembly are shown in

Figure 9 and described in Table 2. The components of the inner portion of the cryogenic cluster cell assembly are presented in Figure 10 and described in Table 3. Both inner and outer portions of the cryogenic cluster cell are connected to the vacuum line by two separate inlets that serve two different functions. The first (inlet #26) allows the volume between the cluster cell and the can (#23) to be evacuated at all times (i.e., insulates the cluster cell from room temperature). The second (inlet #30) is used to evacuate the inner portion of the static cluster cell or load gaseous samples into the static cluster cell.

Inlets #24 and #27 are wire feed-throughs for the temperature diode and resistance heater, respectively. The temperature measuring assembly consists of a model DT-450-SR-13 LakeShore thermal diode (#37; See Fig. 10) connected to a model 201 LakeShore Cryotronics thermometer. The heater components include a ~40 ohm constantan wire heater (#38) connected to model 116B Powerstat variable auto transformer. Component #23, #24, #30, #31, and #32 of Figure 9 were manufactured in the Oklahoma State University Physical Sciences Machine Shop; the other components are standard with an Air Products HC-2 water-cooled closed-cycle helium cryogenic refrigerator that can cool the static cluster cell to ~25 K.

Fig 10A illustrates and Table 3 describes the assembly of the inner portion of the cryogenic cluster cell assembly. The ~40 ohm resistance heater (#38) is wrapped around a copper cylinder that has a lip on one end. The lip serves as a barrier for a brass nut (#43). The brass nut is threaded to fit a copper bolt that is located on the wall of the static cluster cell (#34) which is butt jointed to the copper cylinder (#38). A thin slab of indium is placed between the bolt of the copper cluster cell (#34) and the copper cylinder (#38) to ensure good thermal contact. A bolt with threads to match the brass nut was soldered onto the cluster cell, and is used to connect the cluster cell to the copper cylinder by tightening the brass nut. Thermal contact is maintained for the thermal diode (#37) to the cluster cell (#34) by wrapping the diode in an indium nugget and pressing the indium wrapped diode with the copper tongue assembly (#36) to the cluster cell by

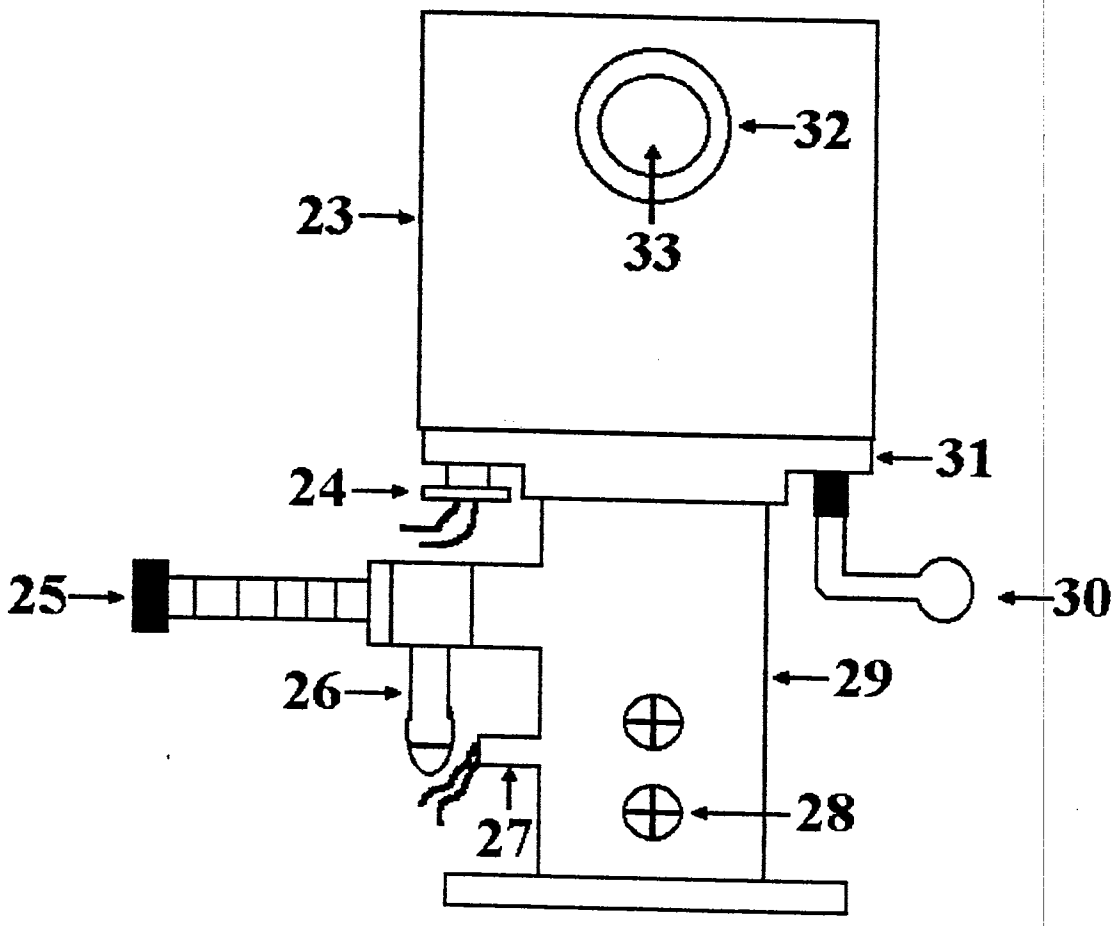

Figure 9. The outer cluster cell assembly

Table 2.
A list of equipment for the cryogenic cluster cell presented in Fig. 9

I.D. number	Representation; Function
23	Outer can; houses the cluster cell in a constant vacuum to eliminate thermal transport.
24	Thermal diode feed through; connect the thermal diode to a Lake Shore digital readout to determine the cluster cell temperature at the windows.
25	Metal valve; allow pumping on the expander unit as well as around the exterior of the cluster cell.
26	Metal-glass joint; connect the vacuum line to the expander unit.
27	Heater wire feed through, connects a 40 ohm heater on the end of the cold finger to a Variac voltmeter.
28	Helium gas connectors; connects the refrigerator to the cell by hoses.
29	Expander unit.
30	Metal-glass joint; connects the vacuum line to the cluster cell.
31	Metal base; connects the expander unit to the outer can.
32	3.8 cm side window stainless steal retainer; protects the KBr window from damage.
33	KBr can side window.

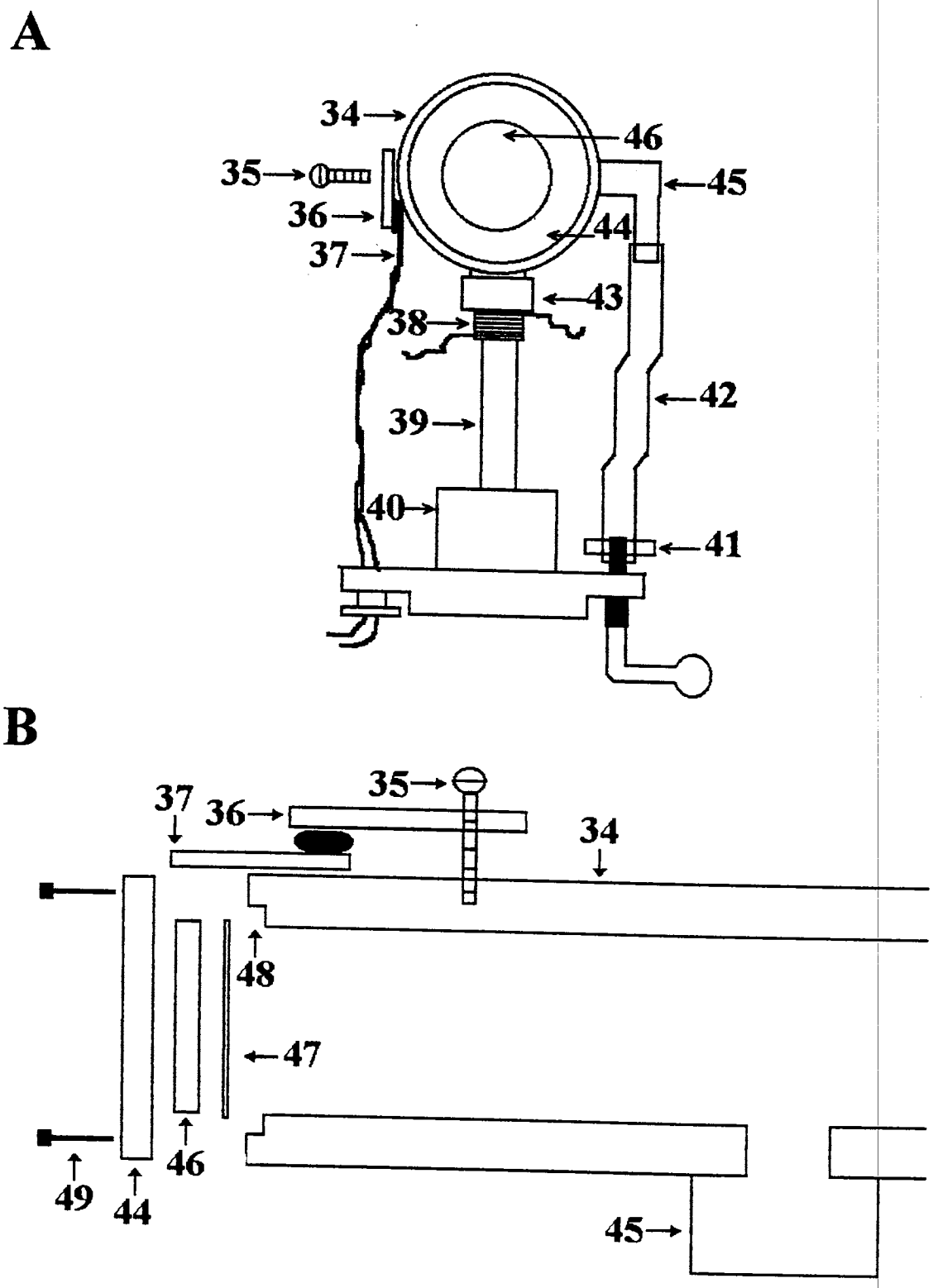

Figure 10. The inner portion of the experimental cluster cell assembly (A), and the cluster cell (B)

Table 3.
A list of equipment for the inner-portion of the cluster cell assembly in Figures 10A and 10B

I.D. number	Representation; Function
34	Brass cluster cell; nanometer sized clusters are formed here.
35	Screw; connects the brass tongue to the cluster cell.
36	Brass tongue; presses the thermal diode to the cluster cell.
37	Thermal diode; used to determine the temperature near the zinc sulfide windows.
38	Metal flange with resistance heater; connects the cryogenic cold finger to the cluster cell, and heats with a 50 ohm resistance heater.
39	Cryogenic cold finger; can cool the cluster cell to ~ 20 K.
40	Metal expander shroud; protects the expander unit and cold finger from damage.
41	Electrician's plastic tie strap
42	3.5mm (i.d) rubber tube; connects the Metal-glass joint to the brass elbow joint.
43	Brass nut; connects the Metal flange with resistance heater to the cluster cell.
44	3 cm brass retainer; protects and aids in pressurizing the zinc sulfide windows onto the cluster cell.
45	Brass elbow joint; connects the rubber tubing to the cluster cell.
46	Zinc Sulfide windows.
47	Indium sheet washer; forms a seal between the cluster cell seat and the zinc sulfide windows to eliminate gas leaks.
48	Cluster cell window seat; allows the windows and indium washers to be deeply seated within the cluster cell, while connecting the cluster cell to the windows.
49	Metal bolts; connects the retainer to the cluster cell and pressurizes the windows to the cluster cell.

tightening the screw (#35). Rubber tubing (#42) is used to connect the cluster cell to the outer vacuum line. The rubber tubing is tightly fitted to nozzles machined on the brass elbow joint #45 and the vacuum inlet #30. The rubber hose is tightened onto the machined nozzles with standard plastic tie straps (#41) as used by electricians.

Many of the components illustrated in Figure 10B and described in Table 3 are illustrated in Figure 10A. However, sealing the ZnS windows has yet to be discussed. Sealing IR transparent windows, which can contain gas pressures of an atmosphere for temperatures ranging from room to 20 K, is difficult. The best procedure (we have found) to seal the windows (#46) of the static cluster cell (#34) is to use two paper-thin indium gaskets (#47) that are placed between the window and the static cluster cell seat (#48). One gasket will not fill every scratch and pit that exist on the window and seat. Therefore, two gaskets are required for each window. The gaskets are cut out of paper-thin sheets of indium by using the equivalent of a cookie cutter (machined at OSU).

A window is pressed against the static cluster cell by tightening the six 7/64 head allen bolts (#49) within the brass retainer (#44) with an even torque. This is achieved by using a Model 6103 Proto allen torque screw driver. Each bolt is tighten to a maximum of 6.5 Kg cm in 5 intervals of 0.7, 2.15, 3.6, and 5.05 Kg cm indicated on the torque screw driver. This limits the shearing stress due to uneven tightening that can crack the window.

II.2.3. Instrument and Interfaced Computer

A digital single beam FT-IR spectrometer is interfaced to a Digilab (Bio-Rad) 3280 data system (Digilab PC) that is based on the Motorola 68000 microprocessor. The specifics about the instrumentation and the FT-IR scan settings for the collecting the experimental data are given in Table 4. Some customization is required to investigate the nanocrystalline ice surface. These changes are to build a mount that suspends the

Table 4.
Description of the spectrometer, data station, and data collection settings

Spectrometer	Spectrometer
Type of interferometer	Single
Interferometer	Michelson interferometer
Spectral range	4000-500 cm^{-1}
Type of beam splitter	KBr/Germanium coated
IR source	Ceramic glower
Detector	Triglycine Sulfate Detector (TGS)
Converter	Analog-to-digital
Resolution at which the spectra are collected	4 cm^{-1} (sometimes 2 cm^{-1})
Purging	Dry air
Computer	Computer
Random access memory	1M
Data storage	801M hard disk drive
Apodization	Triangular
Plotter	Digilab laser printer/plotter
Computation	Fourier transform system

cryogenic cluster cell above the spectrometer, and to transfer data from the older Digilab PC (which uses an UNIX operating system) to an IBM compatible PC (which uses a DOS operating system).

The experimental data are analyzed by a 486 66Mhz DX2 PC that is capable of running more programs for spectral evaluations (such as band fitting with the PeakFit program) at a superior speed to the Digilab PC. This makes data collection from the spectrometer the only significant function of the Digilab PC.

The cryogenic cluster cell, illustrated in Figure 9, can be suspended above the spectrometer from a firmly suspended grooved plate. The components within this arrangement are illustrated in Figure 11 and described in Table 5. A grooved stainless steel plate (#54) is suspended by securing the suspension assembly to the wall (#51) behind and the ceiling (#50) above the spectrometer. By sliding the base of the expander unit (#29) onto the grooved plate (#55), the cryogenic cluster cell can be firmly suspended. Its height and orientation can be manipulated by adjusting the nuts (#56) below the grooved plate. These adjustments allow the maximum IR transmittance through the sample region of the static cluster cell to be achieved. The expander unit is secured by tightening a thumb wheel clamp (#57) that presses the base plate of the expander unit to the grooved plate.

II.3. Experimental Procedures

A major problem that must be overcome to observe surface-defect vibrational modes is having sufficient surface area to observe the surface-defect vibrational modes. This research group employs three methods that produce high surface-to-bulk ratios. These methods are based on gas-phase suspended nanocrystals, window deposited nanocrystals, and amorphous ice. These methods of creating observable ice surfaces are reproducible and easy to do. They are also discussed at length in this chapter.

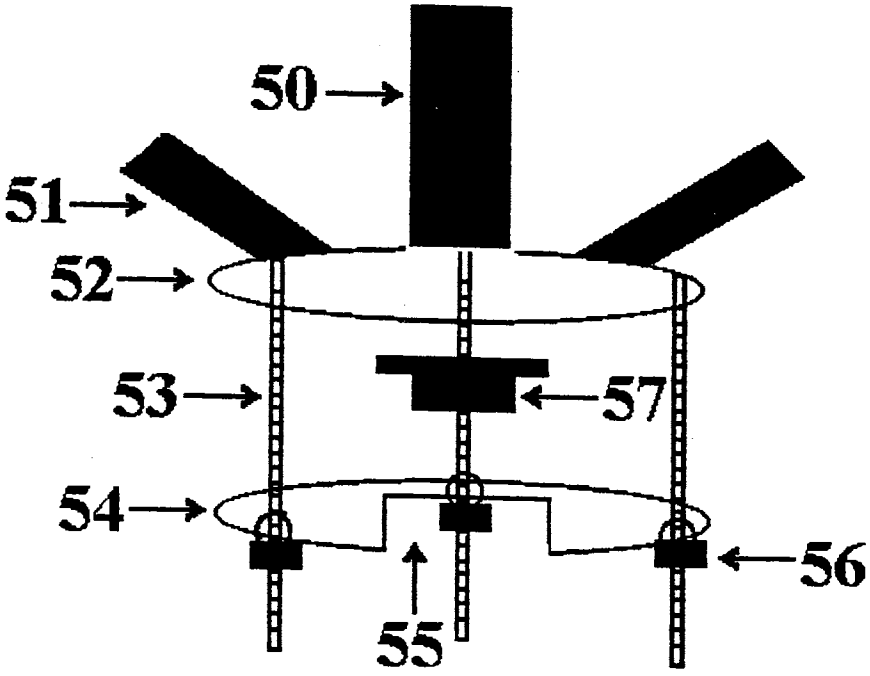

Figure 11. Suspension assembly

Table 5.
Description of the suspension assembly

ID. number	Representation; Function
50	Steal rod; connects the top plate to the ceiling to secure the plate.
51	Steal rod; connects the top plate to the wall to secure the plate.
52	Top stainless steal plate; Allows the grooved stainless steal plate to be suspended, and is securely fastened to the wall and ceiling.
53	Threaded rods; used to connect the grooved plate to the top plate, and to adjust the height of the grooved plate.
54	Grooved stainless steal plate; used to support the cryogenic cluster cell.
55	Groove; groove cut out to allow the expander unit to slide into the grooved plate.
56	Small nuts; threads match the threaded rods, and are used to adjust the orientation and height of the cryogenic cluster cell via the grooved plate.
57	Thumb wheel clamp; secures the base plate of the expander unit to the grooved plate.

Standardized procedures are developed to insure sampling reproducibility for the suspended and deposited nanocrystals.

An obstacle arises from the need to separate the vibrational bands of the interior ice molecules from the surface-defect infrared absorption bands. One method for eliminating the bulk portion of a spectrum has already been discussed. A detailed description for obtaining the annealed difference spectra is given in this section. The annealed difference scheme is not the only scheme to differentiate between the bulk IR bands and the surface IR bands. The adsorbate-shifted difference scheme is also employed to eliminate the bulk contribution to the nanocrystalline spectra. This technique is used to observe the surface-defect vibrational mode behavior in the presence of an adsorbate.

II.3.1. Methods Used to Create Ice Surfaces

The methods that are used to create ice surfaces that are observable by using FT-IR spectroscopy have been discussed. They are suspended nanocrystals, window deposited nanocrystals, and microporous amorphous ice. These methods are not the only methods to create observable H_2O surfaces, but they are simple, rapid, and inexpensive. Each method has advantages and disadvantages, but only the suspended nanocrystals and widow deposited nanocrystalline sample procedures are described here.

II.3.1.1. Suspended Nanocrystals

Gas-phase suspended nanocrystals (the aerosol of crystalline cubic H_2O ice clusters) were the first H_2O ice samples to be studied in the static cluster cell. Surface-defect vibrational bands were first observed for crystalline ice using this sampling method.[19] Also, the suspended nanocrystals serve as analogs of atmospheric ice clusters

that are of interest to atmospheric chemists. A discussion of the experimental procedures, parameters, and advantages will be discussed in the following sections.

Procedures

Loading a gaseous mixture of H_2O (D_2O) with a carrier gas (usually N_2) at ~100/1 molar ratio (N_2/H_2O) into the 5 liter sample bulb (#13) (see Fig. 8) is the beginning of the procedure. Next, the sample bulb (#13) is connected to the vacuum line. It is used to charge the 1 L charging bulb (#15) to a predetermined pressure by closing the 0-10 mm orifice stopcock (#19). During charging with the gaseous sample, the Teflon valve #18 is left open to allow the pressure to be monitored. Once the desired pressure is obtained within the charging bulb, Teflon valves #14 and #12 are closed, and stopcock #19 is opened allowing the gaseous mixture to enter into static cluster cell (#34) (see Fig. 10). Valves #20, #10, #6, and #5 remain open during loading. The purpose of the charging bulb is to insure loading reproducibility.

One preload must be made before good aerosol spectra can be taken. This is due to the excessive uptake of H_2O by the 'dry' experimental equipment. A background spectrum is needed after the initial load, and a new background is also required after every subsequent load to compensate for ice that has deposited on the windows. The background spectra are usually 256 scans at resolution of 4 cm^{-1} (res 4). Once a load is made, spectra that are taken are usually 50-100 scans at res 4. Res 4 is adequate to achieve the quality spectra that are needed to observe the surface-defect IR bands. The resolution of the features that are revealed in spectra taken at a res 2 offer little advantage compared to the res 4 spectra. The decrease in scanning time for res 4 spectra allows more scans to be obtained over a given period of time. The increase in the number of scans results in increased signal-to-noise ratio.

The reason that fewer scans are taken of the suspended nanocrystal than for other methods is that the nanocrystals diffuse and settle out of the aerosol suspension. The half-life for H_2O (D_2O) arosol sample that is suspended in N_2 at 70 K is ~ 7 minutes which is time required to run ~100 scans. The half-lives of the aerosol samples increase with temperature, and triple from 70 K to 120 K.

Unloading a sample from the cluster cell requires closing the Teflon valve #20 and opening valve #12. Closing valve #20 will retain the vacuum that surrounds the static cluster cell (#34), thereby not allowing thermal transport and rapid warming of the static cluster cell to occur. Opening valve #12 connects the vacuum line to the inner portion of the static cluster cell, and evacuates the sampling volume. Once the sampling volume is evacuated, valve #12 is closed, and valve #20 is reopened which allows reloading to begin.

Experimental Variables

Controllable parameters that affect nanocrystal size are pressure, temperature, and the type of carrier gas. A reasonable model for nanocrystal formation needs to be stated. Quite simply, the gas vapors are dumped into the static cluster cell. On the way into the static cluster cell, the H_2O (D_2O) vapors are cooled, and nucleate to form a liquid droplet.[28] After the formation of the liquid droplets, growth and freezing occur thus resulting in nanocrystals of cubic ice. Once the nanocrystals are formed and suspended in the carrier gas, they are depleted by sticking to the walls of the static cluster cell, or the larger nanocrystals can simply settle out.[29] The average diameter of the nanocrystals are calculated to be from 25-70 nm (see appendix A.1).

By varying the temperature and pressure, the average size of the suspended nanocrystals can be altered. The dependence of the average size (of the nanocrystals) on the temperature and pressure is displayed in Figure 12. The average size of the

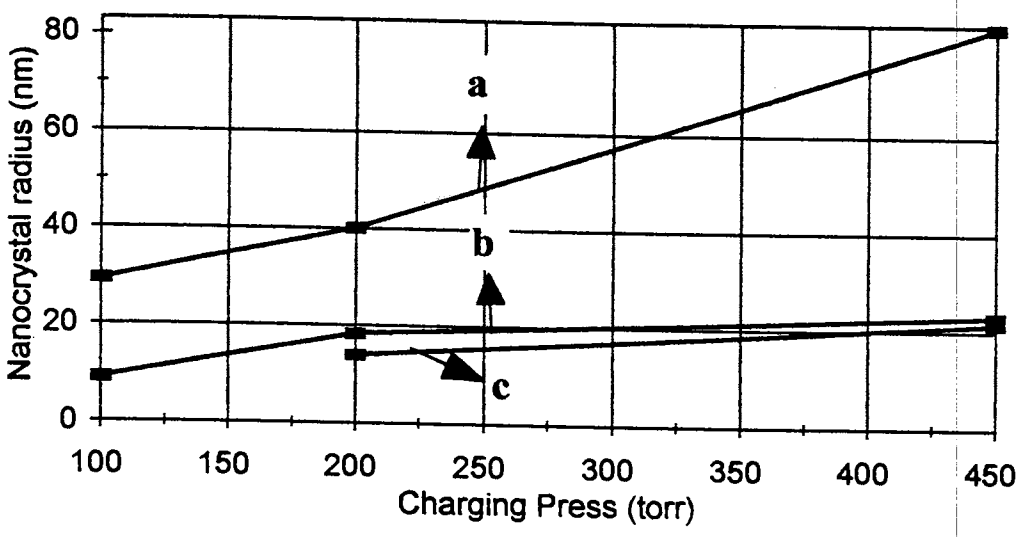

Figure 12. A comparison that shows the general trends of pressure versus the average size of the aerosol H_2O nanocrystals suspended in N_2 at 120 K (a), 85 K (b), and 70 K (c)

nanocrystals increases with increasing pressure, because additional H_2O (D_2O) molecules are available for growth. The average size also increases with increasing temperature which relates to the increase in the size of the critical nucleus for the gas-to-liquid transition. The size increase due to temperature is also observed as a rise in the baseline of the aerosol ice IR spectra due to Mie scattering.[30] The best concentration (which we use to provide ample intensity for analysis) of H_2O (D_2O) in a gaseous sample is a saturated sample of H_2O (D_2O) in one atmosphere to N_2 at and room temperature.

The advantages and disadvantages of using the suspended nanocrystal sampling method have been discussed above, but they are summarized here. The advantages are that surface-defect vibrational modes are observable for temperatures below 120 K, that the clusters can be used as analogs of atmospheric ice clusters, and that the procedures and equipment needed to produce suspended nanocrystals are relatively simple. The main disadvantages are that the nanocrystals diffuse and settle out of the sample (which lowers the intensity), that the ratio of signal-to-noise is not as good as other sampling methods (due to the reduced scanning time), and that a range of temperatures cannot be evaluated for the same load (limited to the loading temperature).

II.3.1.2. Window Deposited Nanocrystals (WDN)

This method of sample preparation has proven to be very valuable in studying the crystalline ice surface. There are many benefits to this method that makes it preferred over the use of suspended nanocrystals or amorphous ice. Presently, WDN represent the preferred way to observe and manipulate ice surfaces (with and without adsorbates) in our group. Several similarities exist between suspended and window deposited nanocrystals sample preparations, but the differences are significant and are discussed.

Procedures

In the suspended nanocrystal section, it was discussed that the suspended nanocrystals diffuse or settle out, and that some of the load will stick on the IR transparent windows. Approximately 7% of the nanocrystals in each load deposits on the windows. Therefore, a 'film' of nanocrystals is created by successive loading of gaseous H_2O (D_2O)/N_2 samples. This is accomplished by using the same procedures outlined for the suspended nanocrystal. However, the exact mechanical procedure for sample preperation of the suspended nanocrystals is repeated approximately 60 times.

A reference spectrum is taken before loading occurs. The WDN procedure requires loading N_2/H_2O (D_2O) (100/1) into the static cluster cell at ~70 K. The charging bulb is pressurized to ~250 torr before the sample is loaded into the cluster cell. The amount of signal intensity for the vibrational modes consistently increases with repetitive loading, but an ample intensity is obtained after 60 loads which takes approximately 3 hours to complete.

Experimental Variables

The temperature and carrier gas effect on the nanocrystal size of one load and multi-loads are discussed here. As with suspended nanocrystals, trends are observed that relate the WDN size to experimental conditions. While suspended in the N_2 carrier gas, the behavior of the nanocrystals is identical to that discussed in the previous section, but the deposition process affects the average nanocrystal size.

The temperature effect on the average sizeof the WDN corresponds to the temperature effect on the size of the suspended nanocrystal. As the temperature increases, the size of the deposited nanocrystal increases. The carrier gas of a sample coats the cluster and prevents further growth as the boiling point of the carrier gas is

approached. The further the temperature is below the boiling point of the carrier gas, the faster it coats and restricts nanocrystal growth. This is observed until liquefaction of the carrier gas becomes significant enough to make the evacuation (through the vacuum line) of the static cluster cell difficult. Figure 13 shows the relationship between the percentage of nanocrystals deposited on the windows and temperature. Argon percentages correspond to those of N_2 with a 10 K shift that corresponds to the 10 K difference between the boiling points of the two gases. The reason that lower temperatures are not used to deposit nanocrystals is that the liquefaction of the carrier gases makes the subsequent evacuation of the static cluster cell difficult.

Advantages and Disadvantages

Similar to the suspended nanocrystals, the surface-defect vibrational modes are observable by the WDN method. However, the IR intensities of the surface vibrational modes for the WDN are much greater than the suspended case because of the repetitive loading that increases the thickness of the WDN samples. The only factor that has been determined to limit the measured intensity for the surface-defect vibrational modes is the endurance of the person performing the deposit. The IR absorption intensity of the surface-defect modes increases upon the continual deposition of nanocrystals. This allows surface-defect vibrational modes to be observed better than for suspended nanocrystals.

The fact that nanocrystals are deposited on the windows allows for interesting options that are not possible for suspended nanocrystal. The pressure of an adsorbing gas (such as N_2, H_2, or CO) can be varied to interrogate surface groups and to measure isotherms that determine the heat of adsorption for adsorbates on the cubic ice surface. WDN allow for particle size selection to be accomplished by annealing; thereby allowing the surface-defect vibrational spectrum to be exposed though the use of difference

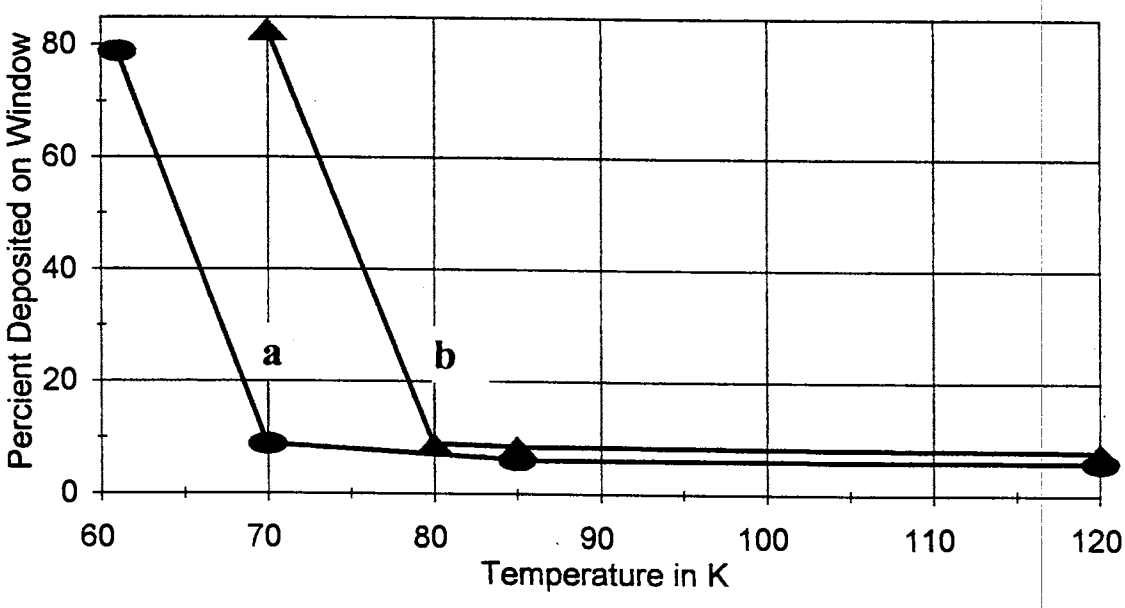

Figure 13. A comparison that shows the general trends between the percentage of a single load of nanocrystals deposited on the windows for N_2 (a) and Ar (b)

spectroscopy. Kinetic experiments that could lead to a better understanding of preferential deuterium bonding and sublimation of ice can also be conducted on the WDN surface.[31,32]

II.3.2. Difference Spectra

The dangling-D band is compared to the bulk stretching-mode absorptions in Figure 14A. Even for small nanocrystals, the bulk region of the IR spectrum dominates the nanocrystalline IR spectrum. Therefore, methods that eliminate the bulk vibrational-mode contribution to the spectrum and that retain the nanocrystalline surface spectrum are devised. Exposing the IR spectrum of the nanocrystalline surfaces is accomplished by employing difference spectra that are created by subtracting spectra taken under different conditions. Two methods for obtaining difference spectra are the annealed difference spectra scheme and the adsorbate-shifted difference spectra scheme.

II.3.2.1. Annealing Difference Spectra Scheme

The preparation of the WDN is achieved by the successive loading of N_2/H_2O (100/1) at ~70 K. After the deposition of nanocrystals is completed, the sample is warmed to 100 K where it is annealed for 30 minutes. The sample is recooled to ~80 K where an IR spectrum is taken. Once the spectrum is taken, the sample is rewarmed and annealed at 150 K for ~30 min. Another spectrum is collected upon recooling to ~80 K, and the spectrum of the 100 K annealed sample is subtracted by the spectrum of the 150 K annealed sample (see Fig 14B). Both spectra are taken at ~80 K to insure that no temperature effects will influence the difference spectrum.

Annealing the deposit is used to increase the average size of the nanocrystals in the deposit, thereby causing the nanocrystals of the sample to lose surface area and gains

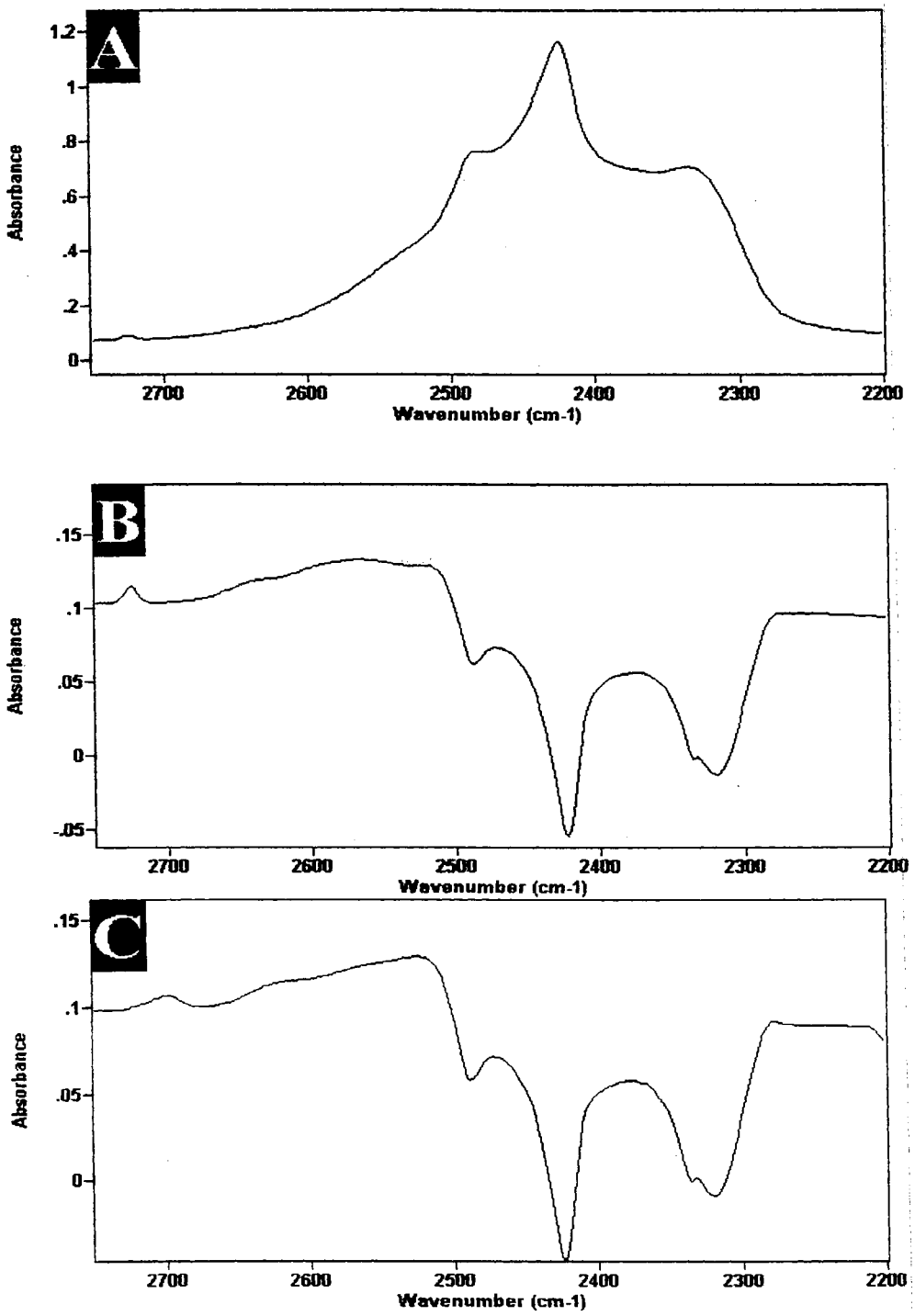

Figure 14. The spectrum of D_2O WDN (A), the annealed difference spectrum of D_2O WDN (B), and the annealed difference spectrum for CO adsorbed on the D_2O WDN (C)

bulk. So, the 100 K annealed nanocrystals are smaller than the 150 K annealed nanocrystals. If the two IR spectra are subtracted, the smaller nanocrystals that have greater surface area are shown as positive IR bands in the difference spectrum, and the larger nanocrystals that have increased bulk and decreased surface area are shown as negative bands in the difference spectrum in Figure 14B.

The effects of adsorbates on the surface-defect vibrational modes are also investigated by using the annealing strategy. The same annealing scheme is applied to the WDN described above. The only difference is that an IR spectrum is collected with an adsorbate present (see Fig. 14C) before and after annealing. The adsorbate-shifted surface-defect vibrational bands for the crystalline ice surface are shown as the positive bands and the bulk vibrational-modes are shown as the negative band.

II.3.2.2. Adsorbate-Shifted Difference Spectra Scheme

The procedures used to create the sample in the adsorbate-shifted difference spectra scheme are similar to the annealing scheme. A sample of WDN is made at ~70 K by using a N_2/H_2O (100/1) gaseous sample and is annealed at 100 K for 30 min. After annealing, the sample is recooled to a temperature where the adsorbate adheres to the nanocrystalline surface. An IR spectrum for the bare ice surface is collected at the chosen temperature. The adsorbate is applied, and a second spectrum is taken. Figure 15 is generated by subtracting an adsorbate-shifted IR spectrum with a spectrum of the bare surface. The positive peaks result from the shifted surface-IR-bands, and the negative bands correspond to the bare surface-defect vibrational mode positions of the bare surface. Adsorbate-shifted difference spectra are more difficult to interpret than annealed difference spectra because the bands shift by different amounts in the presence of different adsorbates, so, a higher frequency band that has a large adsorbate-induced

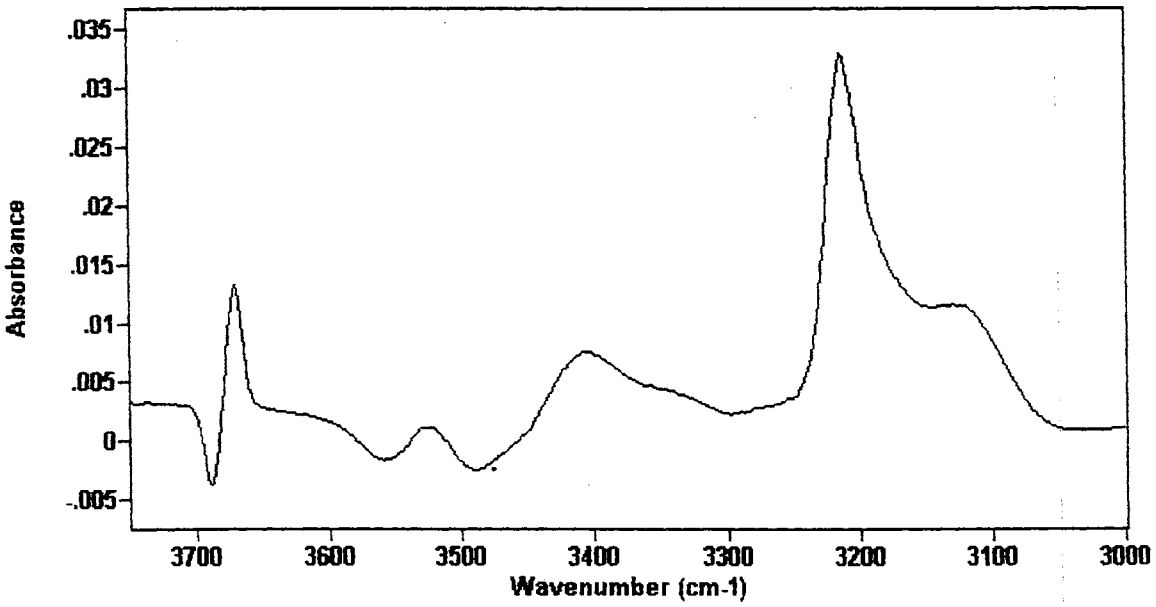

Figure 15. The adsorbate-shifted difference IR spectrum of N_2 adsorbed on H_2O WDN

shift may shift onto a lower frequency band position that has a small adsorbate-induced shift.

II.3.3. Annealing

Annealing the nanocrystals deposited on the windows of the static cluster cell increases the average size of the nanocrystals as the annealing temperature is increased. The use of annealing has already been discussed regarding the production of difference spectra. It also has been stated earlier that the annealed difference spectra exhibit loss of surface area and gain of bulk ice upon increased annealing. The gain in the intensity of the bulk spectral region (negative bands) indicates that the H_2O (D_2O) molecules that are vaporized from the smaller nanocrystals are redeposited on larger nanocrystals (appendix A.2), and are not significantly lost to the cell.

A model for the physical processes that occur during annealing is obtained by using the nanocrystal-vapor pressure relationship that is obtained from classical nucleation theory.[29,33] It can be shown that the vapor pressure exerted by small clusters is greater than the vapor pressure exerted by larger clusters (cluster being defined as small aggregates in any phase). Therefore, the average size of the nanocrystals increases upon annealing at increasing temperatures, because the smaller nanocrystals vaporize and its molecules deposit on the larger nanocrystals. The size of the unstable nanocrystals increases upon annealing at higher temperatures. A semi-quantitave model of the annealing process is presented in appendix A.2.

A distribution of nanocrystal sizes is found for WDN. However, the range of this distribution in WDN size is not yet known. As a sample is annealed, ample time (usually ~30 minutes) is allowed for annealing to occur, thus all the samples annealed at a given temperature have the same average size of the nanocrystals. This is based on the d-H(D) IR band intensity. A plot of the average WDN size versus annealing temperature for a

D_2O deposit, which was annealed at each annealing temperature for ~30 minutes and which was recooled to obtain spectra at 80 K, is presented in Figure 16. The data plotted in Figure 16 are fit an exponential equation that is related to the vapor pressure of the clusters as shown in appendix A.2.

II.4. Band Fitting

Band fitting was used during this research, and was important part in evaluating the surface-defect vibrational mode assignments in the infrared spectrum. Also, the determination of the fractional surface coverage, which was crucial for the evaluation of an adsorbate isotherm on the crystalline ice surface, was made possible by band-fitting the bare and adsorbate-shifted positions of the d-H(D) band. The same band-fitting computer program that was used to determine fractional coverage was also used to fit various theoretical equations to experimental data. For example, the use of the Peakfit program by Jandel is used to determine the heat of adsorption (ΔH_{ads}) for the adsorbates H_2, N_2, and CO (see section IV.4).

Band fitting was used to determine the areas of various surface-defect IR bands. These areas were used to determine the average size of the nanocrystals, to resolve the annealed difference spectra, and to determine the fractional coverage of an adsorbate on the nanocrystalline surface. The band-fitting routine that was used to fit IR spectra was also used to fit various equations (such as the Langmuir isotherm equation) to the isothermal data. General information about the band-fitting program and band fitting in general is included in this section.

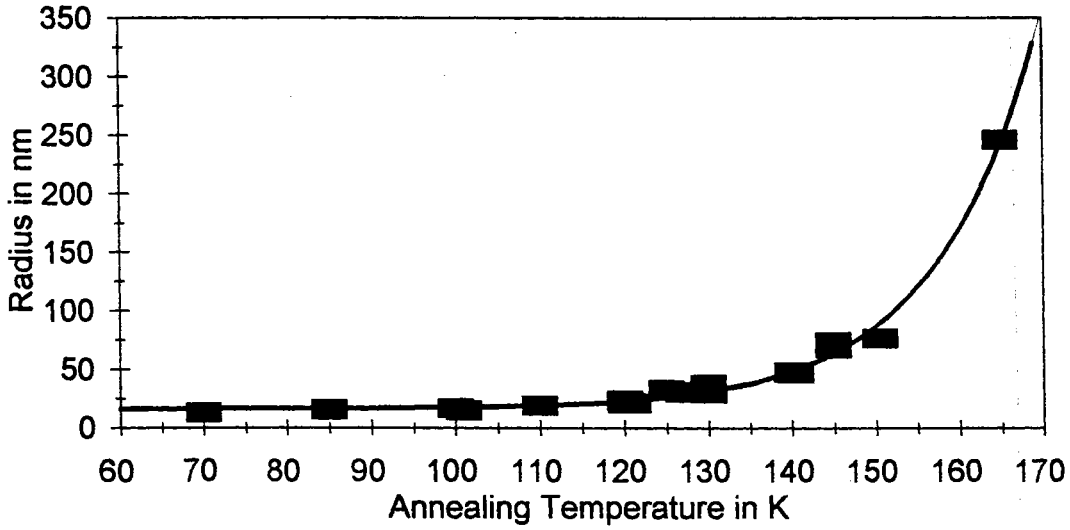

Figure 16. The plot of the average D_2O WDN size versus the annealing temperature of the sample

II.4.1. General

Band fitting has a subjective quality to it. The initial guesses for the band positions, band intensities, choice of bands (e.g., Gaussian, Lorentzian, or Voilt functions), type of background, and the number of bands that are used to fit a given spectrum are all subjective aspects of band fitting. Although the accuracy may be questioned, precision is obtained by fitting a given data set with the same initial parameters. The results yield useful information within a given data set. Other criteria are used to justify the "goodness" of a particular fit, such as comparing results of the fits to theoretical results (simulated IR spectra or *ab initio* calculations), and the conservation of signal. One of the best guides is the question, "Does the fit make physical sense?"

Band fitting is carried out on a Gateway 486DX2-66Mhz IBM capable PC with the "PeakFit" program by Jandel. The program uses a fourth-order polynomial to fit the background, provides a choice of 27 fitting functions, allows manually inserted fitting functions, and can fit up to 8 functions at one time. Other abilities of the PeakFit program are to lock various values that comprise fitting functions (such as the amplitude of a Gaussian function), to manually enter initial guesses for any function, to choose the number of functions that are needed to fit the spectrum, to manually manipulate and lock values for the baseline, and to manipulate the data prior to fitting. The Gaussian function are commonly used to fit the spectral data. Solid state spectral bands tend to be described by Gaussian functions because of the dominance of inhomogeneous broadening.

II.4.2. Nanocrystal Size

The size of the average nanocrystal is determined by obtaining a surface/bulk ratio as shown in appendix A.1. From appendix A.1, the average size of the nanocrystals is calculated by

(1) $r = (A[bulk]/A[d\text{-}H]) \times 1.39 \times 10^{-2}$ nm,

where A[bulk] and A[d-H] are the fitted band areas for the bulk vibrational modes and dangling-H(D) portions of an IR spectrum, respectively. The constant (0.0139) is from appendix A.1, and r is the average radius (in nanometers) of the nanocrystals. The ratio of the areas is determined by fitting the dangling-H(D) and the bulk stretching-mode regions of a nanocrystalline IR spectrum with Gaussian functions. WDN and suspended nanocrystal spectra are fit similarly to determine the surface/bulk ratio.

The fitting procedure for the d-H (D) region of a bare ice surface is identical for all cases, and is displayed in Figure 17A. The d-H(D) portion of an IR spectrum is selected by choosing reasonable end points. To the high frequency side of the d-H(D) band, the points are considered to be on the baseline. To the low frequency side, the points that are selected account for a portion of the out-of-phase d-O band, but the PeakFit baseline fit accounts for this. A non-restricted baseline and a single non-restricted Gaussian function (see Fig.17A.c) are used to fit this portion of the nanocrystalline IR spectrum with consistent results.

Determination of the area of the bulk band included only enough Gaussian functions to yield a good fit (see Fig. 17B). This required six non-restricted Gaussian functions with two of the six Gaussian bands accounting for small amounts of the total area, and a baseline that is restricted by allowing it to only move vertically. None of the fitted bands is assigned to any IR absorption. Only the total area of the bulk bands is used to calculate the average size of the nanocrystals.

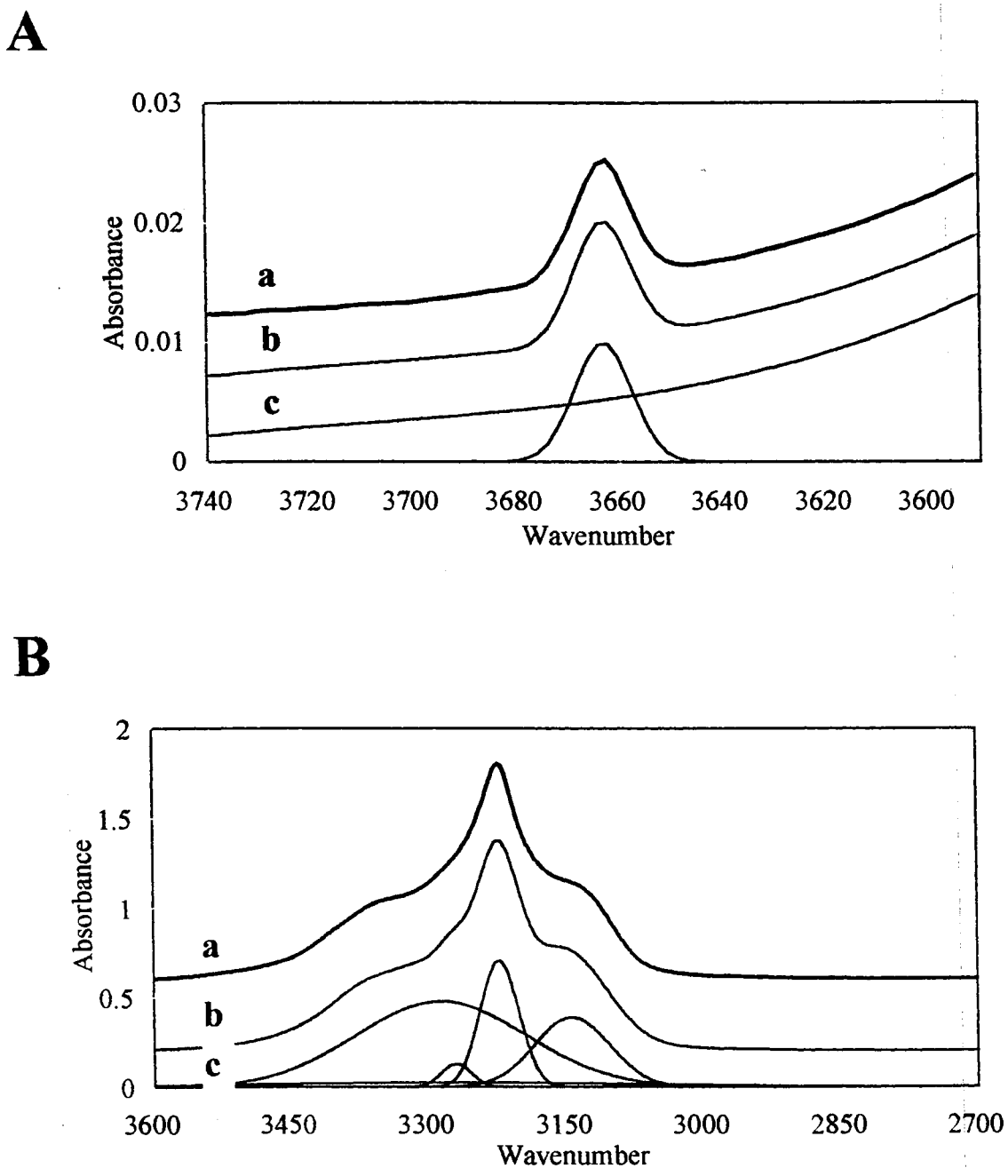

Figure 17. The band fit for the N_2 shifted d-H (A) and bulk (B) portions of an H_2O WDN spectrum

a) the original spectrum b) the fitted spectrum c) the fitting components

II.4.3. Fitting the Surface Portion of the Annealed Difference Spectra

A discussion regarding the procedure that is used to fit the annealed difference spectra is given here for the bare and adsorbed gas cases. Also, an evaluation of the "goodness" of the spectral band-fits is determined for an annealed difference spectrum by reproducing the experimental adsorbate-shifted difference spectrum with the band fitted annealed difference spectrum of a bare surface and band-fitted annealed difference spectrum of a covered surface. The adsorbate-shifted difference spectrum produced by the band-fitted spectra is compared to the true experimental adsorbate-shifted difference spectrum.

The surface bands exposed by the annealing difference scheme were fit with five non-restricted Gaussian functions and a restricted baseline. A flat baseline was imposed as shown in Figure 18A. The initial guesses for the five Gaussian functions were loosely guided by using band positions and band intensities that were theorotically predicted of the in-phase and out-of-phase vibrational modes of S-4. Known assignments were used for the initial band positions for the out-of-phase mode of d-H and d-O. End points were chosen that would fit the bulk region of the IR spectrum, and are shown in Figure 18A. Fitting the bulk region was accomplished by adding three more Gaussian functions which raised the total number of Gaussian fuctions to the maximum of eight functions that are allowed by the program.

Fitting the bulk portion of the difference spectrum was necessary to correctly fit the surface portion of the spectrum. While fitting the surface and bulk regions, the "goodness" of the fit was sacrificed in the bulk region, but this sacrifice gives a good fit in the surface region by accounting for the low frequency bands. Once this fit was obtained, the bulk bands were frozen, and two new end points were chosen that accounted for the surface IR spectrum only. The fitting routine was rerun to obtain a better fit for the surface region (see Fig.18B). The adsorbate-shifted annealed difference

A

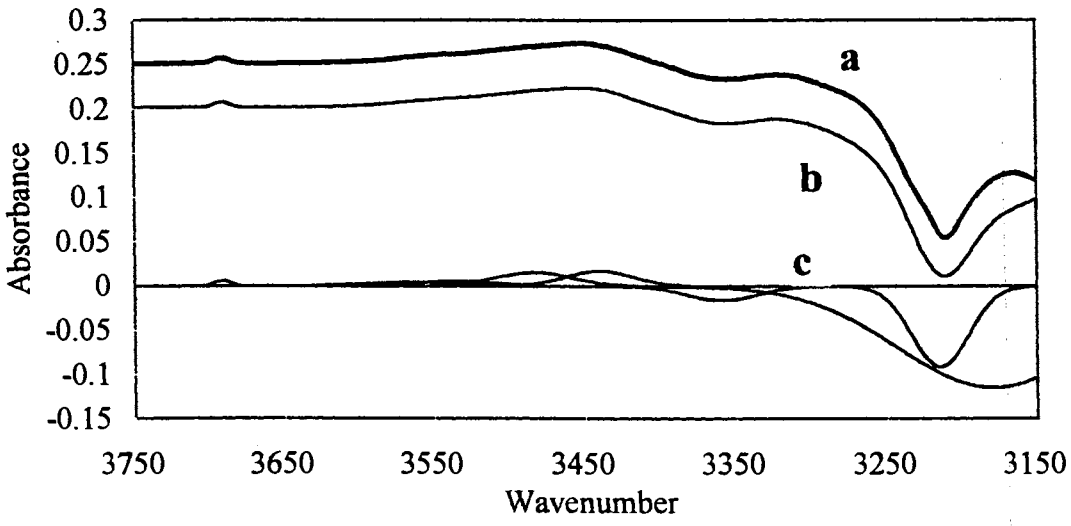

B

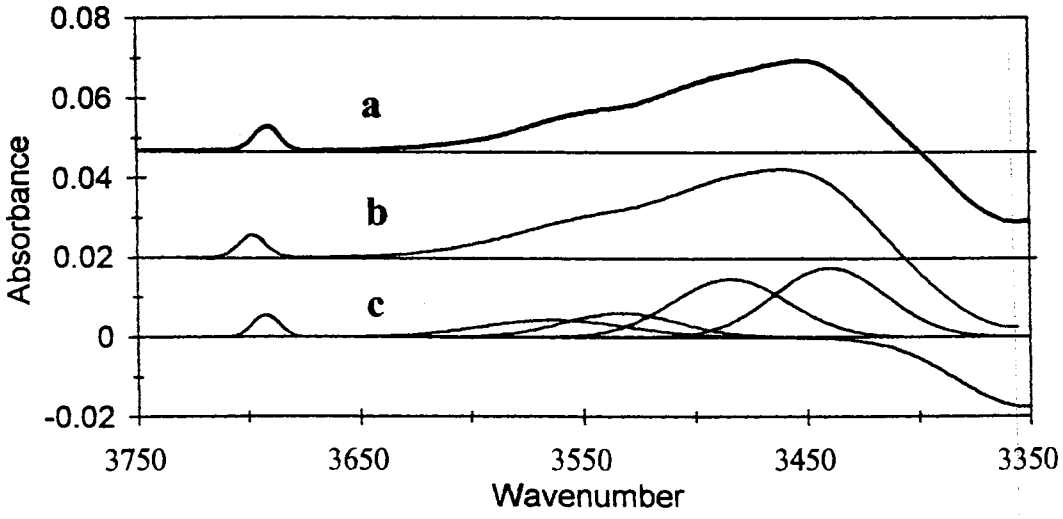

Figure 18. The band fits for the annealed difference spectrum of H_2O WDN that includes the surface and bulk portions (A), and the surface portion only (B); a) the original spectrum b) the fitted spectrum c) the fitting components

spectra were fit in a similar manner; except all the Gaussian bands were shifted to lower frequencies (see Fig. 19B).

The experimental adsorbate-shifted difference spectrum (see Fig. 20a) is reproduced by subtracting the band fit of the band-fitted adsorbate-shifted annealed difference spectrum with the band fit of the band-fitted annealed difference spectrum of the bare surface (see Fig. 20b). However, this is only a fit that reproduces the experimental adsorbate-shifted difference spectrum, and other fits that are better may exist. The agreement between the experimental and fitted spectra (see Fig. 20) aids in validating the choice of Gaussian functions that reproduces the 3750-3350 cm^{-1} portion of the difference spectrum. The assignments of the fitted bands to surface-defect vibrational modes may not be accurate, but some justification is given by their spectral reproducibility.

II.4.4. Isotherms

Fractional coverage for the saturation of d-D surface-defect sites with adsorbed molecules is determined by fitting the d-D band positions for the bare and adsorbed surfaces. Fitting the d-D region of the nanocrystalline IR spectrum to determine fractional coverage is similar to fitting the d-D region of the bare surface; except that extra Gaussian functions are needed to account for the adsorbate-shifted d-D band. The consistency of the fits is determined by using the conservation of signal. As in the bare case, the baselines are unrestricted for CO, N_2, and H_2 induced shifted bands. The isothermal data obtained from fitting the d-D spectral region are fit by using the Langmuir and custom isotherm equations.

The conservation of signal comes from the fact that a certain number of d-D oscillators remain constant after annealing the sample at a given temperature. The IR band for a limited number of d-D oscillators shifts and exhibits an intensity enhancement

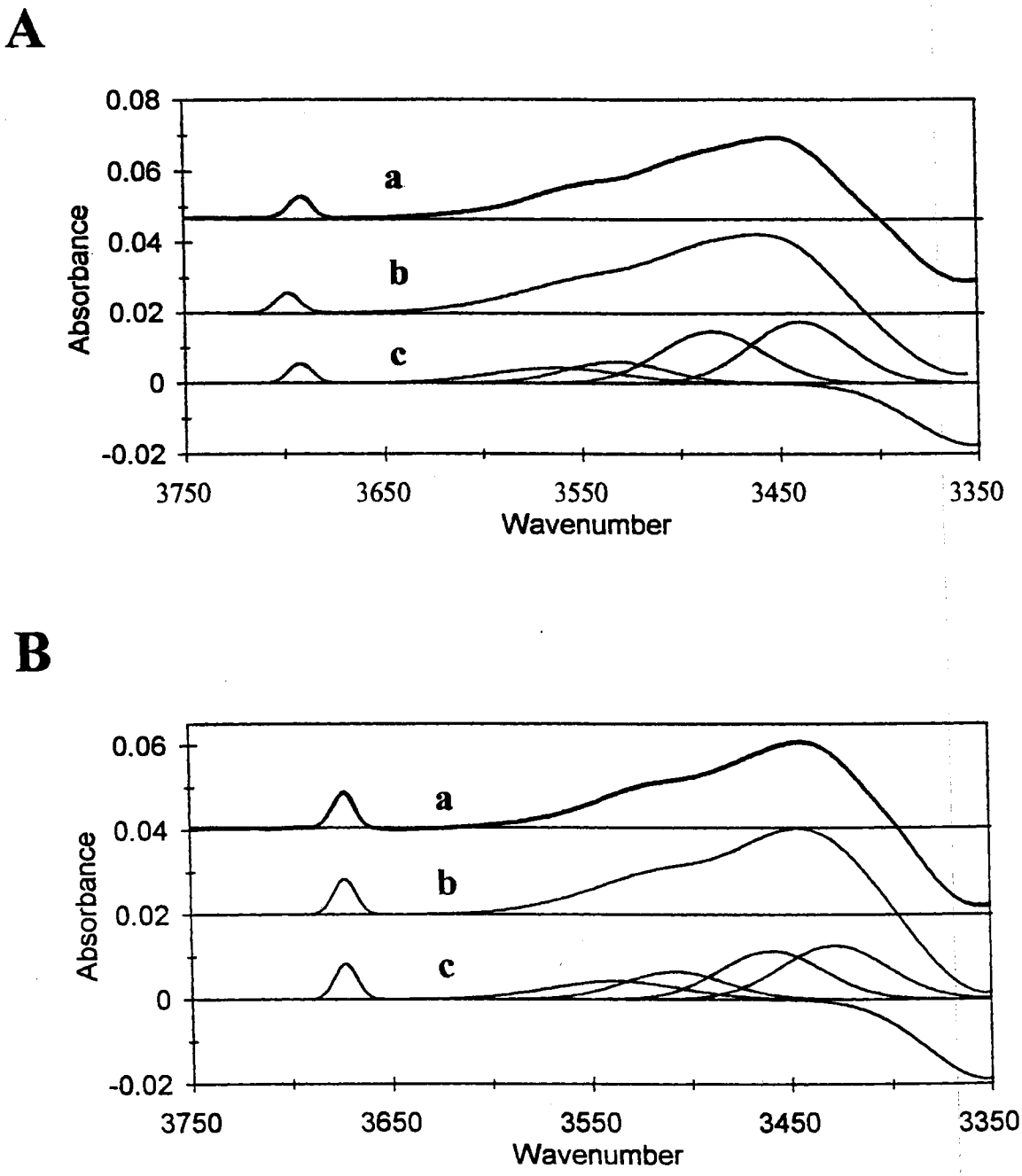

Figure 19. The band fits for the bare (A) and N_2 adsorbate-shifted (B) annealed difference spectra of H_2O WDN

a) the original spectrum b) the fitted spectrum c) the fitting components

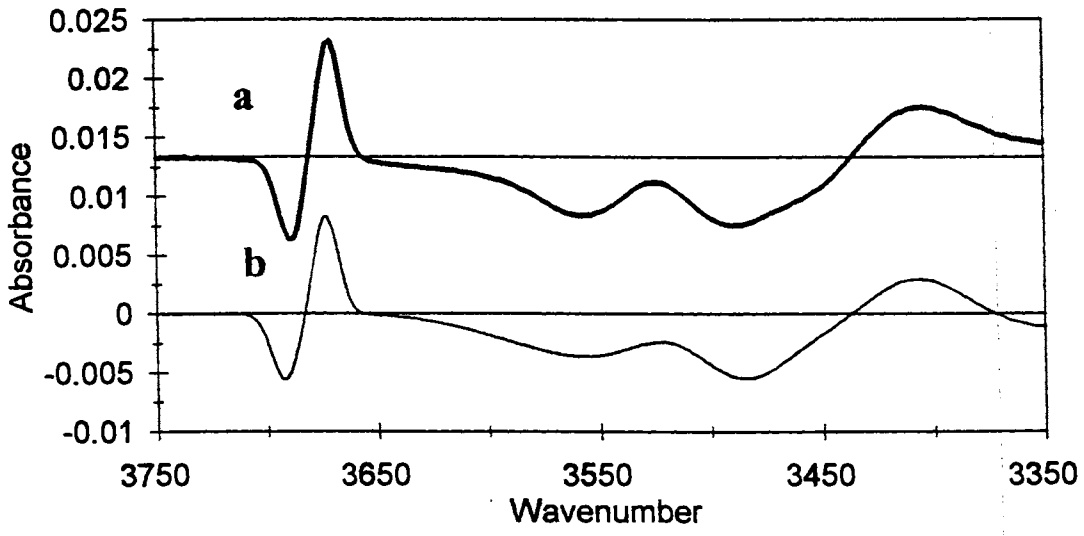

Figure 20. The experimental N_2 adsorbate-shifted difference spectrum (a), and the resultant N_2 adsorbate-shifted difference spectrum from the annealing difference band-fits (b)

upon interaction with a particular adsorbate. So, the number of d-D oscillators corresponds to the area under the d-D IR absorption bands and is given by

(2) A[total d-D bare] = A[d-D bare] + (1/(Enh)) x A[d-D shifted],

where A[d-D bare], A[d-D shifted], and A[total d-D bare] are the fitted areas for the unshifted d-D band, adsorbate-shifted d-D band, and the total unshifted d-D band, respectively. The variable Enh represents the intensity enhancement factor for a specific adsorbate. The A[total d-D bare] is used to evaluate the consistency of the band fits within a given data set. Usually, the A[total d-D bare] values are within 10% of each other, and allow the use of a statistical test to accept or reject various fits.[34]

The band fit for the partial coverage of CO on d-D sites is displayed in Figure 21A. Two unrestricted Gaussian functions are used to fit the CO-shifted d-D band, and a single unrestricted Gaussian function is used to fit the unshifted d-D band. Two bands are needed to fit the adsorbate-shifted d-D region because of the probable CO molecular orientations on the d-D sites and/or the asymmetry of the broad CO-shifted d-D band. *Ab initio* calculations of the CO-H_2O complex show that the interaction of the CO with an H_2O molecule prefers the carbon atom to interact with an H_2O,[35] but both orientations of CO interacting with the d-D surface sites are possible.[35] Also, the CO-shifted d-D IR band moves with respect to the amount of surface saturation, and has an average intensity enhancement factor of 2.1.

Spectra of N_2 and H_2 adsorbed on the d-D surface sites are fit by using identical procedures, and are displayed in Figures 21B and 21C. One unrestricted Gaussian function is used to fit the adsorbate-shifted IR band, and another Gaussian function with a restricted band center is used to fit the unshifted d-D band. Restricting the unshifted d-D position is needed to produce consistent and meaningful results. Other reasons for freezing the unshifted d-D band center are that the amount of shift between the adsorbate-shifted band position and the unshifted band position is small (8-15 cm^{-1}), and that shifts in the unshifted band position towards the adsorbate-shifted band positions at

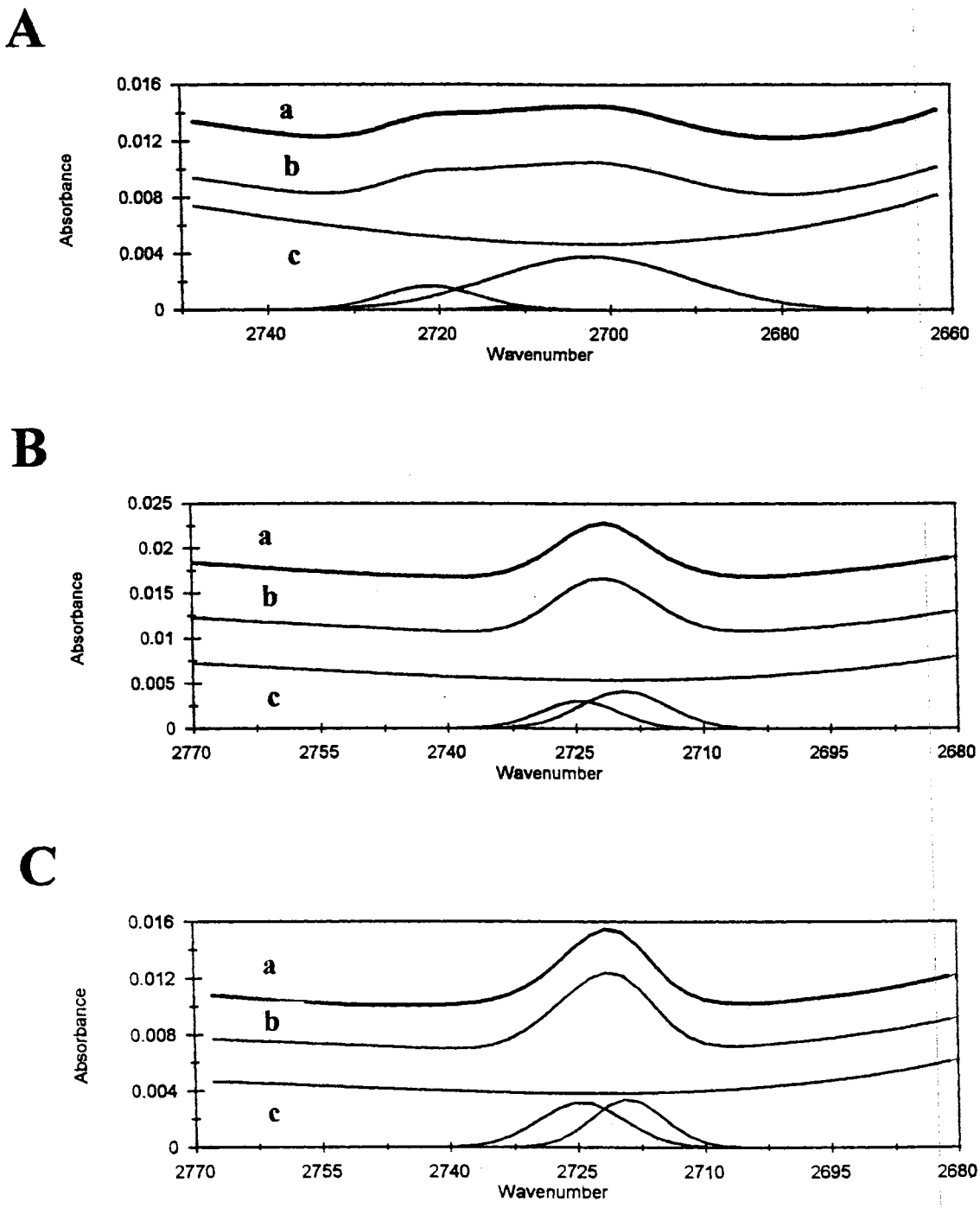

Figure 21. The band fits of the d-D region for CO (A), N_2 (B), and H_2 (C) adsorbed on the WDN

a) the original spectrum b) the fitted spectrum c) the fitting components

intermediate coverages yield unphysical results. Also, consistent results are obtained by locking the unshifted band center. The average intensity enhancement factors are 1.1 for N_2 and 0.85 for H_2.

PeakFit is also used to fit the fractional coverage results with the Langmuir isotherm equation and a custom isotherm equation (see appendix A.3). The "user defined function" option is used to enter various equations into the program, and the baseline is frozen at the zero value. Some initial values that are used to curve fit an equation are guessed, except for the cases where some experimental data existed.[56,57] A discussion of the physical relevance of the isotherm equations and a derivation of the custom isotherm equation are presented in the adsorbate chapter IV and in appendix A.3.

III. Infrared Spectra of the Surface-Defect Vibrational Modes

III.1. Review

As discussed in the experimental chapter II, depositing icy nanocrystals on infrared (IR) transparent windows permits major increases in the surface-defect infrared band intensities with improved signal-to-noise levels compared to that for suspended nanocrystals. The resulting spectra obtained from window deposited nanocrystals (WDN) clearly reveal the surface-defect vibrational mode of the 3-coord d-H(D) (see Fig.14a; Section II.3.2.1). To eliminate the bulk "ice" vibrational modes from the spectra of the deposited nanocrystals, the annealing difference scheme or the adsorbate-shifted difference scheme is used to uncover and display the surface-defect vibrational modes (see Fig. 14b, 14c, and 15; Section II.3.2.1). The purpose of this chapter is to the assign the surface-defect vibrational mode in the IR spectra and to discuss the justification of these assignments.

An ice surface (particularly a crystalline ice surface) can be viewed as being composed of individual surface-defect components of 3-coord d-H(D), 3-coord d-O, and 4-coord S-4 (see Fig. 3; Section I.2.2). Also, the IR spectrum of $(H_2O)_{20}$ clusters is similar to the H_2O WDN surface spectrum above 3400 cm^{-1} (see Fig. 22A and 22B), thereby confirming that the IR spectrum of the crystalline ice surface is composed of surface-defect vibrational-modes that are separated into individual bands that correspond to specific groups of surface sites, and that the IR spectrum for d-H, d-O, and S-4 H_2O molecules in any phase (nanocrystalline surface, amorphous ice surface, or $(H_2O)_{20}$ cluster) is similar. The number of IR bands that are produced by the surface-defect vibrational modes must be known to separate the IR surface spectrum into individual bands. If the three surface-defect groups have out-of-phase and in-phase stretches, then a

A

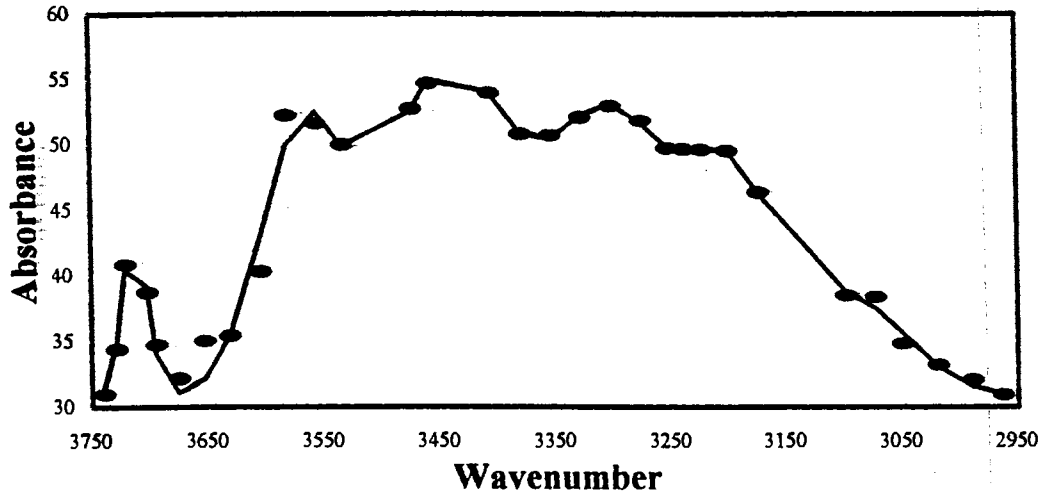

B

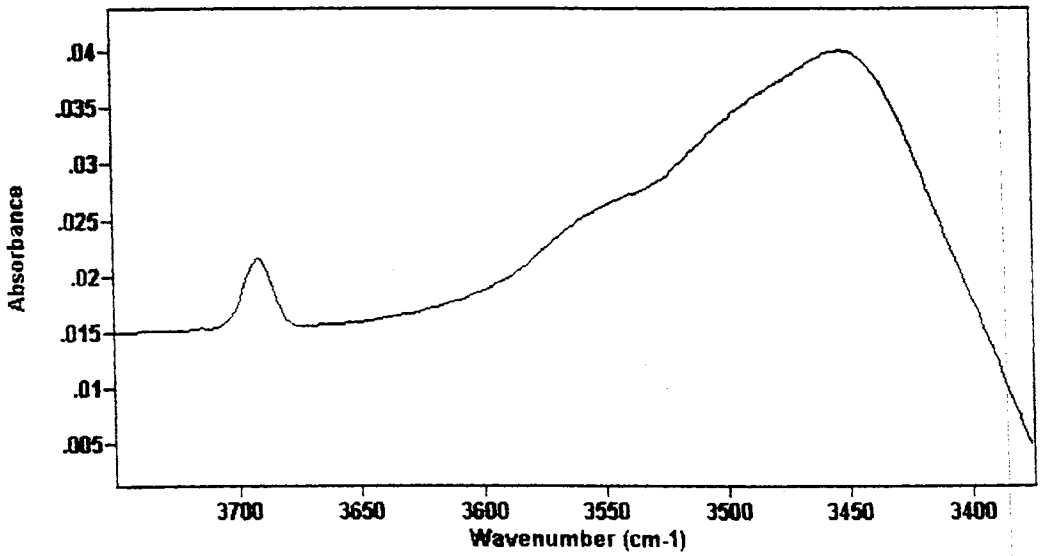

Figure 22. Page et al. $(H_2O)_{19}$ IR spectrum (A) and the surface portion from the annealed difference surface spectrum (B)

Figures 22A and 22B are Figures 4 and 2B, respectively, and are displayed here to provide and easy comparison between the spectra.

minimum of six bands are expected in the stretch-mode infrared spectrum of the WDN surface. Also, three IR bands are expected in the bending region of the surface spectrum.

Assignments for the surface-defect IR bands are not straightforward. Dimer and H_2O molecular beam cluster data were used to assign the out-of-phase d-H at ~ 3700 cm^{-1}. However, dimer frequency assignments led to an incorrect assignment of the in-phase stretch of d-H as 3563 cm^{-1}.[36] Accurate theoretically calculated frequencies were needed to provide guidance in assigning the surface-defect vibrational frequencies below 3694 cm^{-1}, and were obtained from the computational studies done by Leutwyler et al.[37], Hermansson et al. [38], and Buch et al.[39]

III.2. Theory

Numerous H_2O dimer frequency calculations and experimental H_2O dimer stretching-mode assignments have been reported.[10-13] Vibrational frequencies of the H_2O dimer are well known and understood. Fewer publications exist on H_2O ring structures, and their corresponding frequency assignments.[14,37,40] Rings such as the $(H_2O)_5$ (see Fig 23A) offer insight to the out-of-phase and in-phase stretches of two-coordinate H_2O molecules, but not 3-coord H_2O molecules which are the lowest coordinated molecules observed on the crystalline ice surface.[40] Theoretical frequency calculations on 3-coord d-H(D), 3-coord d-O, and S-4 are needed to model the IR surface spectrum and to aid in assigning the IR bands of the ice surface. Only a few computational studies have been conducted for these types of frequency calculations.

III.2.1. Leutwyler et al.

The structure of the $(H_2O)_8$ cluster (see Fig. 23B) was optimized by using the GAUSSIAN-86 program with the 4-31G basis set.[37] This SCF calculation is apparently

A

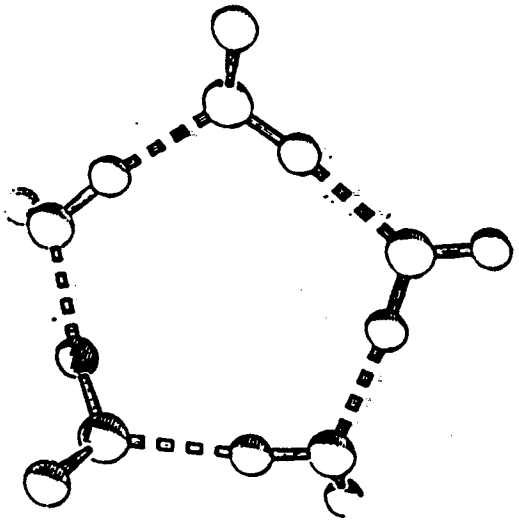

B

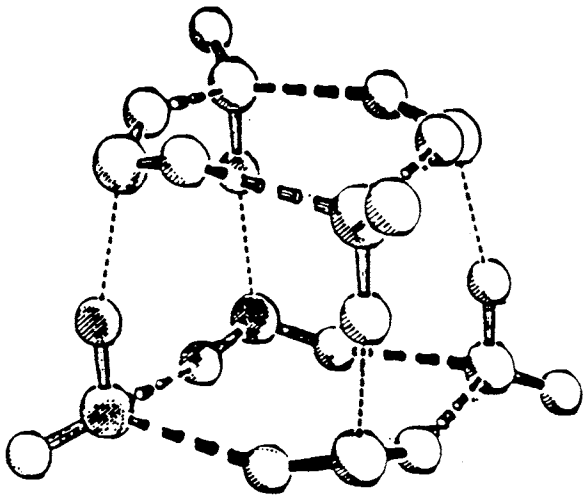

Figure 23. Leutwyler et al. $(H_2O)_5$[14] (A) and $(H_2O)_8$[37] (b) structures

the only *ab initio* calculation for the vibrational frequencies of small cage-like water clusters. The significance of this structure is that it contains the 3-coord d-H and the 3-coord d-O molecules with frequency calculations for both groups. Although Buffey et al.[25] and Jordan et al.[26] (see sections I.2.2.1) had minimized the geometry and potential energy for the $(H_2O)_{20}$ structures, they did not calculate vibrational frequencies for any of the clusters they studied.[25,26]

Leutwyler et al.[37] calculation assigns the out-of-phase stretch of d-H at ~3740 cm^{-1} and the in-phase stretch at ~3200 cm^{-1}. The d-O out-of- and in-phase stretches are located in the ~3600 cm^{-1} region, and are not individually assigned. Assignments are made for the bending modes of d-H and d-O molecules at 1680 cm^{-1} and 1720 cm^{-1} with overtones in the ~3400 cm^{-1} region. Although the vibrational frequency calculations were incomplete (no S-4 molecules are present), the work of Leutwyler et al. offers the only computational results that aid in assigning the bending modes of the d-H and d-O surface sites.

III.2.2. Ojamae and Hermansson

Ojamae and Hermansson used an *ab initio* approach to calculate the binding energies for an H_2O molecule that is tetrahedrally surrounded by four other H_2O molecules (see Fig. 24A).[38] By selectively removing H_2O molecules from around the central H_2O molecule, binding energies were calculated for geometries that match the 3-coord d-O (16 Kcal/mol) and d-H (15.8 Kcal/mol) geometries (see Fig 24B and 24C). A binding energy was calculated for a structure that corresponds to the S-4 (22 Kcal/mole) structure (Fig. 24A) which is formed by not removing H_2O molecules from around the central H_2O molecule. Hermansson et al.[41] also did calculations for interior H_2O molecules in bulk ice. The IR frequency assignments and IR intensity enhancements for the d-H, d-O, and S-4 structures were calculated by Ojamae and Hermansson, and

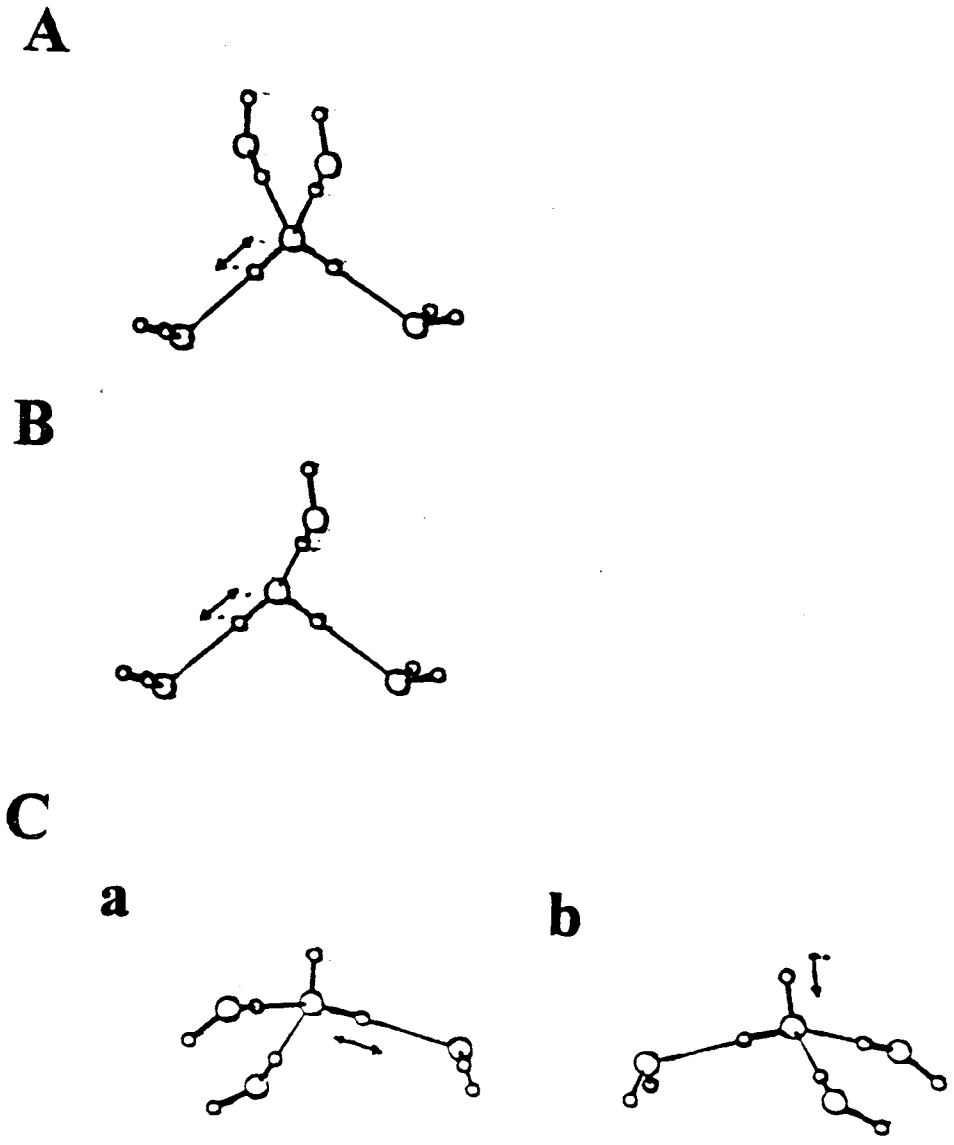

Figure 24. Ojamae and Hermansson[38] S-4 geometry (A) with the OH stretch indicated, d-O geometry (B) with the OH stretch indicated, and the d-H geometry (C) with the free OH stretch (b) and the internal OH stretch (a) indicated

Hermansson et al.[38,41]

The vibrational frequency calculations for S-4, d-O, and d-H are the same structures as those in the binding energy calculations. The S-4 vibrational frequency is calculated for the tetrahedrally bonded H_2O molecule (see Fig. 24A). The d-O frequency is calculated for a structure where the central H_2O molecule has both hydrogens bonded to other H_2O molecules, and one H_2O molecule bonded through the lone pair of electrons on the central H_2O molecule (see Fig. 24B)). Finally, the d-H structure is represented by surrounding a central H_2O molecule with three H_2O molecules in a tetrahedral arrangement, where two of the surrounding H_2O molecules are bonded through the lone pair of electrons on the central H_2O molecule, and the remaining H_2O molecule is bonded through a hydrogen of the central H_2O molecule (see Fig. 24C).

The frequency calculations are for localized OH stretches. This eliminates intramolecular coupling, and focuses only on the intermolecular static field effect on vibrational frequencies. The calculated decoupled frequencies are analogous to the vibrational frequencies that are determined for the O-H stretch of isolated HOD. With this in mind, only one vibrational frequency is calculated for S-4 at 3534 cm^{-1}, and one vibrational frequency is calculated for d-O at 3628 cm^{-1}. The calculations yield external (out-of-phase) d-H(O) and internal (in-phase) d-H(I) vibrational frequencies of 3788 cm^{-1} and 3473 cm^{-1}, respectively (see Fig 24C a and b). If calculated out-of-phase d-H(O) frequency value is scaled to the experimentally observed d-H value of 3694 cm^{-1}, the scaling factor could be used to adjust the internal vibrational-mode value for d-H, and scale the d-H(I) assignment to 3377 cm^{-1}. The adjusted S-4 and d-O vibrational frequencies would be observed at 3438 cm^{-1} and 3532 cm^{-1}, respectively.

The intensities that correspond to the given vibrational modes are also determined by Ojamae and Hermansson[38], and are important here and to Buch et al. simulated IR spectra.[39,46,72] It is observed that vibrational stretching frequencies red-shift from the H_2O gas phase frequencies due to increased hydrogen bonding, and that an increase in IR

intensity corresponds to shifts. The intensities for the vibrational modes of d-H, d-O, S-4, and "bulk" H_2O molecules are not explicitly given, and had to be inferred from the information that is available in Hermansson et al. publications.[38,41]

Figure 25A shows a chain of seven H_2O molecules. From the chain structure, the relationship between the infrared intensity and the vibrational frequency shifts is obtained. By plotting this relationship, a linear relationship between the frequency shifts and infrared intensities is given in Figure 25B. The intensities for the d-H, d-O, S-4, and "bulk" H_2O molecules are shown on the plot in Figure 25B. The ratios of the intensities of d-O/d-H (3.86), S-4/d-H (5.53), and S-4/d-O (1.44) were useful in validating the experimental assignments discussed later in the chapter.

III.2.3. Buch et al.

Buch created an amorphous $(H_2O)_{450}$ cluster by employing classical trajectories to simulate H_2O condensation .[27] Annealing was simulated by adding energy to the amorphous cluster to form a fully annealed $(H_2O)_{450}$ cluster. A "Morse basis"[42] was used to describe each localized OH (or OD) oscillator.[42] The ground state is described by the product of all the Morse ground states, and the excited state was described by a linear combination of the "Morse basis" with one quantum placed in a localized Morse oscillator which is located on an OH bond with all remaining bonds set to zero.[42] Frequency calculations were then done for the 450 molecule cluster. An OH bond for a classically determined cluster structure was described by a "Morse basis" that is used to calculate the OH vibrational frequency for each OH stretch in the cluster.

Buch et al. calculated the vibrational frequencies specifically for surface-defect vibrational modes.[39] The frequency results of the calculations are expected to agree with the experimental surface-defect vibrational frequencies because the calculations were conducted for the purpose of studying the ice surface. The out-of-phase vibrational

A

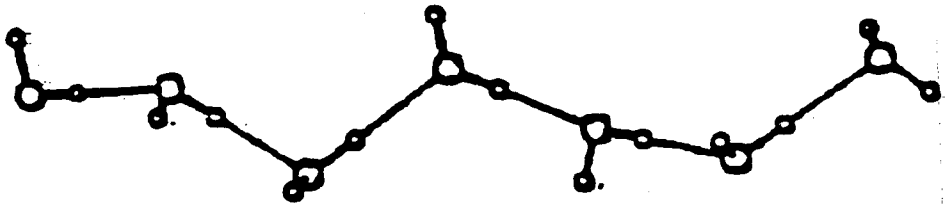

B

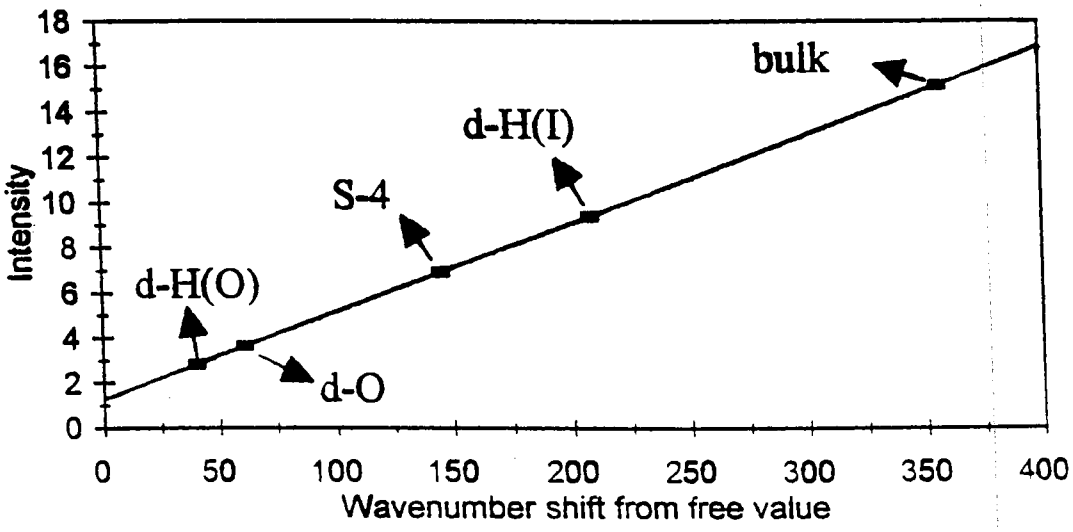

Figure 25. Ojamae and Hermansson heptimer chain (A), and calculated intensity plot (B)

modes for the d-D, d-O, and S-4 molecules were calculated to be 2700 cm^{-1}, 2590 cm^{-1}, and 2490 cm^{-1}, respectively. The in-phase bands for d-D and S-4 groups were calculated to be at 2380 cm^{-1} and 2390 cm^{-1}. The calculated out-of-phase and in-phase vibrational mode assignments for the d-O are smeared within the 2600-2300 cm^{-1} frequency range. The theoretical approach of Buch et al. produces an IR spectrum for the $(H_2O)_{450}$ fully annealed cluster. In the cluster, 360 H_2O molecules out of 450 are either d-D, d-O, or S-4 molecules. Therefore, the simulated fully-annealed cluster spectrum is effectively a surface spectrum with bands for the interior vibrational mode omitted. The intensity assigned to each OH vibrational mode was extrapolated from Ojamae and Hermansson data.

Figure 26A shows the simulated $(D_2O)_{450}$ fully annealed cluster spectra of the d-D (solid line), d-O (dot-dashed line), S-4 (dashed line), and the total cluster spectrum (dot). The spectrum in Figure 26B is generated by subtracting the fully annealed cluster spectrum by a previously simulated spectrum of bulk ice.[42] The positive bands correspond to the surface-defect vibrational modes, and the negative bands correspond to the bulk vibrational modes as in the experimental annealed difference spectrum. Similarities exist between the experimental annealed difference spectrum (see Fig. 22B; Section II.3.2.1) and the simulated difference spectrum (see Fig. 26B). This agreement between theory and experiment is discussed in the following section regarding the experimental frequency assignments.

III.3. Experimental Assignments

In the experimental chapter, the difference schemes that are employed to eliminate the bulk IR bands from the surface-defect vibrational bands are discussed in detail. The experimental spectrum that demonstrates the relationship between an experimental spectrum for D_2O nanocrystals and the simulated annealed difference

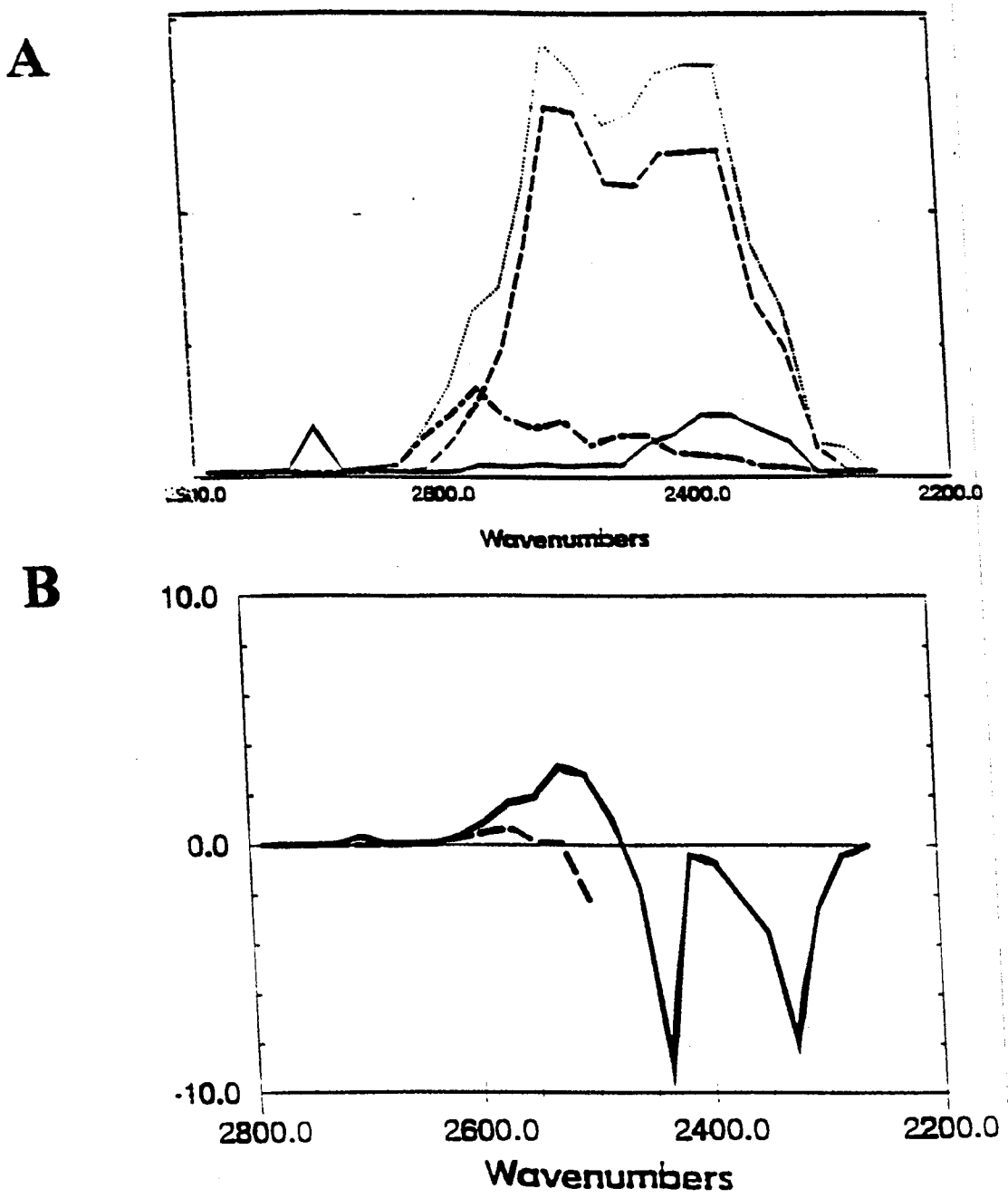

Figure 26. Buch et al.[72] simulated $(H_2O)_{450}$ cluster spectrum (A), and the simulated surface-interior difference spectrum (B)

spectrum is the annealed difference spectra. A one-to-one correspondence is observed between the experimental and simulated spectrum, where the bands in the experimental annealed difference spectrum qualitatively agree with the bands of simulated annealed difference spectrum. The obvious assignments from the spectra that are presented in Figures 27a and 27b are the out-of-phase vibrational modes of d-D, d-O, and S-4 at 2725 cm^{-1}, 2645 cm^{-1}, and 2580 cm^{-1}, respectively.

Further assignments are obtained by band fitting the experimental annealed difference spectra. The band-fitting procedure that is used to resolve the experimental surface spectrum is discussed in the experimental chapter. Briefly, Ojamae and Hermansson[38] infrared intensity data and the simulated vibrational frequency assignments are used to guide the band fitting of the experimental spectrum, which is displayed in Figure 28B. The out-of-phase and in-phase bands that compose the surface portion of the annealed difference spectrum are assigned to the vibrational-modes of d-D, d-O, and S-4. The initial Gaussian band centers for the out-of-phase modes of d-D, d-O, and S-4 are taken from spectral results. The initial band centers for the in-phase vibrational modes are taken from theoretical results.[72]

Figures 28A and 28B demonstrate the relationship between the cluster simulated spectrum of the fully annealed cluster and the band-fitted experimental spectrum. The fitted band positions of the surface-defect vibrational modes and their respective intensities qualitatively agree with the simulated spectrum. This experimental fit of the surface-defect IR spectrum reveals that the in-phase vibrational modes of d-D(I), d-O(I), and S-4(I) cannot be confidently assigned. The fitted band at ~2490 cm^{-1} is broad, and is composed of in-phase d-D, d-O, and S-4 bands that cannot be resolved into individual bands (because the band centers of the three bands are too close to each other). Sub-surface vibrational modes could also be located in the ~2500 cm^{-1} region which further complicates the interpretation of the fit. Sub-surface vibrational modes are the vibrational modes of the D_2O (H_2O) molecules that are located within a few layers from

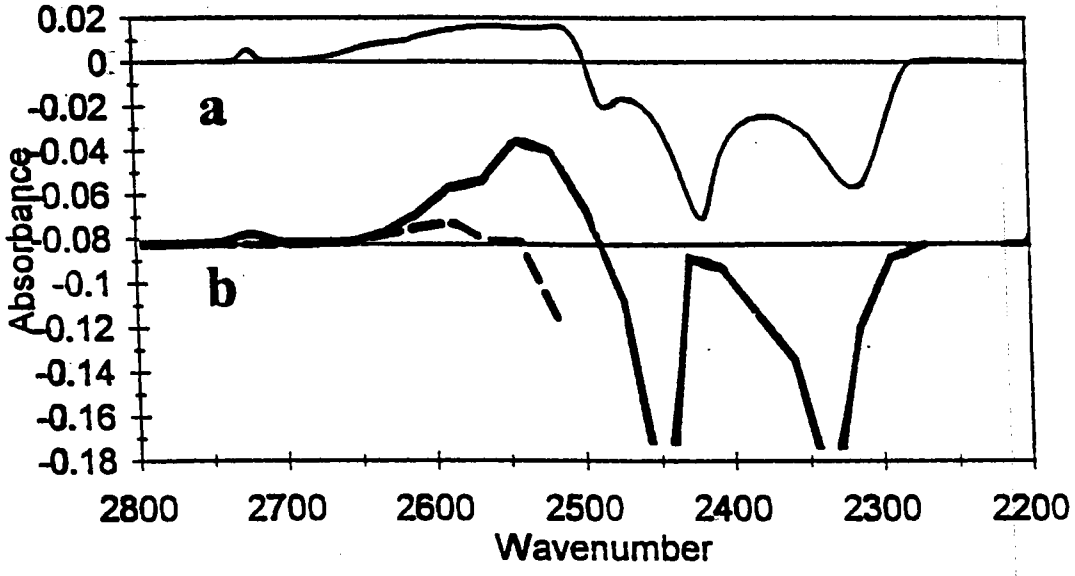

Figure 27. Comparisons between the D_2O experimental annealed difference spectrum (a) and the simulated annealed difference spectrum[72] (b)

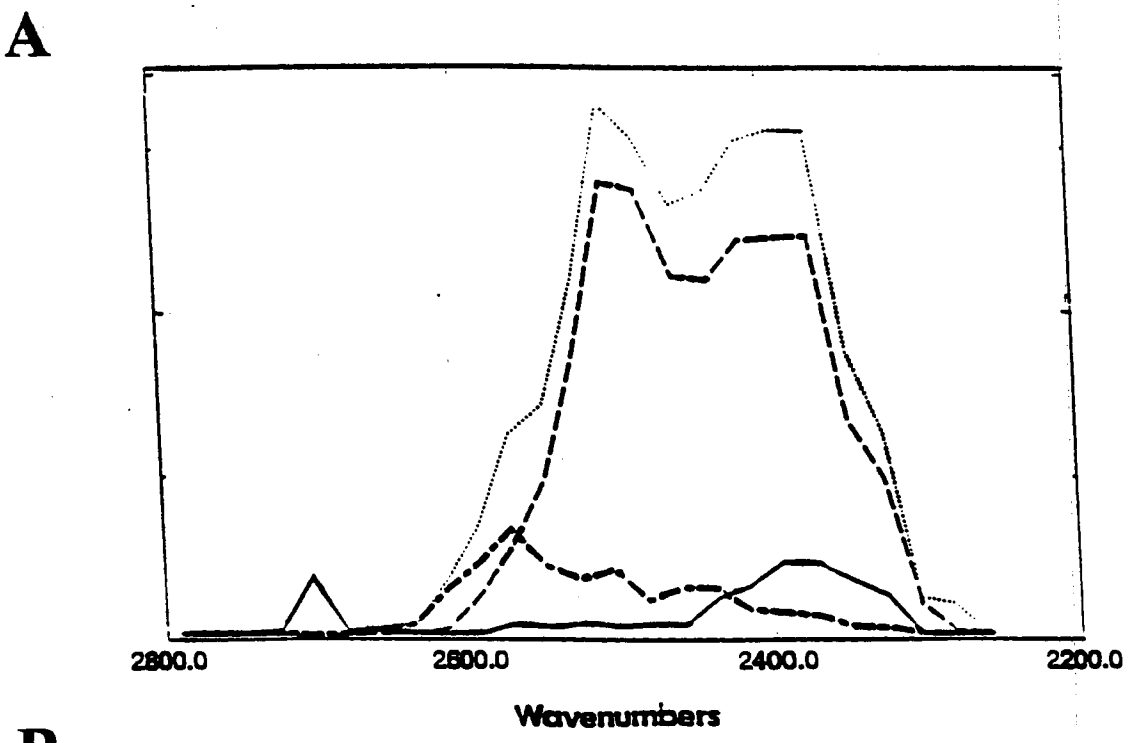

Figure 28. Buch et al.[72] simulated surface spectrum (A), and the band-fitted experimental spectrum (B)

the surface. So, the 2490 cm^{-1} band in the fitted experimental spectrum is composed of many bands.

The out-of-phase surface-defect vibrational modes for the d-D, d-O, and S-4 are confidently assigned 2725 cm^{-1}, 2640 cm^{-1}, and 2564 cm^{-1}, respectively. The reason for the confidence is because of the agreements between theoretical and experimental assignments. As seen in Figures 29A and 29B, the ratios of fitted experimental infrared band intensities for the out-of-phase bands agree with ratios of intensities calculated by Hermansson et al.[41] for the surface-defect groups (see Fig. 29A), and the assigned experimental frequencies are between Ojamae and Hermansson[38] and Buch et al.[46,72] calculated frequencies (see Fig. 29B).

Two bands are singled out in the d-O region of the simulated cluster spectrum. A sharp band for the out-of-phase d-O mode is assigned to ~2600 cm^{-1}, and a broader underlying band for the in-phase d-O mode is assigned to ~2500 cm^{-1}. The out-of-phase d-O is experimentally observed at 2640 cm^{-1} in Figure 28, and the band centered at 2600 cm^{-1} in Figure 28 accounts for the asymmetry in the out-of-phase d-O and S-4 bands.

Band fitting is not necessary to assign bands in the bending region of the ice surface spectrum. In Figure 30, the bending mode region of an experimental annealed difference spectrum is compared to the unadjusted IR bending spectrum of nanocystalline ice. The computational study of Knochemuss and Leutwyler[37] identifies the bending mode of d-O at 1690 cm^{-1} and the bending mode of d-H at 1650 cm^{-1}. In the experimental annealed difference spectrum (see Fig. 30a), there is an intense band at 1650 cm^{-1} that is assigned to the bending mode of d-H and broader band at 1690 cm^{-1} that is assigned to the bending mode of d-O. Also, the bending mode bands assigned in the annealed difference spectrum correspond to a horn and a shoulder that are observed in the bending region of the unadjusted standard spectrum (see Fig. 30b). The close agreement between theory and experiment gives credibility to these assignments.

A

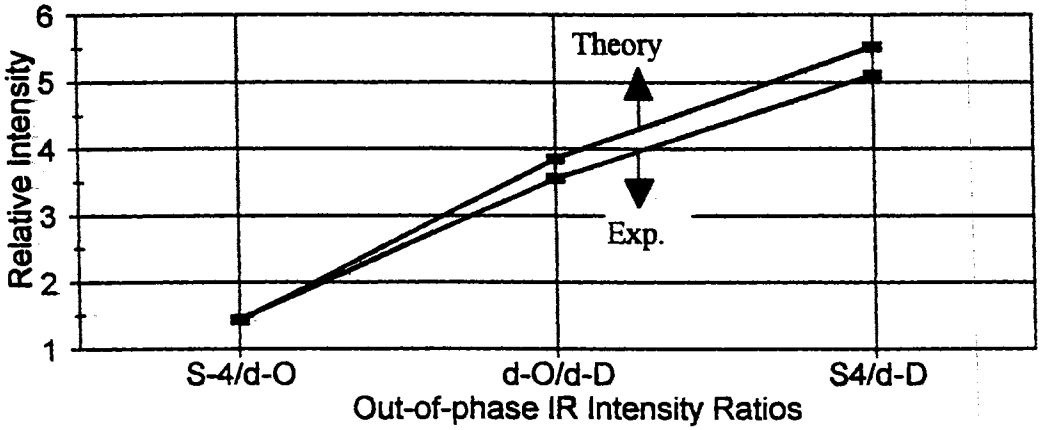

B

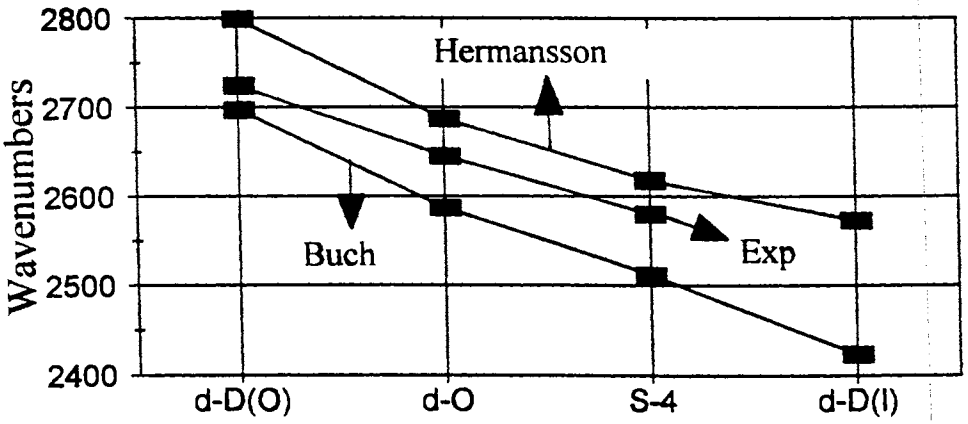

Figure 29. Experimental intensity ratios (A), and a comparison between calculated and experimental assignments for vibrational surface-defect modes (B)

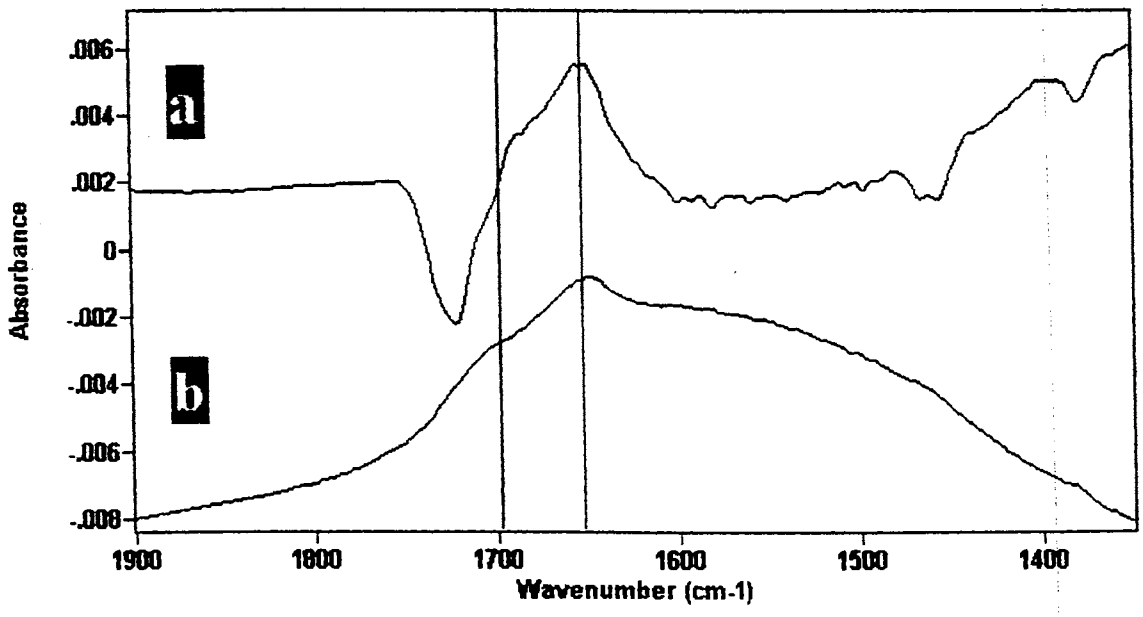

Figure 30. Bending spectra of the annealed difference spectrum (a) and the standard IR spectrum of ice nanocrystals (b)

The assignments of the surface-defect vibrational modes emerge by comparing theoretical and experimental assignments. Table 6 lists the assignment information for the experimental vibrational modes of the bare surface. Figure 29 displays the trends that are apparent for the theoretical and experimental frequencies of the surface-defect vibrational modes. The experimental assignments of the vibrational modes agree within the range of theoretical assignments which are shown in Figure 29B, and the fitted ratios of the experimental band intensities agree with the ratios of the theoretical band intensities which are also shown in Figure 29A. Therefore, the assignments for the out-of-phase vibrational modes are considered by us to be correct, and the assignments of the bending modes are also considered by us to be reasonable. The assignment for in-phase vibrational modes of S-4 is based on the band at 2490 cm^{-1} that we consider dubious, and the assignments for the in-phase d-D and d-O modes are based solely on the simulated spectrum of Buch et al.

Table 6.

Summary of vibrational frequency assignments in cm^{-1}

	H_2O			D_2O			
	d-H	d-O	S4	d-D	d-O	S4	
out-of-phase	3692	3564	3485	2725	2640	2564	
in-phase	3150*	3300*	3440	2350*	2450*	2490	
bending	1650	1690	?	1215	1235	?	

	3-coord	HOD
	d-H	d-D
free stretch	3688	2712

* The frequency values for D_2O are taken from the simulated IR spectrum, and the H_2O frequency values are extrapolated from corresponding D_2O values by using the isotopic shift factor of ~1.35.

IV. Adsorbates

IV.1. Introduction

The D_2O (H_2O) crystalline ice surface is a bilayer consisting of three distinct surface-defect groups. These are the 3-coordinate dangling-D (d-D), dangling-O (d-O), and the surface 4-coordinate groups (S-4) (see Fig. 3; Section I.2.2). The surface-defect groups have out-of-phase and in-phase vibrational modes as well as bending modes. The assignments for the D_2O (H_2O) out-of-phase vibrational modes of d-D (d-H), d-O, and S-4, are 2725 (3692) cm^{-1}, 2640 (3564) cm^{-1}, and 2564 (3485) cm^{-1}, respectively. The assignments for the D_2O (H_2O) in-phase vibrational modes of d-D (d-H), d-O, and S-4 are 2350 (3150) cm^{-1}, 2450 (3300) cm^{-1}, and 2490 (3440) cm^{-1}, respectively. Also, the D_2O (H_2O) bending modes of d-D (d-H) and d-O are assigned 1215 (1650) cm^{-1} and 1235 (1690) cm^{-1}. The band-fitted D_2O and H_2O annealed difference spectra, which are used to assign the surface-defect vibrational modes, are displayed in Figures 30B and 20A (see sections III.3 and II.4.3).

Assignments of the surface-defect vibrational modes allow the H_2O ice surface to be separated into individual bands that correspond to specific surface sites. This allows a site-specific view to be derived from the resolvable surface IR bands. Also, this site-specific view of the ice surface is used to study adsorption onto the ice surface by employing the FT-IR techniques, which are described in the experimental chapter 2. Adsorbed molecules have a significant effect on the IR spectra of the ice surface. Observation of the effects that adsorbed molecules have on the surface-defect sites is achieved by using the methods of difference spectroscopy (the adsorbate-shifted difference spectrum and the adsorbate-shifted annealed difference spectrum), and by using the standard unadjusted spectra of WDN.

Adsorbates on the ice surface cause red shifts relative to the surface-defect IR bands of the bare surface, and enhance the intensities of the adsorbate-shifted IR bands relative to those for the bare ice surface. Data gained by applying adsorbates allow for a qualitative and quantitative description of the adsorption process (site specificity), of the interaction strength, of the heat of adsorption, of the ice surface morphology, and of other aspects that give insight into the interactive nature of the ice surface. This information is site specific and adsorbate specific. The binding energies of the adsorbed molecules are site dependent, and thus cause different spectral characteristics for each group of sites on the surface (such as the magnitude of the adsorbate induced IR shift of the d-H(D)).

The topic of the adsorption on the ice surface is too broad to be completely covered in depth in this thesis. However, the information presented in this thesis should provide a reasonable model of the ice surface, and its interactive nature. A review of the literature on adsorption, general information about adsorption that was obtained in our research, information obtained from our experimental isotherms, and an adsorption study of CF_4 on the H_2O (D_2O) ice surface are presented.

IV.2. Literature

Few surfaces described in the literature have specific surface groups that can be used as probes of surface interactions. To our knowledge, the only reasonable analog to the dangling groups of the ice surface are the dangling-OH groups on the zeolite surface.[43] An infrared study of adsorbed molecules on the H-ZSM-5 zeolite surface reveals a downward shift in the bare dangling-H band located at 3640 cm^{-1} for Ar, O_2, CH_4, CO, and C_2H_4. This red shift of the d-H frequency mimics the adsorbate-induced shifts observed for the same adsorbates on the ice surface. The d-H adsorbate-induced shifts on the zeolite surface qualitatively agree with the observed shifts on the H_2O ice surface. These d-H shifts occur in the same order of increasing adsorbate interaction

($Ar<O_2<CH_4<CO<C_2H_4$) for both surfaces. However, the magnitudes of these shifts differ by a factor of ~10 with the shifts in adsorbate-shifted d-H zeolite band being greater than those for the ice surface.

The IR intensity enhancement was observed for the d-H band of an adsorbate covered zeolite surface. The ratios of the adsorbate-enhanced IR intensities versus the d-H intensities for the bare ice surface increase linearly with the magnitude of the adsorbate-shifted d-H position (for a fully covered surface). Therefore, C_2H_4 adsorption causes a greater enhancement in the d-H intensity than CO adsorption, and the order of increasing intensity enhancement is $Ar<O_2<CH_4<CO<C_2H_4$. This linear relationship was calculated by Hermansson et al.[38] (see section III.2.2), and was used by Buch et al.[39] (see section III.2.3) to assign intensities for the bands of the simulated surface spectra. Intensity enhancement is the result of the charge flux that is due to the charge transfer and polarization along the hydrogen-bond axis.[44]

Results have been reported by Devlin et al.[45,46,49] for H_2, N_2, CO, Ar, C_2H_2, C_2H_4, and CF_4 adsorbed on amorphous and crystalline ice surfaces. The ortha-para conversion of H_2 molecules on the ice surface was investigated.[45] Nitrogen, Ar, C_2H_2, C_2H_4, and CO were adsorbed onto the ice surfaces to study the effect on d-H(D) sites.[46] Infrared spectra of the CO stretch and Raman spectra of the C_2H_2 C-C stretch revealed that the fundamentals are split into two bands.[47,48] This indicates that the adsorbed molecules occupy two strongly perturbing groups of surface sites. The transverse optical and longitudinal optical (TO-LO) splitting of CF_4 is used to determine surface morphology.[49] Most of the previously reported adsorbate studies on ice surfaces are directly related to this thesis, and are discussed in this chapter. H_2 ortha-para conversion and C_2H_2 adsorption are not directly related to this thesis and are not be discussed in this thesis.

Ab initio calculations for complexes of an H_2O molecule with a H_2, N_2, HF, CO, C_2H_2, CO_2, C_2H_5OH, or CH_2O molecule give estimations for the adsorption interaction

strengths, and for the site (d-D(H) or d-O) that the adsorbing molecules prefer to occupy.[33, 50-55] The calculated complexes of the dimer are arranged such that a molecule interacting with the H_2O molecule bonds through a hydrogen of the H_2O (the proton donor complex) (see Fig. 31A), or bonds through the lone pair of electrons on the oxygen of the H_2O molecule (the Lewis base complex) (see Fig. 31B). The proton donor complex corresponds to an adsorbed molecule interacting with a d-H site, and the Lewis base complex corresponds to an adsorbed molecule interacting with a d-O site. The dimer results that are used in this thesis are those for the H_2O molecules binding with H_2, N_2, and CO.[55]

Isotherms determined by using IR absorption (optical isotherms) have been reported for H_2 and CO adsorbed on the crystalline surface of NaCl.[56,57] Optical isotherms were obtained by following the IR spectra of the adsorbed molecules. The H_2 and CO isothermal data for adsorption on the NaCl surface were fit by the Langmuir isotherm equation, which accounts for the adsorbate molecule-surface site interaction only. The Langmuir isotherm equation has no provisions for the adsorbate molecule-adsorbate molecule interaction or any other interactions. The heats of adsorption (ΔH_{ads}) for H_2 and CO adsorption on the NaCl surface are determined to be -0.81 Kcal/mol and -3.35 Kcal/mol, respectively. The binding energies for CO and H_2 on the H_2O ice surface were also determined by Sandford and Allamandola. They followed the vibrational intensity of the adsorbates as a function of the desorption time, and calculated binding energy values of 3.5 and 1.1 Kcal/mol for CO and H_2 adsorption, respectively.[58,59]

A

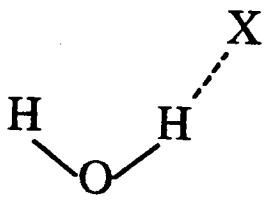

B

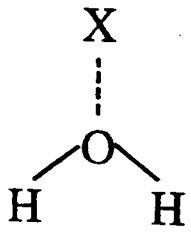

Figure 31. The proton donor complex (A) and the Lewis base (B) complex for the H_2O--X dimer

IV.3. Adsorption on the Ice Surface

The selection of molecules that we adsorbed on the surface of the WDN was dictated more by practicality than curiosity. In some cases, the available literature encouraged the use of various adsorbates at cryogenic temperatures (N_2, H_2, CO), but there exist minimal requirements that guide adsorbate selection. Because of the design of the static cluster cell (see Fig. 10; Section II.2.2), the adsorbing gases must pass through a precooled rubber tube (#42), inlet #45, static brass cluster cell (#34), and penetrate the nanocrystalline window deposit. The adsorbing molecules must also adsorb on the ice surface in a monolayer not a multilayer. The maximum temperature that surface-defect vibrational modes can be observed for the WDN is ~160 K. This must be considered while selecting adsorbates.

The practicality of the selected adsorbate molecule is also determined by the temperature range that the application and spectral evaluation of an adsorbate on the ice surface can be conducted. For example, CO_2 is a poor choice for a WDN sample that is not annealed to temperatures above 120 K, because the amount of time that is required to evacuate CO_2 for another trial would be hours if at all. Carbon dioxide cannot be evacuated within an hour from the ice surface at temperatures below 120 K with our vacuum equipment. The same is true for evacuating N_2 out of the static cluster cell at ~60 K. Carbon dioxide is a good choice for experimental conditions that allow the annealing temperature to exceed 130 K. So, (depending on the purpose of the experiment) the adsorbing gas needs a vapor pressure of a ~half torr to be evacuated within an hour. This requirement for a particular adsorbate limits its use to certain experiments.

As positions on the D_2O (H_2O) ice surface are occupied by the adsorbed molecules, the surface-defect vibrational modes (d-D, d-O, and S-4) shift to lower frequencies. Several examples of the adsorbate-shifted d-D IR bands are displayed in

Figure 32, and the IR frequencies of various adsorbate-induced d-D and d-O shifts are listed in Table 7. Also, IR intensity enhancements are observed by comparing the area under the adsorbate-shifted out-of-phase d-D band (see Fig. 32b-e) to the area under the unshifted out-of-phase d-D band (see Fig. 32a). The intensity enhancements are quantified in this thesis by band fitting the out-of-phase d-D bands.

Ab initio calculations of dimer complexes are suggested as a good estimation of surface-defect site that an adsorbate molecule occupies first. The exact behavior of adsorbed molecules on the ice surface is only speculation at this time. However, these calculations accurately predict the surface-defect sites that are preferentially occupied at low surface coverage (except for C_2H_2[47]). The potential energies of the experimental interactions between the adsorbed molecules and the d-D and d-O sites are predicted by the calculations of the dimer complexes, and serve as a guide to determine the amount of preference that one set of surface sites have relative to another. However, the magnitudes of the predicted binding energies may not agree with the experimental binding energies due to cooperative effects that are caused by increased H-bonding of the surface-defect sites.[38]

The adsorbate-shifted difference spectra of H_2 adsorbed on the ice surface give validation to the calculated site preference. Hydrogen is predicted (by the *ab initio* calculations of the dimer complexes) to prefer the d-O sites over the d-H(D) sites. Therefore, the majority of adsorbed H_2 molecules at low surface coverages are expected to occupy the d-O sites, and the d-D sites should be occupied as the vapor pressure of the adsorbing gas increases. So, intensity of the d-D adsorbate-shifted band increases at higher pressures, once the d-O sites are occupied. An adsorbate-shifted difference spectrum for which most of the d-O sites are occupied is shown in Figure 33a. An adsorbate-shifted difference spectrum with additional H_2 added to cover the remaining d-D sites is displayed in Figure 33b. The d-O and S-4 regions in Figure 33b changed little upon increasing the H_2 surface coverage (this indicates that these surface-defect sites are

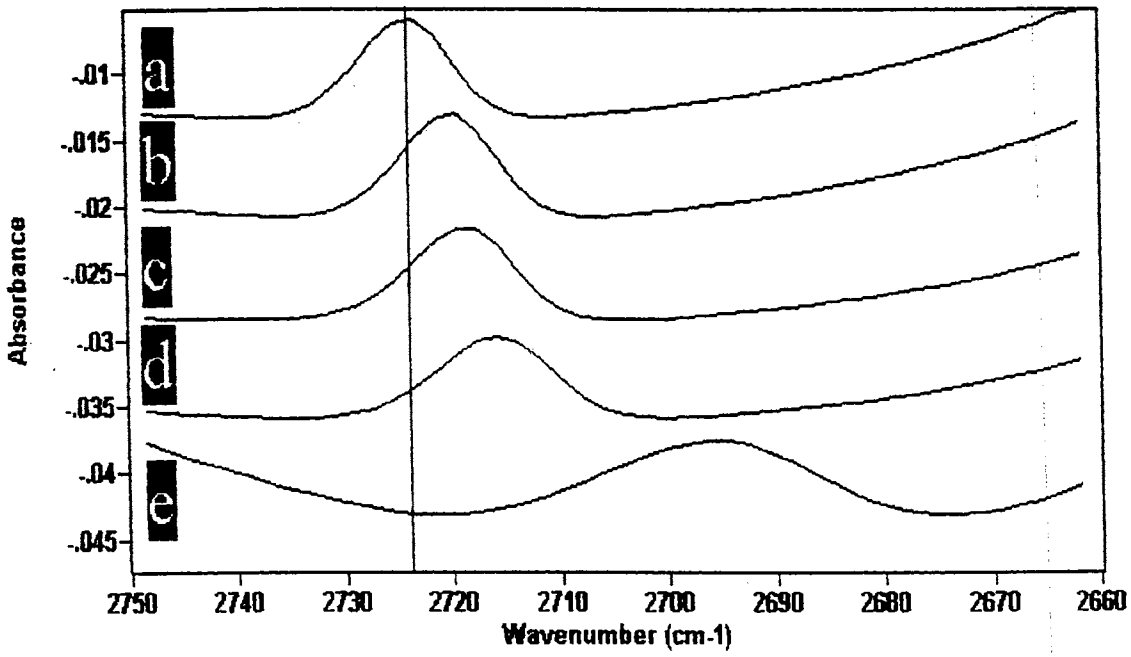

Figure 32. The adsorbate-shifted d-D band for bare (a), CF_4 (b), H_2 (c), N_2 (d), and CO (e) covered WDN

Table 7.

Summary of some adsorbate-shifted D_2O surface-defect vibrational frequencies

Adsorbate	d-D position	d-O position
Bare	2725	2645
H_2	2719	2631
CF_4	2719	2617
N_2	2712	2625
CO	2696	2619
C_2H_4	2671	2595

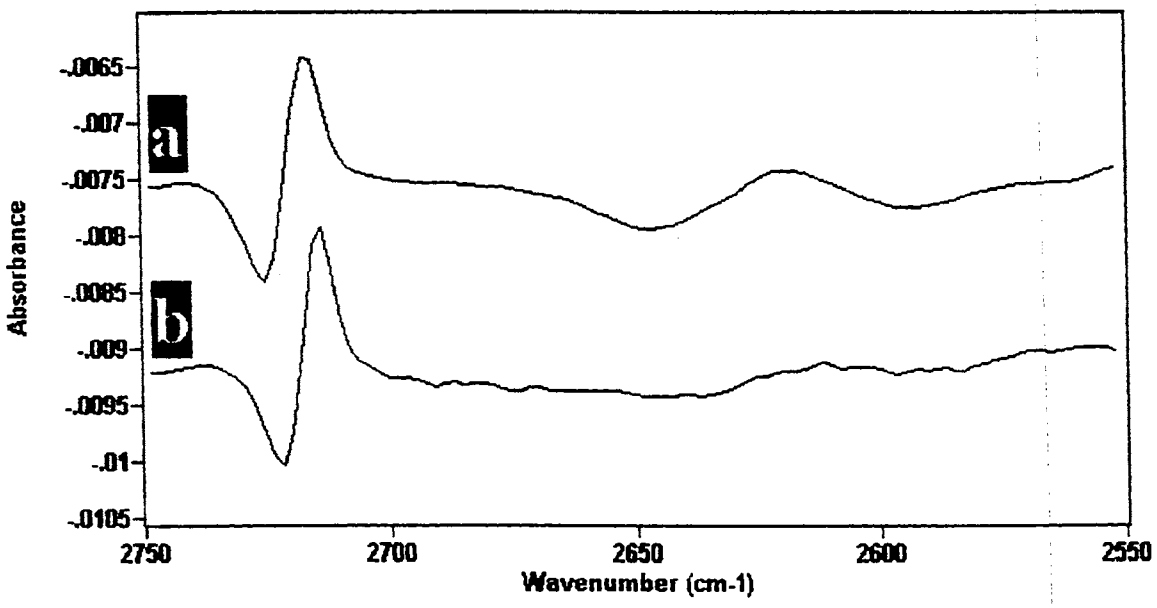

Figure 33. The adsorbate-difference spectrum for almost saturated d-O sites (a), and the difference spectrum that is obtained after adding H_2 past the d-O saturation point (b); Taken from reference 72

already saturated with adsorbate molecules), but the adsorbate-shifted d-D band increases significantly. This agrees with the dimer prediction that the d-O sites are occupied at lower pressures, and the d-H(D) (and d-O) sites are occupied at higher pressures.

The areas of the out-of-phase d-D and d-O IR bands at the unshifted band positions are determined by band fitting the adsorbate-shifted spectra for partially covered surfaces. The band-fitted areas may not be accurate , but the fits are consistent and do show trends (see section II.4.1). As seen in Figure 34, the areas of the d-D and d-O bands are determined by band fitting the adsorbate-shifted difference spectrum with unrestricted Gaussian functions. The ratios of the d-O and the d-D band areas at the unshifted band positions of the bare ice surface (A[d-O]/A[d-D]) are used to show site preference. The unshifted band positions are used to determine the ratio of the areas because of the reproducibility and simplicity of the fits. If the d-D sites are preferred (i. e., are lower in potential energy), the ratio of the areas is "small" at a low surface coverage because the d-D band area dominates the ratio. The ratio of the areas increases with the increase in surface coverage because more d-O sites are occupied. However, the opposite is expected for adsorbates that prefer the d-O sites.

Carbon monoxide is an adsorbate for which the *ab initio* calculations of the dimer complexes predict d-D(H) preference. The d-D(H) sites are predicted to be more stable than the d-O sites by 1.09 Kcal/mol.[55] Band fitting is used to evaluate the d-D and d-O band areas of the adsorbate-shifted difference spectra. The band fits of the spectra are displayed in Figure 34, and the ratios of the areas with their corresponding surface coverages of d-D sites are listed in Table 8. The ratios increase with increasing surface coverage , which agrees with the theoretically predicted d-H(D) site preference for CO.

Nitrogen adsorption onto the ice surface is predicted to prefer the d-D sites over the d-O sites by 0.56 Kcal/mol.[55] The areas of the d-D and d-O bands at the unshifted band positions are obtained by band fitting the adsorbate-shifted spectra. The fitted spectra are displayed in Figure 35, and the ratios of the band areas are listed in Table 8.

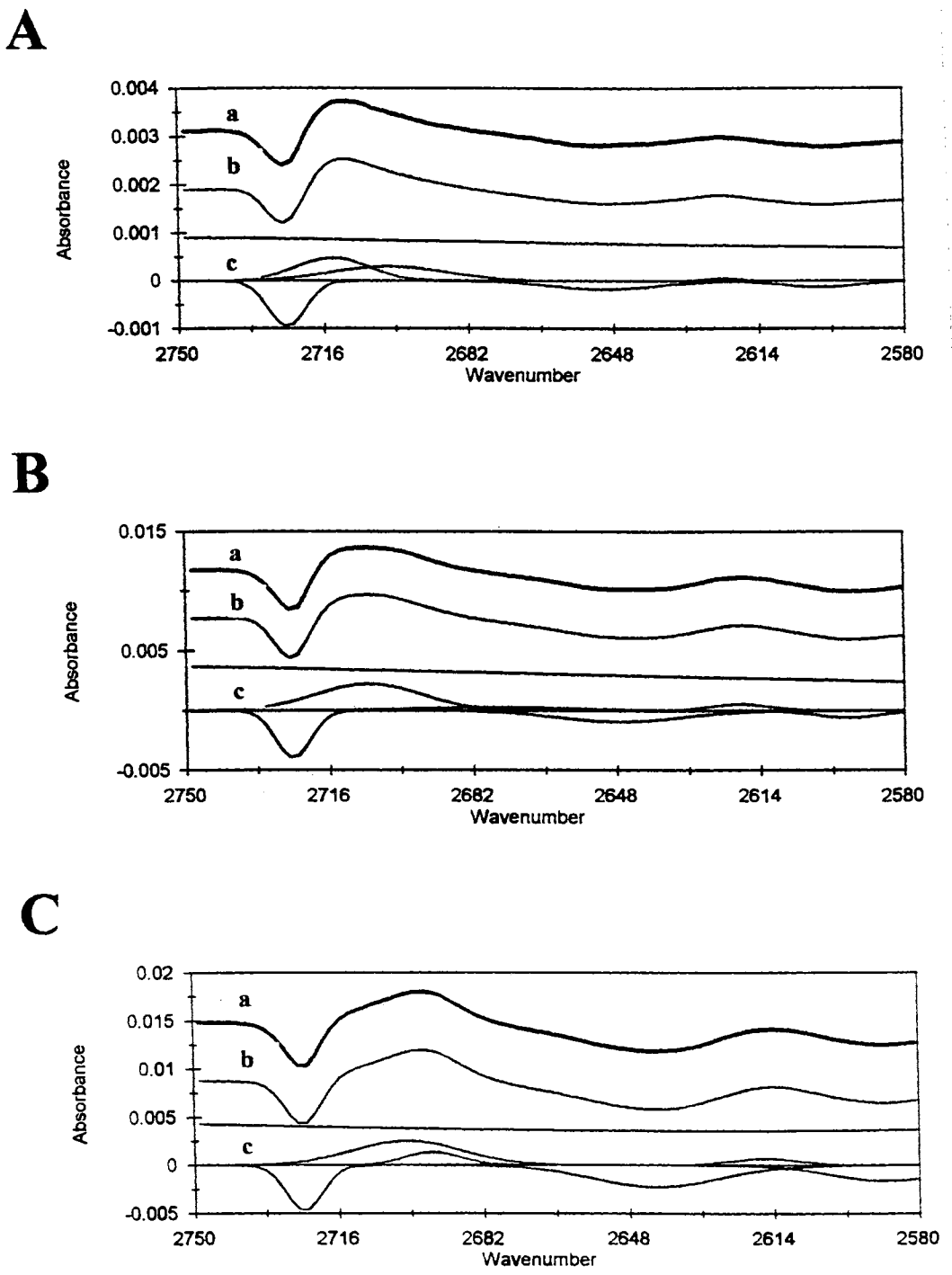

Figure 34. The band-fitted CO adsorbate-shifted difference spectra used to determine site preference for 4% (A), 63% (B), and 98% (C) d-D coverage the original spectrum a), fitted spectrum b), and fitting components c)

Table 8.

Summary of the band-fitted adsorbate difference spectra for CO, N_2, and H_2

* the area of the d-D was taken from the adsorbate-shifted position

CO

% coverage d-D	area d-O	area d-D	area ratio of (d-O/d-D)
4	0.005	0.010	0.500
63	0.033	0.041	0.805
98	0.083	0.050	1.66

N_2

% coverage d-D	area d-O	area d-D	area ratio of (d-O/d-D)
31	0.014	0.026	0.538
57	0.035	0.059	0.593
81	0.075	0.116	0.646

H_2

% coverage d-D	area d-O	area d-D*	area ratio of (d-O/d-D)
32	0.014	0.014	1.00
47	0.027	0.027	1.00
65	0.038	0.045	0.844

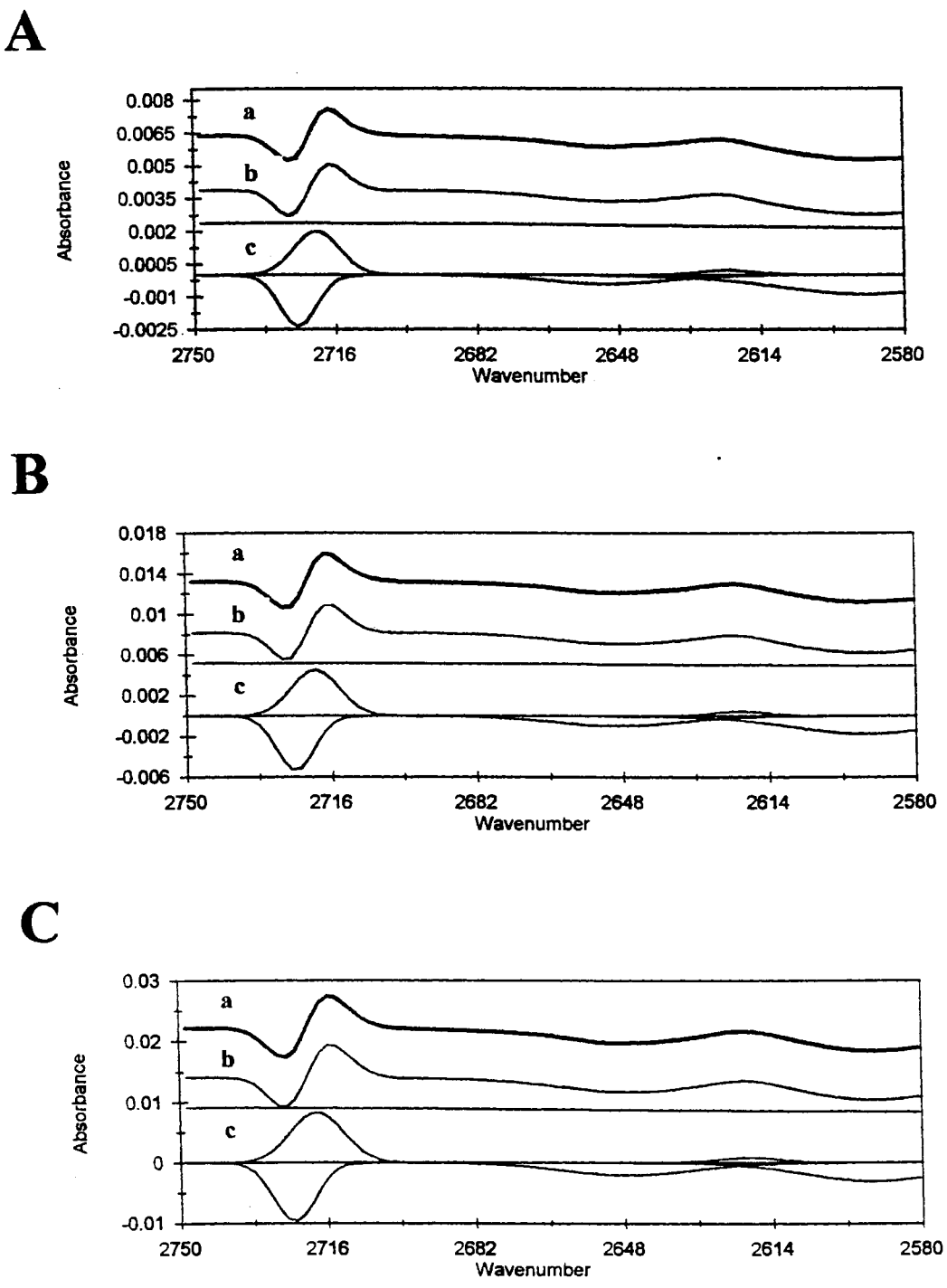

Figure 35. N_2 band-fitted adsorbate-shifted difference spectra used to determine site preference for 31% (A), 57% (B), and 81% (C) d-D coverages the original spectrum a), fitted spectrum b), and fitting components c)

The values of the ratios for N_2 increase with the increase in the surface-site coverage of d-D sites, but the rate of increase in the ratios is less than for CO adsorption. So, the d-D sites are preferred by the adsorbing N_2 molecules, but the preference of N_2 for the d-D sites is not as great as CO preference for the d-D sites.

The experimental ratios of the band areas for H_2 adsorption are obtained, and agree with the predicted behavior for an adsorbate that prefers the d-O sites. Hydrogen is calculated to prefer the d-O sites by 0.11 Kcal/mol over the d-D sites.[55] Thus, the ratios of the band-fitted areas decreased with increasing surface coverage of H_2. The band-fitted adsorbate-shifted difference spectra are shown in Figure 36, and the ratios are listed in Table 8. The adsorbate-shifted d-D band position is used to determine the d-D area because of the errors fitting the unshifted band position of the bare ice surface, and the unshifted band position of the d-O is used to evaluate the d-O area. Site preference predictions from the calculations of the dimer complexes agree with the trends observed in the experimental ratios of the band areas.

IV.4. Isotherms

Isotherms are used to calculate values such as the heat of adsorption (ΔH_{ads}) for a particular adsorbate on the ice surface. This is done by using the pressure dependent equilibrium that exists between adsorbate gas-phase molecules and the adsorbed molecules on the ice surface. A detailed derivation of an isotherm equation, which is used to fit the H_2 isothermal data, is presented in appendix A.3.

The selection of an isotherm equation to fit the isothermal data that include fractional d-D surface coverages and their corresponding pressures indicates the nature of adsorbed molecule-ice surface interactions. If the adsorbate-site interaction is localized, the isothermal data are fit with the Langmuir isotherm equation. The Langmuir isotherm equation is

A

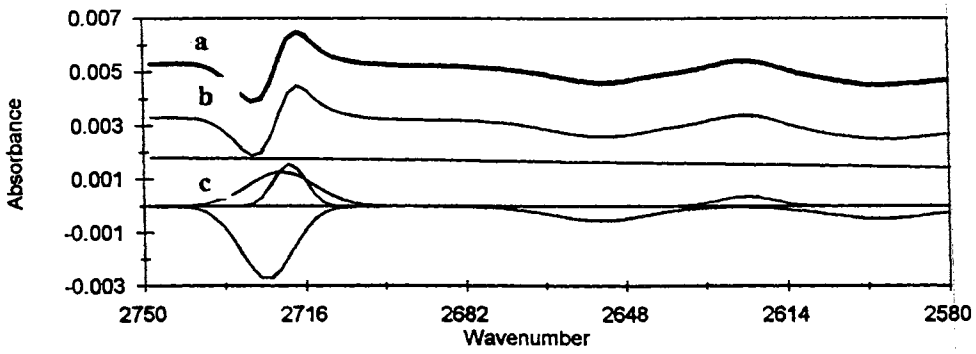

B

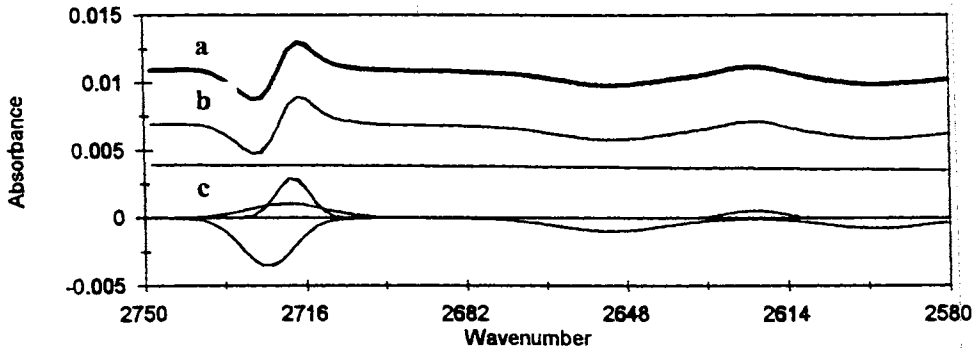

C

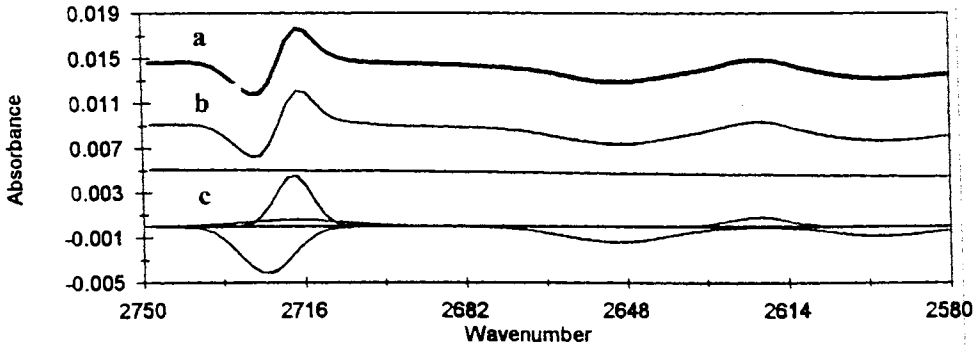

Figure 36. H_2 band-fitted adsorbate-shifted difference spectra used to determine site preference at 32% (A), 47% (B), and 65% (C) d-D coverage

the original spectrum a), fitted spectrum b), and fitting components c)

(1) $\theta = Xp/(1+Xp)$,

where θ and p are the fractional coverage and pressure, respectively, and X represents a ratio of partition functions of the adsorbed and the 'free' gas-phase molecules. The adsorbed molecules have significant interactions only with the surface-sites, and have trivial (not accounted for in the isotherm equation) interactions with other adsorbed molecules.[56,60,61] The Langmuir isotherm equation is the simplest isotherm equation that can be used to fit isothermal data. However, other isotherm equations are available to fit the isothermal data, and can account for other interactions such as the interaction between adsorbed molecules.[60-63]

An intriguing property of the crystalline ice surface is observing the adsorbate molecules interacting with specific groups of surface sites (d-D, d-O, and S-4). This is possible because the vibrational spectrum of the surface-defect modes allows site-specific adsorption to be followed. The fractional coverage for a specific group of surface sites is determined by following the intensity of a particular adsorbate-shifted band such as the out-of-phase d-D band.

In this thesis, the out-of-phase d-D band is chosen to determine the fractional surface coverage because of its distinct and easily observed band position at 2725 cm^{-1} in the unadjusted WDN IR spectrum. The other surface-defect vibrational bands are not sufficiently resolvable (i.e., can be separated into individual bands) to follow their fractional coverages. Therefore, the ΔH_{ads}, which is calculated by using the isothermal data, is site specific for the adsorbate-d-D interaction.

IV.4.1 The CO Isotherm

Review of Spectral Information

Spectra that demonstrate the intensity transfer from the d-D IR band position for a bare surface to the adsorbate-shifted d-D band position as a function of d-D site saturation are displayed in Figure 37A for CO. The band-fitted IR bands, which are necessary to determine the fractional d-D site coverage from Figure 37A, are shown in Figure 37B. The "goodness" of the fitted spectra that are used to determine fractional coverage is determined by the conservation of signal, and a statistical test[34] is used to either accept or reject the fitted results (the band-fitting procedure is outlined in section II.4.4). The fractional coverage of d-D sites with adsorbed CO molecules is obtained for different pressures and temperatures. Drifts in the CO-shifted d-D band position from a maximum shift of ~30 cm^{-1} to adsorbate-induced shifts of less than ~30 cm^{-1} are observed (see Fig. 37A) as the coverage of the d-D sites decreases. However, the IR intensity enhancement of the CO-shifted d-D band remains unchanged with the drifts in shifted frequencies. The experimental results for the CO isotherms are summarized in Table 9.

Ab initio calculations of the dimer complexes predict that CO molecules prefer the d-D sites over the d-O sites. From these calculations, a binding energy for the proton-donor complex is calculated to be 1.76 Kcal/mol, and a binding energy for the Lewis base complex is calculated to be 0.667 Kcal/mol.[55] Therefore, CO is theoretically expected to prefer the d-D sites, and is experimentally observed to prefer the d-D sites (see section IV.3).

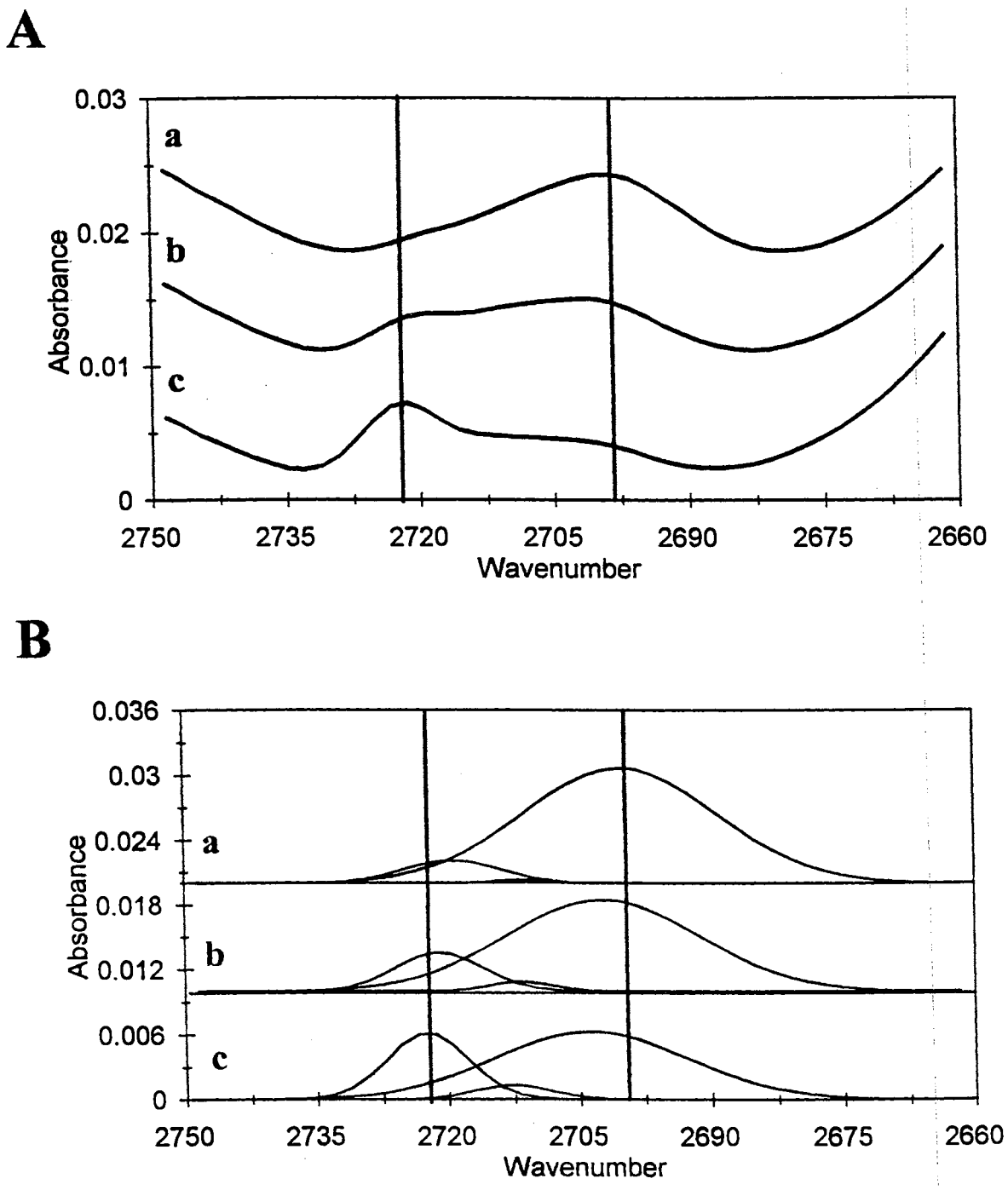

Figure 37. The CO adsorbate-shifted d-D band as a function of surface coverage (A), and the corresponding fitted bands (B) at 100% (a), 63% (b), and 45% (c) d-D surface coverage

Table 9.

Summary of CO isothermal data for an ice surface annealed at 120 K

Isotherm taken at 85.1 K Pressure in torr	Freq d-D Bare	Freq d-D CO	Area d-D Bare	Area d-D CO+ghst	Fraction Surface Coverage	Conservation of Signal
0.0	2724.3		0.0400	0.0079	0.09	0.0439
1.5	2723.7	2710.5	0.0190	0.0360	0.43	0.0366
3.3	2723.2	2700.2	0.0159	0.0483	0.57	0.0396
5.2	2722.9	2702.1	0.0107	0.0536	0.63	0.0370
7.2	2722.6	2700.7	0.0085	0.0612	0.72	0.0385
10.2	2721.5	2699	0.0063	0.0672	0.80	0.0392
20.6	2720	2698.7	0.0038	0.0777	0.92	0.0418

Isotherm taken at 90.1 K Pressure in torr	Freq d-D Bare	Freq d-D CO	Area d-D Bare	Area d-D CO+ghst	Fraction Surface Coverage	Conservation of Signal
0.0	2724.4		0.0450	0.0000	0.00	0.0450
1.2	2724.1	2705.3	0.0409	0.0035	0.04	0.0426
5.3	2723.4	2703.4	0.0257	0.0349	0.42	0.0429
10.1	2722.5	2703.9	0.0181	0.0470	0.56	0.0412
14.0	2721.9	2703.3	0.0153	0.0529	0.63	0.0412
19.8	2721.1	2702.4	0.0114	0.0609	0.72	0.0412
24.6	2720.5	2701.8	0.0104	0.0645	0.77	0.0420
30.5	2720	2701.1	0.0089	0.0690	0.82	0.0427
40.3	2719.5	2700.2	0.0073	0.0744	0.89	0.0438
61.4	2720	2698	0.0044	0.0738	0.88	0.0406
89.9	2720	2696.6	0.0025	0.0791	0.94	0.0413
115.3	2720	2696	0.0013	0.0820	0.98	0.0415
151.7		2694.9	0.0000	0.0840	1.00	0.0412

Isotherm taken at 95.1 K

Pressure in torr	Freq d-D Bare	Freq d-D CO	Area d-D Bare	Area d-D CO+ghst	Fraction Surface Coverage	Conservation of Signal
0.0	2724.4		0.0393	0.0108	0.13	0.0446
4.3	2723.9	2700.1	0.0336	0.0276	0.33	0.0472
11.1	2723.6	2700.6	0.0220	0.0442	0.52	0.0436
16.8	2723.2	2702.5	0.0178	0.0508	0.60	0.0427
21.6	2722.9	2702.8	0.0148	0.0542	0.64	0.0414
27.1	2722.6	2702.7	0.0122	0.0593	0.70	0.0413
34.6	2722.3	2702.7	0.0092	0.0637	0.76	0.0404
40.2	2722.2	2702.5	0.0075	0.0668	0.79	0.0402
50.2	2720.9	2702.2	0.0086	0.0679	0.81	0.0419
59.9	2720	2701.6	0.0077	0.0719	0.85	0.0430
87.1	2720	2700.2	0.0053	0.0757	0.90	0.0424
143.4		2697.4	0.0000	0.0797	0.95	0.0391
195.7		2696.5	0.0000	0.0798	0.95	0.0391
300.3		2695.3	0.0000	0.0842	1.00	0.0413

The CO Isotherm

Carbon monoxide isotherms that were determined by using the IR spectrum of CO to determine the surface coverage were obtained for CO adsorption on a NaCl surface.[57] The determination of the fractional coverage of CO is achieved by following the IR intensity of the C-O vibrational stretching mode. The resulting isothermal data are fit with the Langmuir isotherm equation which requires that the CO interaction with the NaCl surface to be "localized". The Langmuir isotherm equation does not involve any adsorbate interactions other than the interaction of adsorbed molecules with a certain set of surface sites. Therefore, interactions of the CO molecules with themselves (adsorbate-adsorbate interaction) and/or interactions of CO molecules with neighboring surface sites are considered trivial because of the fit of the Langmuir isotherm equation to the isothermal data.[56-62] The resulting ΔH_{ads} value for CO adsorption on a NaCl surface is -3.35 Kcal/mol.[57] The binding energy of CO adsorption on an H_2O surface, which was obtained in a non-equilibrium study that differs from Ewing et al.[56,57,62] and our equilibrium studies, is calculated to be 3.05 Kcal/mol.[59]

The adsorption of CO on the crystalline ice surface is similar to the adsorption of CO on the NaCl surface. Isothermal data that were obtained at temperatures of 85.1, 90.1 and 95.1 K for a 120 K annealed WDN surface are shown in Figures 38A a, b, and c, respectively. The solid lines that are shown in Figures 38A a, b, and c, are fits of the Langmuir isotherm equation to the isothermal data . Fits of the isothermal data with the Langmuir equation allow the determination of ΔH_{ads} by using the van't Hoff equation, and the fits justify a localized description of CO adsorbed on d-D sites. The van't Hoff equation is

(2) $\Delta H_{ads}/R=d(\ln(p))/d(1/T)\,|_{0.5}$,

where T, P, and R are the temperature, pressure, and the gas constant, respectively. The van't Hoff equation is evaluated at 50% d-D coverage. From the slope of the line in

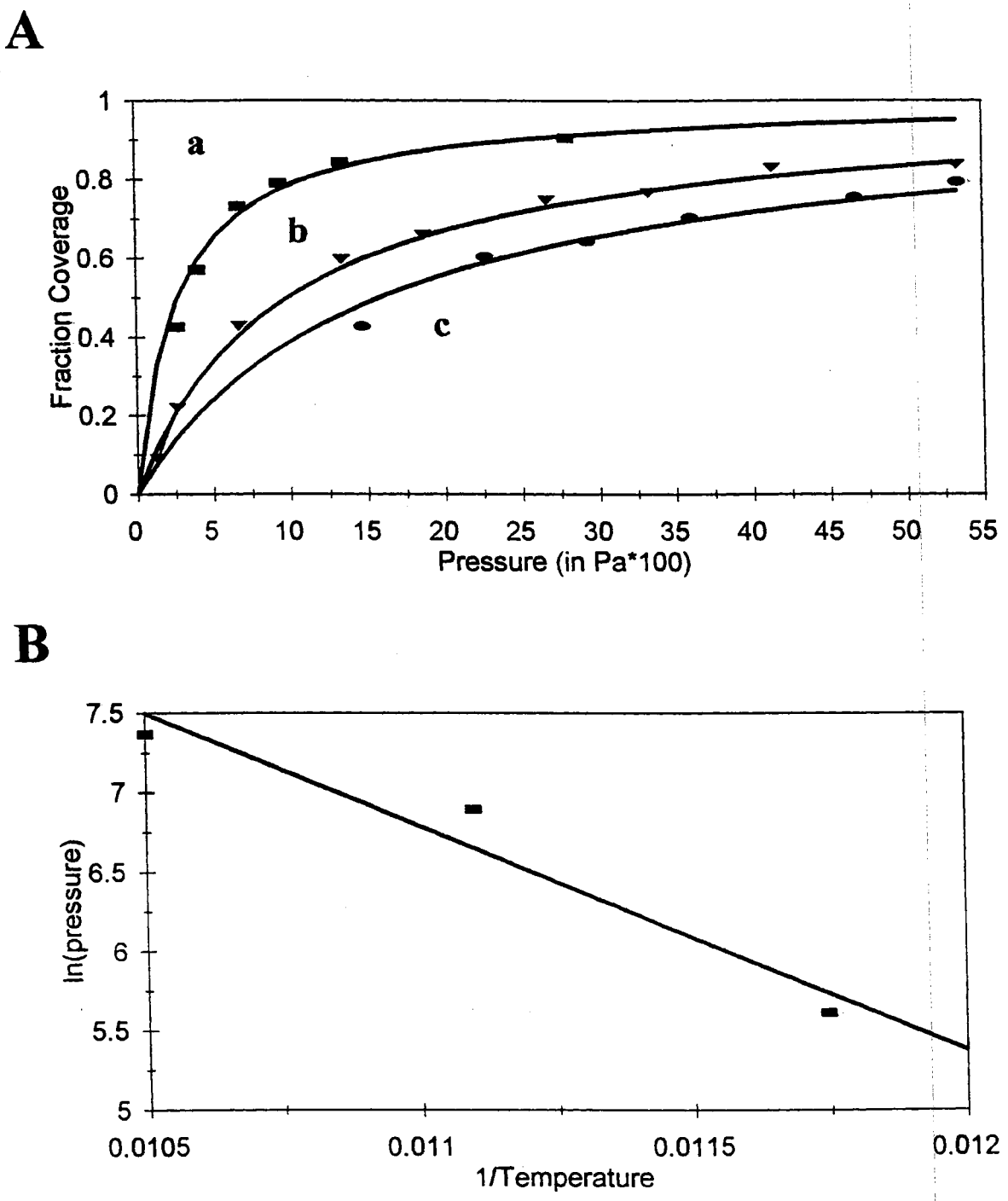

Figure 38. Fits of the Langmuir equation to the isothermal data (A) at 85.1 K (a), 90.1 K (b), and 95.1 K (c), and the corresponding fit of the van't Hoff equation to determine ΔH_{ads} (B)

Figure 38B (van't Hoff equation), a ΔH_{ads} value of -2.80 Kcal/mol is calculated for CO adsorption onto the d-D surface-defect sites.

The following model is proposed for CO adsorption on the crystalline ice surface with respect to the d-D sites. The CO molecules prefer to occupy the d-D sites over the d-O sites. Therefore, most of the CO molecules occupy d-D sites at low surface coverage. The CO molecules adsorbed on the d-O sites do not appreciably interact with empty d-D sites, because the amount of d-O sites occupied at lower adsorbate coverages are less than the number of occupied d-D sites, and the isothermal data can only be fit with the Langmuir isotherm equation if the adsorbate interactions are localized. The previous statement requires some conjecture, but all interactions other than the CO-d-D interaction are trivial, and the CO-d-D interaction is considered "localized".

The term "localized" must be used carefully. If the interaction is exclusively localized, the spectra would exhibit two out-of-phase d-D IR bands (for intermediate fractional coverages) at the unshifted band position and at the full CO adsorbate-shifted position. No intermediate positions of the CO-shifted d-D band would exist. This on-off adsorption model is clearly not applicable for the observed CO adsorption (see Fig. 37). However, CO interactions, other than the CO-d-D interaction, are small enough to be ignored.

IV.4.2. The N_2 Isotherm

Review of Spectral Information

The behavior of N_2 adsorption on crystalline ice surface parallels the behavior of CO adsorption. The positions of the N_2-shifted d-D IR bands as a function of the fractional coverages of the d-D sites are given in Figure 39A. The "goodness" of the band fits to obtain the fractional coverage are determined in the same manner as for the

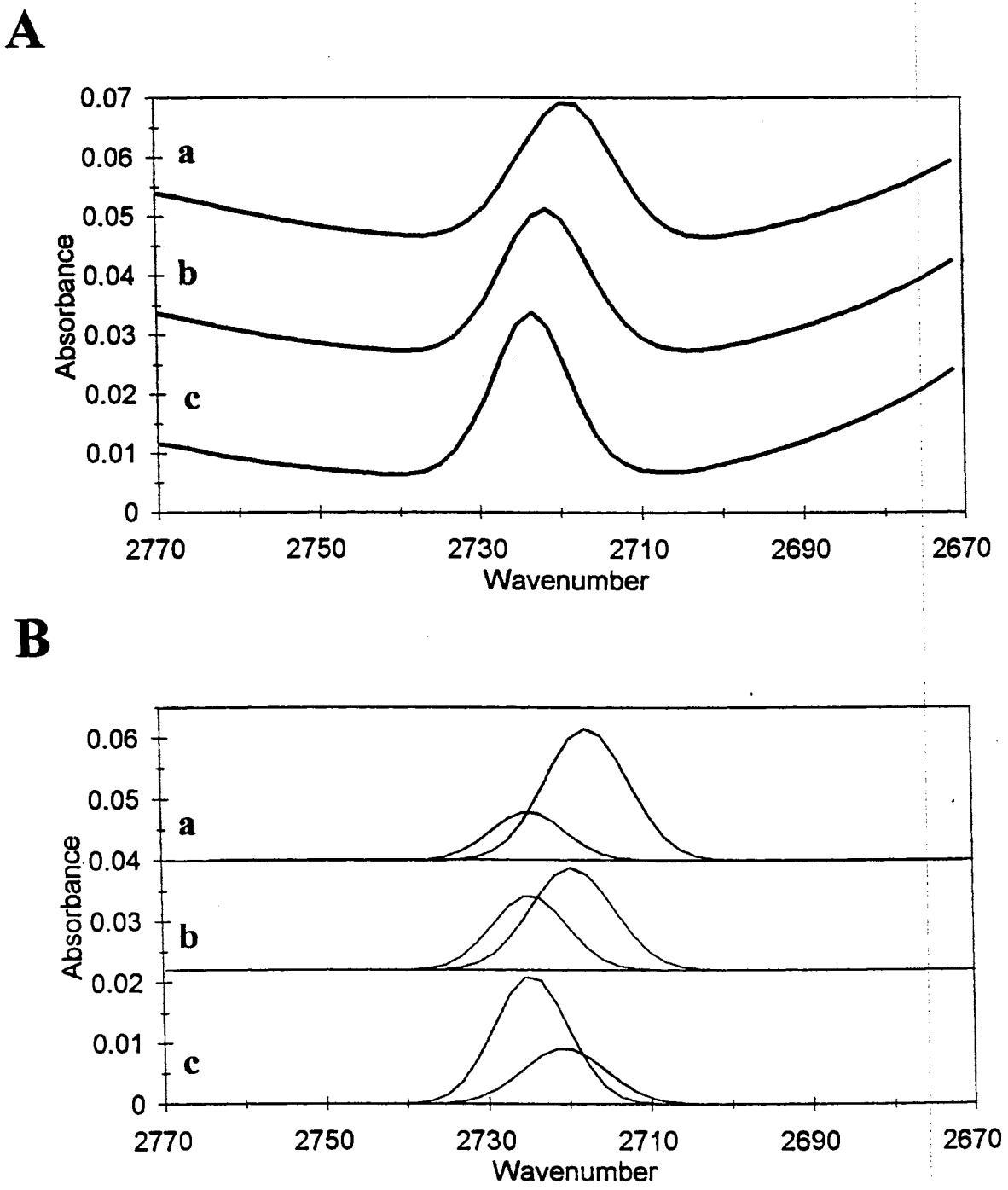

Figure 39. The N_2 adsorbate-shifted d-D band at various adsorbate surface coverages and the corresponding band fits (B) at 73% (a), 57% (b), and 30% (c) d-D surface coverages

CO data, and the band-fitting procedure is discussed in the experimental chapter (see section II.4.4). Drifts in the out-of-phase adsorbate-shifted d-D band position to adsorbate-shifted band positions less than the maximum shift of ~11 cm^{-1} are observed. The IR intensity enhancement of the N_2-shifted d-D band is independent of the shifted-band position with respect to the adsorbate coverage of the ice surface. The isothermal data collected for N_2 adsorption on the WDN surface are summarized in Table 10.

Nitrogen molecules are predicted by *ab initio* calculations of the dimer complexes and experimentally shown to prefer the d-D sites on the ice surface.[55] Binding energies of 1.15 and 0.577 Kcal/mol are calculated for the proton-donor and the Lewis base complexes, respectively.[55] Calculations of the dimer complexes also show that the N_2 preference for d-D sites is less than CO. This result is verified experimentally by evaluating A[d-O]/A[d-D] as a function of fractional d-D coverage (see section IV.3).

The N_2 Isotherm

To our knowledge, nitrogen isotherms studied by optical techniques have not been reported. Isotherm equations[56-63] that accounts for non-localized adsorbate interactions with the ice surface were used to fit the N_2 data that accounted for the adsorbate molecules interacting with the surface in a non-localized manner, but the best fit of an isotherm equation was obtained by using the Langmuir isotherm equation. This is expected because of the existing computational and experimental agreements between N_2 and CO adsorption. Describing the interaction that exists between the adsorbed N_2 molecules and the d-D sites reduces to the simple "localized" model as offered in the CO case.

The N_2 isothermal data for a 100 K annealed crystalline ice surface at 70, 75, 80, and 85 K are displayed in Figure 40A. The solid lines represent the fits of the Langmuir isotherm equation to the isothermal data. The van't Hoff equation, which is used to

Table 10.

Summary of N_2 isothermal data for an ice surface annealed at 100 K

Isotherm taken at 69.9 K						
Pressure in torr	Bare d-D Position	N_2-shifted d-D Position	Area d-D Bare	Area d-D Coverage	Fraction Surface Coverage	Conservation of Signal
0.0	2724.7		0.0899	0.0000	0.00	0.0899
0.5	2724.7	2720.7	0.0381	0.0507	0.51	0.0844
0.9	2724.7	2719.2	0.0319	0.0583	0.59	0.0850
1.3	2724.7	2718.5	0.0279	0.0629	0.64	0.0852
2.0	2724.7	2717.5	0.0230	0.0694	0.70	0.0863
4.3	2724.7	2716.2	0.0164	0.0798	0.81	0.0891
6.1	2724.7	2715.5	0.0136	0.0860	0.87	0.0921
8.2	2724.7	2715	0.0111	0.0918	0.93	0.0948
10.4	2724.7	2714.6	0.0097	0.0955	0.97	0.0968

Isotherm taken at 74.8 K						
Pressure in torr	Bare d-D Position	N_2-shifted d-D Position	Area d-D	Area d-D Coverage	Fraction Surface Coverage	Conservation of Signal
0.0	2724.7		0.0896	0.0000	0.00	0.0896
0.7	2724.7	2720.8	0.0603	0.0294	0.31	0.0882
1.2	2724.7	2720.8	0.0428	0.0457	0.48	0.0861
2.2	2724.7	2719.5	0.0352	0.0539	0.57	0.0865
4.2	2724.7	2718.2	0.0270	0.0636	0.67	0.0874
6.1	2724.7	2717.5	0.0228	0.0691	0.73	0.0885
10.2	2724.7	2716.5	0.0179	0.0772	0.82	0.0912
19.9	2724.7	2715.3	0.0122	0.0883	0.94	0.0960

Isotherm taken at 79.9 K

Pressure in torr	Bare d-D Position	N_2-shifted d-D Position	Area d-D	Area d-D Coverage	Fraction Surface Coverage	Conservation of Signal
0.0	2724.6		0.0808	0.0000	0.00	0.0808
1.2	2724.6	2719.9	0.0659	0.0165	0.19	0.0813
2.8	2724.6	2719.9	0.0494	0.0332	0.38	0.0803
5.5	2724.6	2719.9	0.0288	0.0519	0.60	0.0772
9.7	2724.6	2718.6	0.0228	0.0593	0.69	0.0781
15.1	2724.6	2717.7	0.0186	0.0651	0.75	0.0794
19.8	2724.6	2717.2	0.0158	0.0690	0.80	0.0802
38.1	2724.6	2715.9	0.0109	0.0778	0.90	0.0835

Isotherm taken at 85.0 K

Pressure in torr	Bare d-D Position	N_2-shifted d-D Position	Area d-D	Area d-D Coverage	Fraction Surface Coverage	Conservation of Signal
0.0	2724.6		0.0810	0.0000	0.00	0.0810
8.8	2724.6	2719.4	0.0461	0.0384	0.44	0.0822
13.8	2724.6	2719.4	0.0319	0.0517	0.60	0.0804
19.8	2724.6	2719.4	0.0198	0.0623	0.72	0.0783
24.8	2724.6	2718.8	0.0181	0.0648	0.75	0.0789
31.6	2724.6	2718.3	0.0156	0.0678	0.79	0.0793
40.7	2724.6	2717.7	0.0135	0.0709	0.82	0.0800
53.0	2724.6	2717.1	0.0121	0.0743	0.86	0.0818
72.6	2724.6	2716.5	0.0100	0.0776	0.90	0.0829

A

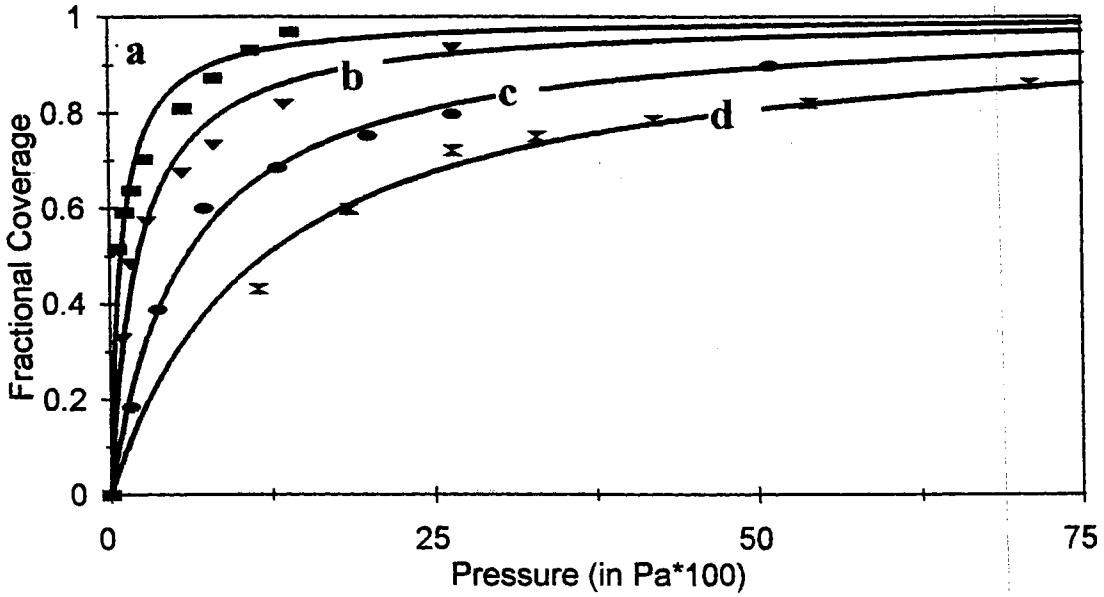

B

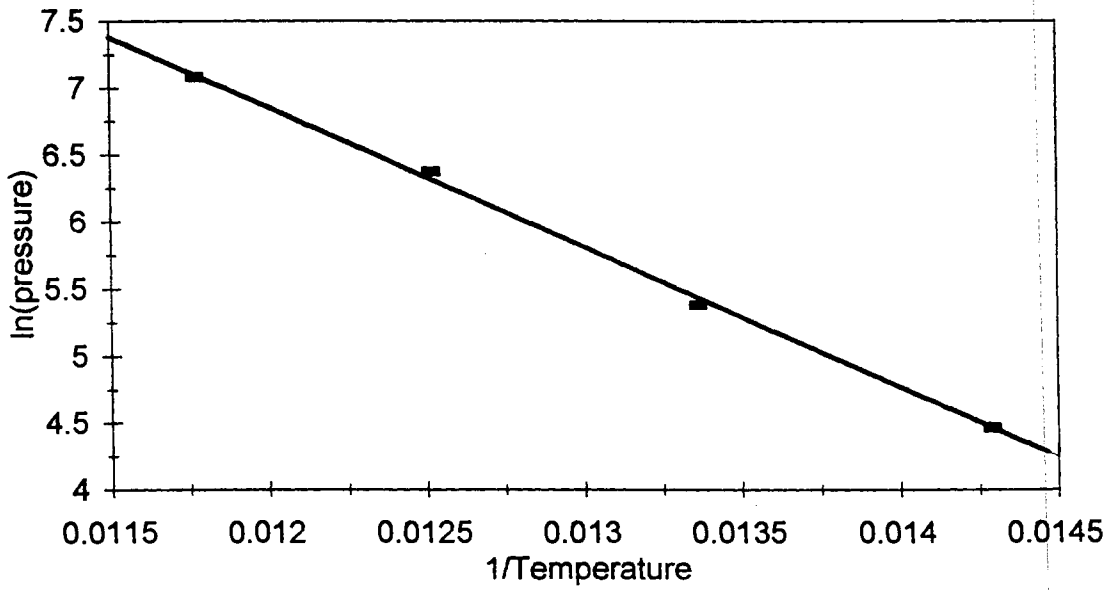

Figure 40. Fits of the Langmuir equation to the N_2 isothermal data (A) at 70 K (a), 75 K (b), 80 K (c), and 85 K (d), and the corresponding fit of the van't Hoff equation to determine ΔH_{ads} (B)

determine the ΔH_{ads} value, fits of the Langmuir results to a line shown in Figure 40B. The ΔH_{ads} value (-2.08 Kcal/mol) for N_2 adsorption was determined in the same manner as for CO adsorption (see section IV.4.1).

The proposed model of N_2 adsorbed on the ice surface is identical to CO adsorption. The interaction between N_2 molecules is trivial compared to the N_2-d-D interaction. The effects of N_2 adsorbed on surface sites that are neighbors to d-D sites at low pressure are trivial compared to the N_2-d-D interaction. However, this model of N_2-d-D interaction being completely "localized" is not accurate because of the same argument used for the CO-d-D interaction (see IV.4.1), but the "localized" model of adsorption agrees with the theoretical predictions for N_2 adsorbed on the ice surface.

IV.4.3. The H_2 Isotherm

Review of Spectral Information

The unshifted and H_2-shifted d-D IR bands at various adsorbate coverages of the crystalline ice d-D surface sites are displayed in Figure 41A. Band fitting the d-D region of the IR spectrum (to determine the H_2 fractional surface-coverage) is described in the experimental chapter (see section II.4.4), and is shown in Figure 41B. The position of the H_2-shifted d-D band is observed to drift between the maximum H_2-induced shift of ~6.5 cm^{-1} and the unshifted band position (see Fig. 41B). The IR intensity enhancement of the H_2-shifted d-D band is independent of the H_2-shifted d-D band position (see Fig. 41B; This is also observed for N_2 and CO adsorptions). The isothermal data for H_2 adsorbed on the WDN surface are listed in Table 11.

Unlike CO and N_2, the *ab initio* calculations of the dimer complexes predict that H_2 molecules prefer the d-O sites over the d-D sites.[55] Binding energies of 0.44 and 0.55 Kcal/mol are calculated for the proton-donor and the Lewis base complexes,

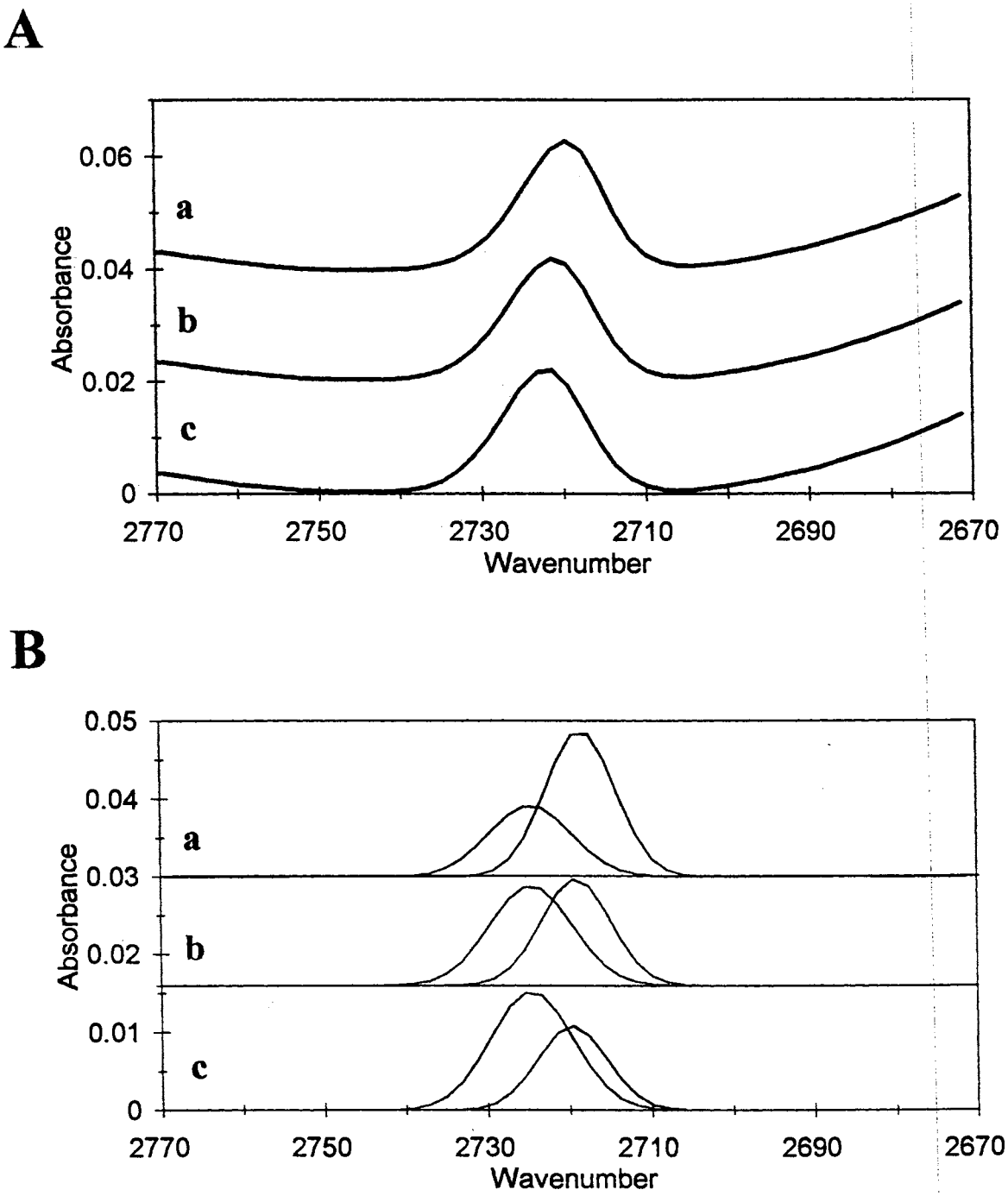

Figure 41. The H_2 adsorbate-shifted d-D band at various adsorbate surface coverages and the corresponding band fits (B) at 72% (a), 52% (b), and 41% (c) d-D surface coverages

Table 11.

Summary of H_2 isothermal data for an ice surface annealed at 75 K

Isotherm taken at 25.9 K Pressure in torr	Bare d-D Position	H_2-shifted d-D Position	Area d-D	Area d-D Coverage	Fraction Surface Coverage	Conservation of Signal
0.0	2724.6		0.0801	0.0000	0.00	0.0801
0.5	2724.6	2719.9	0.0425	0.0318	0.45	0.0786
1.0	2724.6	2719.6	0.0392	0.0353	0.50	0.0792
1.3	2724.6	2719.5	0.0371	0.0375	0.53	0.0796
1.7	2724.6	2719.3	0.0351	0.0397	0.56	0.0801
2.2	2724.6	2719.1	0.0333	0.0420	0.59	0.0808
2.7	2724.6	2719.0	0.0309	0.0447	0.63	0.0815
3.0	2724.6	2718.9	0.0299	0.0462	0.65	0.0823

Isotherm taken at 29.8 K Pressure in torr	Bare d-D Position	H_2-shifted d-D Position	Area d-D	Area d-D Coverage	Fraction Surface Coverage	Conservation of Signal
0.0	2724.6		0.0827	0.0000	0.00	0.0827
1.1	2724.6	2720.2	0.0547	0.0223	0.32	0.0812
2.1	2724.6	2719.9	0.0503	0.0262	0.38	0.0813
3.1	2724.6	2719.7	0.0477	0.0285	0.41	0.0816
4.1	2724.6	2719.6	0.0453	0.0306	0.44	0.0816
6.0	2724.6	2719.4	0.0426	0.0338	0.49	0.0827
8.0	2724.6	2719.2	0.0401	0.0363	0.52	0.0832
10.2	2724.6	2719.1	0.0373	0.0394	0.57	0.0841
15.9	2724.6	2718.9	0.0342	0.0428	0.61	0.0850
20.3	2724.6	2718.8	0.0320	0.0458	0.66	0.0863

Isotherm taken at 35.0 K

Pressure in torr	Bare d-D Position	H_2-shifted d-D Position	Area d-D	Area d-D Coverage	Fraction Surface Coverage	Conservation of Signal
0.0	2724.4		0.0839	0.0000	0.00	0.0839
10.1	2724.4	2719.1	0.0539	0.0243	0.35	0.0830
15.1	2724.4	2719.0	0.0504	0.0272	0.39	0.0829
20.2	2724.4	2718.9	0.0475	0.0297	0.42	0.0831
24.8	2724.4	2718.9	0.0456	0.0316	0.45	0.0835
30.1	2724.4	2718.8	0.0438	0.0339	0.48	0.0843
35.1	2724.4	2718.8	0.0420	0.0354	0.51	0.0843
40.7	2724.4	2718.7	0.0409	0.0366	0.52	0.0846
60.3	2724.4	2718.5	0.0370	0.0408	0.58	0.0859

respectively.[55] This site preference is experimentally observed by evaluating the adsorbate-shifted difference spectra with respect to H_2 coverage of the d-D sites (see Fig. 33, Section IV.3), and observed by following the A[d-O]/A[d-D] ratios in the same manner (see Table 8; Section IV.3). The change in surface site preference infers a change in the type of isotherm equation that is used to fit the H_2 isothermal data, and that is used to describe the interaction of the H_2 molecules with the ice surface.

The H_2 Isotherm

Hydrogen adsorption on a NaCl surface was followed by observing the H-H vibrational stretching-mode to determine the surface coverage.[56] For H_2 and CO, the isothermal data are fit with the Langmuir isotherm equation that requires a localized adsorbate-site interaction, and that requires all other adsorbate interactions to be trivial.[56] So, the H_2-H_2 interaction is considered to not contribute to the overall H_2-surface interaction. The ΔH_{ads} value that is calculated for H_2 adsorption on a NaCl surface is -0.81 Kcal/mol.[56], and a binding energy for H_2 adsorbed on H_2O ice surface is calculated to be 1.1 Kcal/mol by Sandford et al..[58] Isothermal data for H_2 adsorbed onto the WDN surface are not successfully fit with the Langmuir isotherm equation. Furthermore, isotherm equations that included a parameter for adsorbate-adsorbate interaction are also unsuccessful at fitting the H_2 isothermal data.[60-62] Therefore, a new isotherm equation that is used to fit the H_2 isothermal data is derived in this thesis (see appendix A.3).

The derived isotherm equation (using information provided in reference 61) is named the adsorbate-neighbor isotherm equation (ANIE), and incorporates a parameter that accounts for adsorbed H_2 molecules interacting with unoccupied d-D sites (d-D sites that are not occupied with adsorbed molecules). The adsorbate-neighbor isotherm equation is

(3) $p=(\theta/(1-\theta))\ X\ e^{(-(\theta-1)w/(kT))}$,

where θ, p, w, k, and T represent the fractional coverage, pressure, interaction energy (the important new term), Boltzman constant, and the temperature, respectively. The ratio of partition functions for the adsorbed and the gas-phase molecules is represented by X. The derivation of the adsorbate-neighbor isotherm equation is presented in appendix A.3.

The isothermal data for H_2 adsorbed on the WDN surface at 25.9, 29.8, and 35.0 K is given in Figure 42, and the solid lines represent the ANIE fits to the isothermal data. The Clausius-Clapeyron relationship is used to calculate a ΔH_{ads} value for H_2 adsorption, and a ΔH_{ads} value of -0.644 Kcal/mol is calculated (see Fig. 43). The Clausius-Clapeyron equation is expressed as

(4) $\Delta H_{ads}/RT^2=d(\ln(p))/dT$.

A procedure for solving the ΔH_{ads} value is given in appendix A.3 and this chapter.

The model for the behavior of the adsorbed H_2 molecules with respect to the d-D sites differs from the model of CO and N_2 adsorbed on the ice surface. The H_2 molecules do not prefer the d-D sites, therefore, H_2 on other surface-defect groups can interact with unoccupied d-D sites at low adsorbate coverages. The function of the S-4 sites is not known for H_2, N_2, or CO adsorptions, but the H_2 on the surface-defect sites that surround the d-D sites, which includes S-4 and d-O sites, significantly effect the d-D sites.

IV.4.4. Justification of Isothermal Results

The ΔH_{ads} results for CO and N_2 isotherms are -2.80 and -2.08 Kcal/mol, and are similar to the binding energies of 1.76 and 1.14 Kcal/mol that are reported for the calculated proton-donor complexes.[55] The ΔH_{ads} value for CO adsorbed on WDN surface d-D sites differs by 25% of the ΔH_{ads} value for CO adsorbed on a NaCl surface

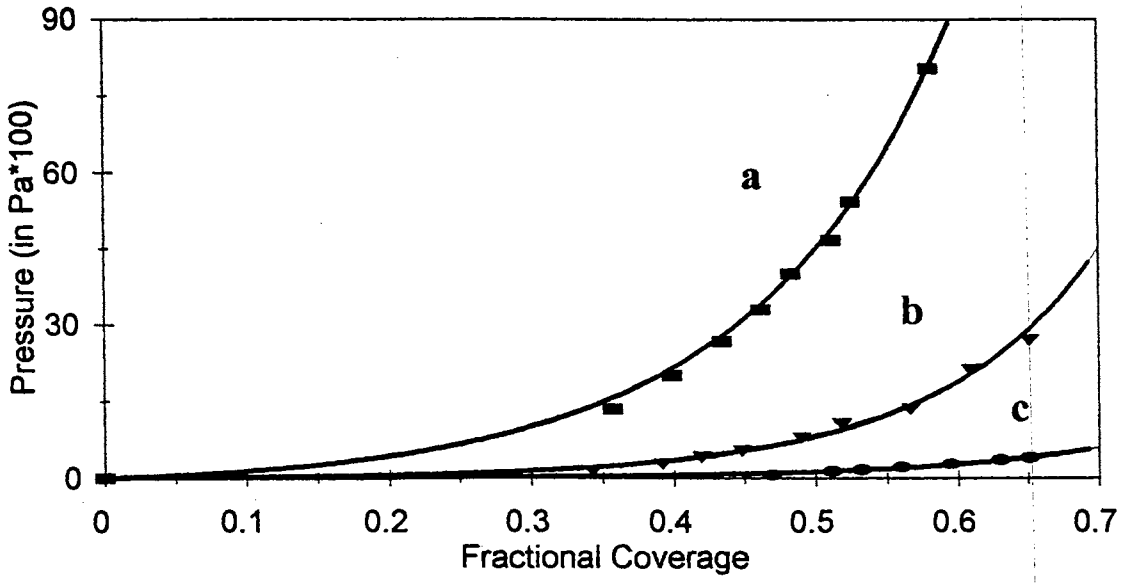

Figure 42. Curve fits of the ANIE equation to the H_2 isothermal data (A) at 25 K (a), 29.8 K (b), and 30.5 K (c)

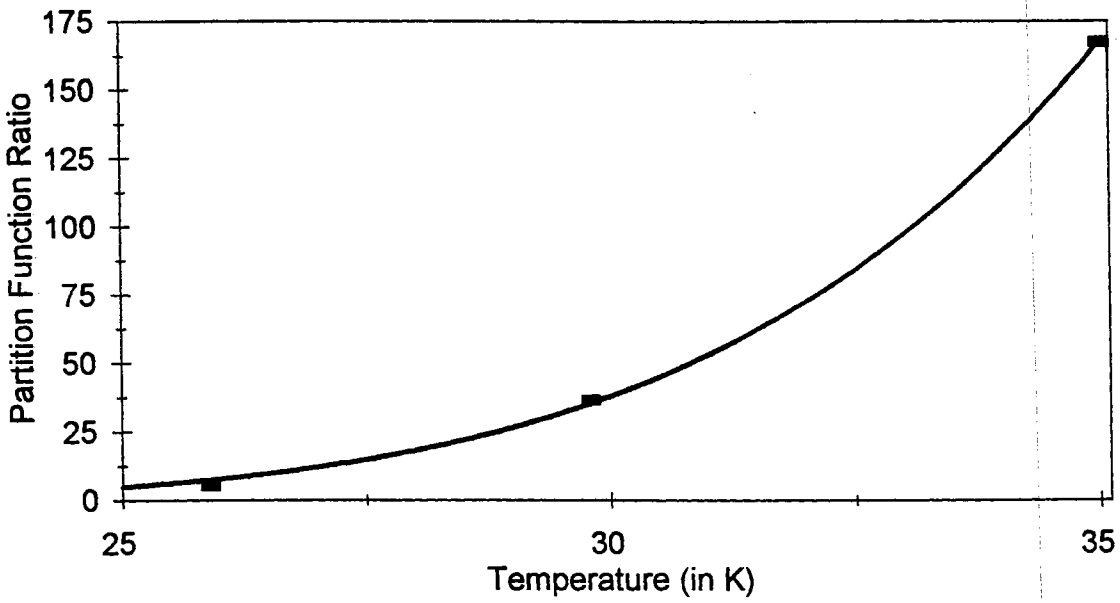

Figure 43. Fit of the H_2 ratios of the partition functions versus temperature to determine ΔH_{ads}

(-3.4 Kcal/mol).[57] Also, our ΔH_{ads} for CO differ by 25% from the experimental binding energy determined for CO adsorption on the crystalline ice surface (3.5 Kcal/mol).[59] We believe that the ΔH_{ads} result for CO is credible because our ΔH_{ads} value agrees with the published results of Ewing et al[57] and Sandford et al.[59], and the fits of the established Langmuir isotherm equation to the isothermal data.[60,61] Although we have found no isothermal data for N_2 to compare with our results, we believe that our ΔH_{ads} value for N_2 adsorption onto a crystalline ice surface is good because of the fits of the Langmuir isotherm equation to the N_2 isothermal data.

The Adsorbate-neighbor isotherm equation (ANIE) is also used to fit the isothermal data, and calculates values for the ratio of the partition functions (X) and the interaction energy (W) that are used to calculate ΔH_{ads}. The ANIE equation is

(4) $p=(\theta/(1-\theta))\ X\ e^{(-(\theta-1)*w/(k*T))}$,

where X is determined for isothermal data that were obtained at different temperatures, and plotted against the corresponding temperature (see Fig. 43). The resulting plot is fit with the equation

(5) $X = ((2\pi mkT/h^2)^{3/2}\ kT)\ (1-\exp(-A/T))\ (1-e^{(-B/T)})2\ e^{(-u0)}$,

which is displayed as the solid line in Figure 43. The terms m, k, T, h, and u_0 represent the molecular mass, Boltzman constant, temperature, Plank's constant, and the zero point binding energy, respectively. A and B are

(6) $A = h\nu_Z/k$, and $B = h\nu_X/k$,

where ν_Z and ν_X values represent the "rattling" frequencies (see appendix A.3) for an adsorbed molecule trapped on a d-D site. The ΔH_{ads} is calculated by substituting the values from equations 5 and 6 into

(7) $\Delta H_{ads} = -(5/2)RT + RT\ [e^{(-A/T)}\ (A/T)/(1-e^{(-A/T)})] + 2RT\ [e^{(-B/T)}\ (B/T)/(1-e^{(B/T)})$ $- u_0 + W/2$.

There are three observations that we believe justify the validity of the ANIE results. The first observation is the agreement between CO and N_2 ΔH_{ads} values that are

obtained from the fits of the with ANIE and the Langmuir isotherm equations to the isothermal data. When same procedures that are used to determine the ΔH_{ads} value for H_2 adsorption are applied to CO and N_2 adsorptions, the ANIE results reproduce the Langmuir results. The fits of ANIE to the CO isothermal data and the fit of equation 5 to the ANIE results, which is used to determine the ΔH_{ads} value, are given in Figures 44A and 44B. Also, the fits of ANIE to the N_2 isothermal data and the fit of equation 5 to the ANIE results are shown in Figures 45A and 45B. The ΔH_{ads} values that are calculated by using the ANIE procedures for CO and N_2 adsorption on the WDN ice surface are -2.81, and -2.10 Kcal/mol, respectively. Therefore, the ΔH_{ads} value that is calculated by the ANIE model agrees with the ΔH_{ads} value that is calculated by the established Langmuir model. We believe that this agreement adds credibility to the use of ANIE. A listing of these results is presented in Table 12.

The second observation, which is used to justify the use of ANIE, is the comparison between the experimental ΔH_{ads}, ν_z, and ν_x values for H_2 adsorption and the corresponding literature values. The ΔH_{ads} value of -0.64 Kcal/mol differs by ~25% from the ΔH_{ads} value that is calculated for H_2 adsorption onto the NaCl surface,[56] and differs by 70% from the experimental binding energy that is determined for H_2 adsorbed onto the crystalline ice surface.[58] Also, Our ΔH_{ads} value by ~30% from the binding energy of the proton-donor dimer complex.[55] Our values for ν_z (256 cm^{-1}) and ν_x (55 cm^{-1}) are close to the ν_z (193 cm^{-1}) and ν_x (63 cm^{-1}) values for H_2 adsorbed on the NaCl surface. So, The values generated by and within the ANIE model agree with literature values.

The third observation, which is used to justify the use of ANIE, is that the direction and magnitude of the interaction energy (W; see equation 4) agree with the thermodynamical behavior that is predicted for adsorbed CO, N_2, and H_2 molecules on the ice surface. As seen in Table 12, the interaction energy is positive for CO, and N_2 adsorption. The reasons are that adsorbed molecules prefer the d-D sites (or interact with

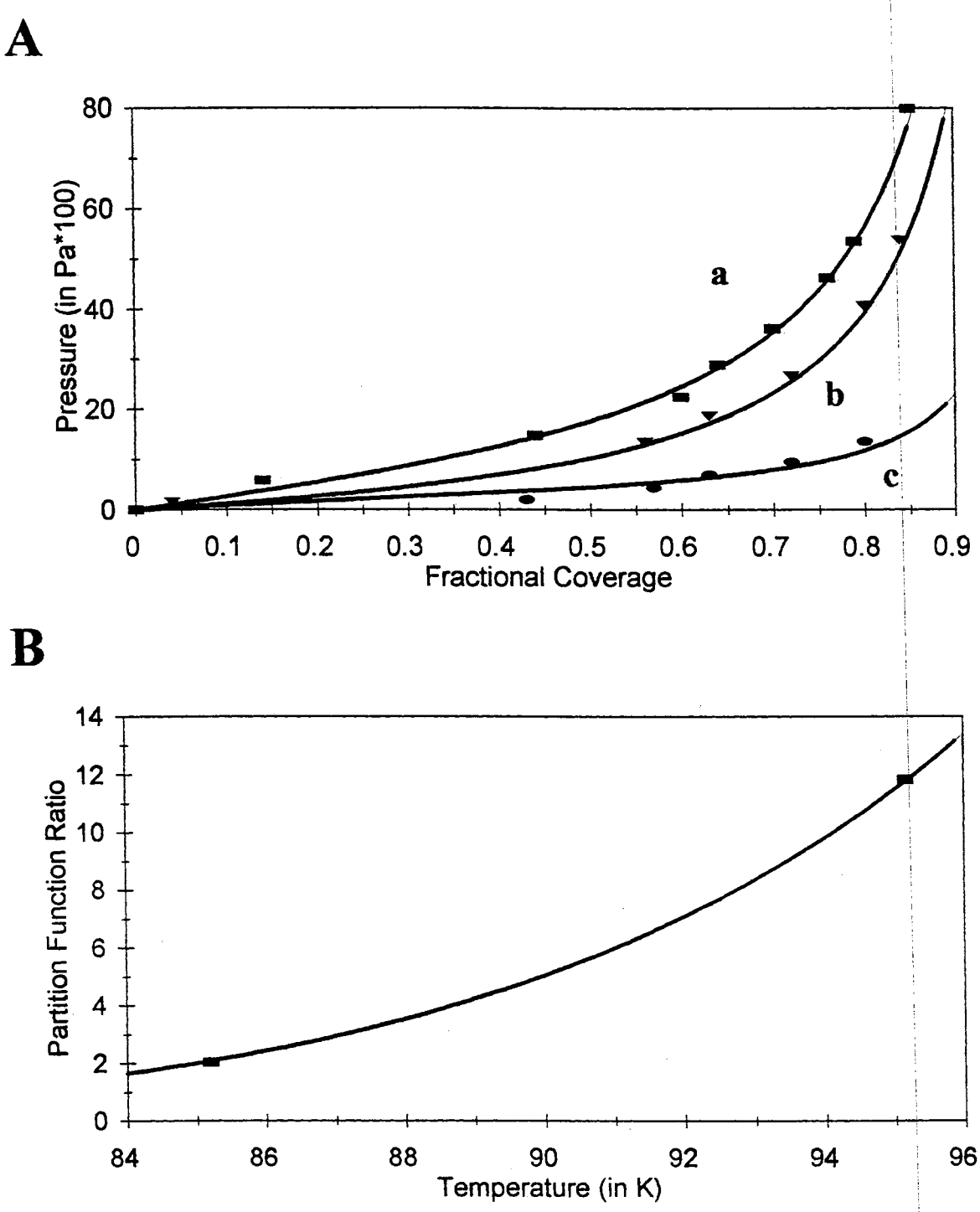

Figure 44. The fits of the CO isothermal data with ANIE (A), and the subsequent fit of the ratios of the partition functions versus temperature to determine ΔH_{ads} (B)

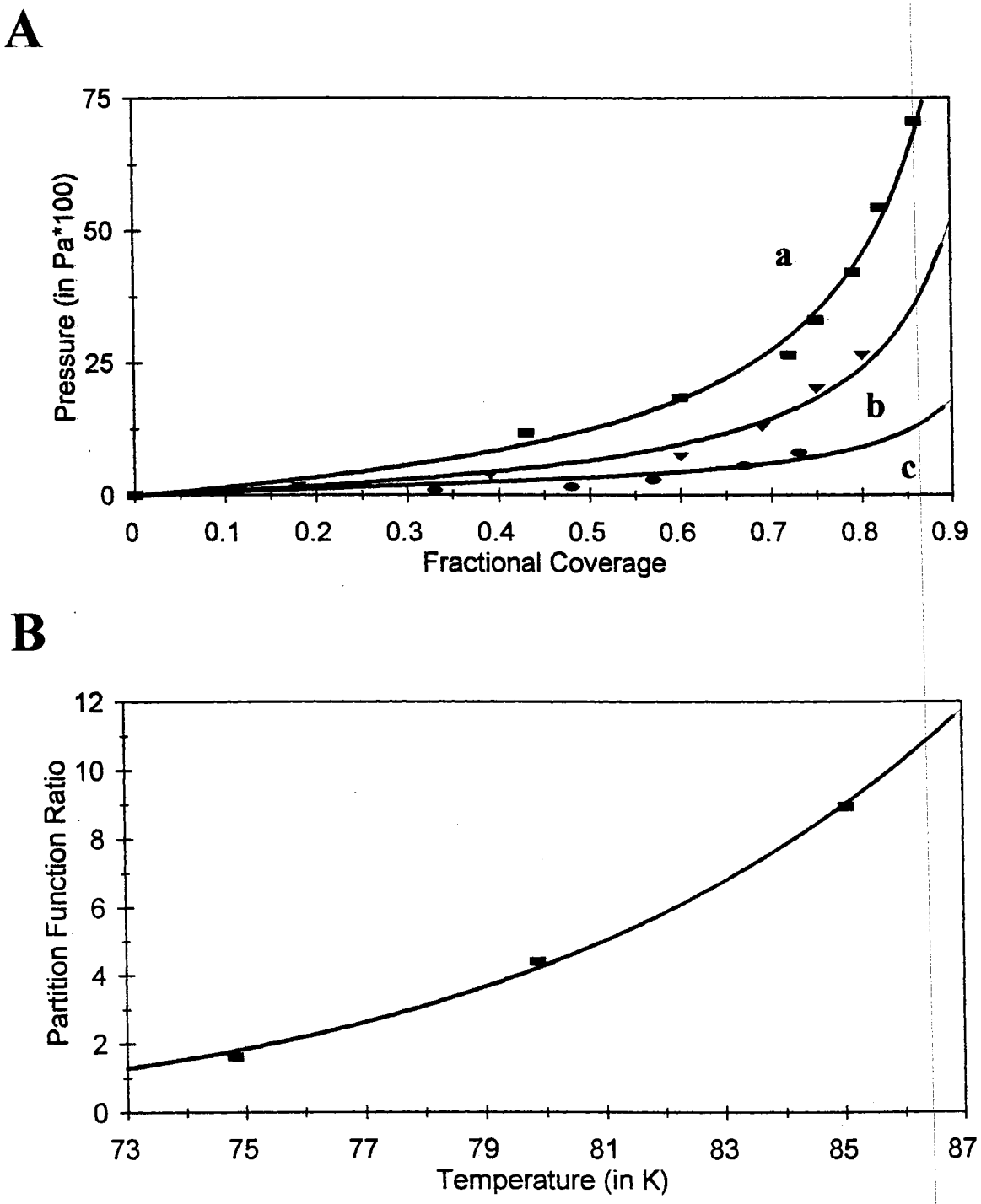

Figure 45. The fits of the N_2 isothermal data fit with ANIE (A), and the subsequent fit of the ratios of the partition functions versus temperature to determine ΔH_{ads} (B)

Table 12.

A summary of the ΔH_{ads} values for CO, N_2, and H_2 on the WDN surface for the Langmuir results (a) and the ANIE results (b)

Isotherm	U_0	W	ΔH
CO^a	------	------	-2.81
CO^b	2.66	2.64×10^{-4}	-2.80
N_2^a	------	------	-2.08
N_2^b	2.00	1.05×10^{-4}	-2.03
H_2^b	0.508	-1.11×10^{-3}	-0.644

the d-D sites stronger than the other sites), and that the adsorbed molecules must adsorb energy to leave the d-D sites. *Ab initio* calculations of the dimer complexes predict that CO binds stronger to d-D sites than N_2.[55] This is evident in the magnitude of the interaction energy for CO and N_2 adsorption in which CO is greater. The interaction energy is negative for H_2 adsorption. This agrees with the theoretical prediction that H_2 molecules prefer the d-O sites over the d-D sites.[55] Therefore, energy is released as the adsorbed H_2 molecules leave the d-D sites.

IV.5. Other Adsorbates

Several adsorbates have been studied on the crystalline D_2O (H_2O) ice surface, and their effects on the d-D IR band are given in Figures 32 and in Table 7 (see section IV.3). Although each adsorbate can offer a unique insight to the interactive nature of the ice surface, the majority of the adsorbates that were applied to the crystalline ice surface were not studied in depth. The reasons were lack of time and the lack of spectacular spectral results that were obvious to us. Carbon monoxide, Nitrogen, and Hydrogen adsorbed on the WDN surface are chosen to be studied in greater detail than the other adsorbates because of the information and interest that exist about them in the literature, and because of their vapor pressures at temperatures below 120 K (easy to measure isotherms).

An adsorbate that exhibits spectral results that are of interest to us is CF_4. A property that CF_4 exhibits is the splitting of the triply degenerate ν_3 mode into transverse optical (TO) and longitudinal optical (LO) components upon application onto the WDN surface.[49] This split in the ν_3 vibrational-mode arises from the long range intermolecular coupling between CF_4 molecules.[64] The amount of coupling is evident in the magnitude of the split between the TO-LO band and in the shape of the TO-LO bands. The TO and LO bands region of the IR spectrum is used to determine surface

morphology by using a monolayer of adsorbed CF_4 molecules to produce the TO-LO spectrum.

Spectra of CF_4 on the crystalline ice surface and the amorphous ice surfaces are given in Figures 46a and 46b. The TO - LO splitting of the ν_3 CF_4 band is best shown in Figure 46a, where the TO and LO bands are centered at ~1330 cm^{-1} and ~1250 cm^{-1}. For adsorption on the crystalline surface, there exist little intensity between the TO-LO band positions, which indicate strong dipole coupling between the CF_4 molecules and a smooth surface. For adsorption on the amorphous surface, considerable intensity exists between the TO and LO IR band positions, which indicate weak dipole coupling and a rough surface that causes pooling of the CF_4 molecules within micropores on the surface of amorphous ice. The CF_4 spectrum for CF_4 molecules adsorbed on amorphous ice surface is reproduced by adsorbing CF_4 molecules on the surface of silicate smokes.[65] Silicate smokes are known to be amorphous and have a very rough, disordered, and spiked surface that is observed by using scanning tunneling microscopy.[66] The resulting spectrum for CF_4 molecules adsorbed on the silicate smoke surface (see Fig. 46c) resembles the spectrum of CF_4 adsorbed on the surface of amorphous ice (see Fig. 46b) because of the IR intensity between the TO and LO band positions. The effect of surface morphology on the TO-LO split of the ν_3 band allows CF_4 to be used to determine the morphology of a surface.

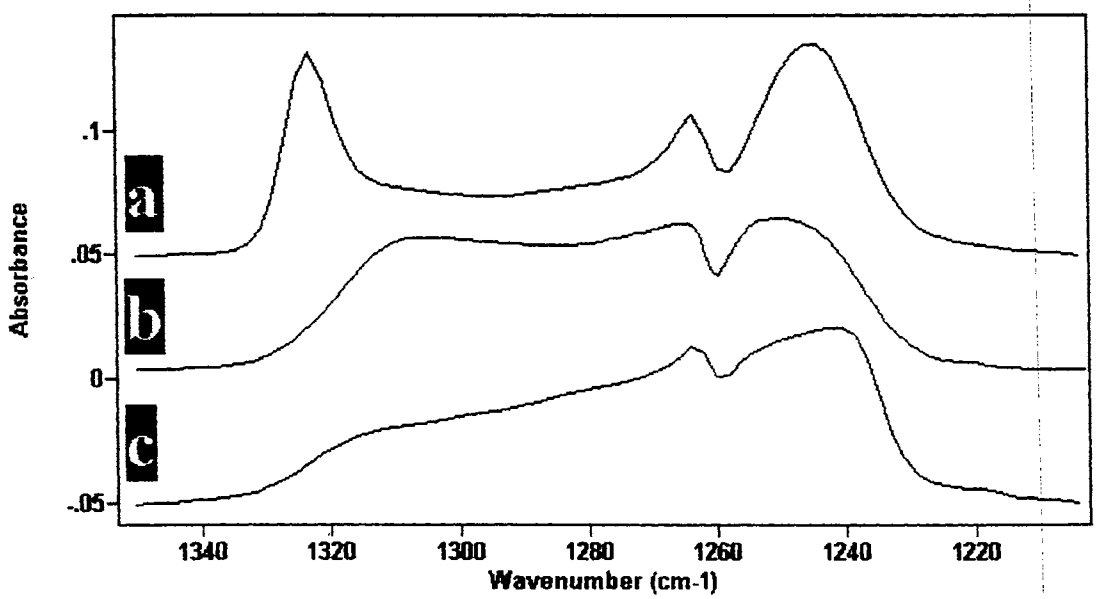

Figure 46. The spectra of CF_4 adsorbed onto the crystalline ice (a), amorphous ice (b), and silicate smoke (c) surfaces

V. Summary and Further Studies

V.1. Summary

Defects in the tetrahedrally hydrogen-bonded H_2O network of cubic and hexagonal ices occur at the surface. By viewing the cleaved surface of crystalline ice (see Fig. 3; Section I.2.2), the ice surface is modeled as being composed of a bilayer. The first (top) layer of the bilayer has H_2O molecules that are involved in three hydrogen bonds (3-coordinate), and the second layer has H_2O molecules that are involved in four distorted hydrogen-bonds (4-coordinate). Water molecules in the first layer of the bilayer are further divided into two groups. Water molecules that have two hydrogen bonds through the hydrogen of H_2O with a third hydrogen-bond through the oxygen are defined as the 3-coordinate dangling-O (d-O) molecules. Water molecules that have one hydrogen bond through the hydrogen of H_2O and two hydrogen-bonds through the oxygen, are defined as the 3-coordinate dangling-H (d-H(D)) molecules. The distorted tetrahedral H_2O molecules in the second layer of the bilayer are the surface 4-coordinate molecules (S-4).

Surface-defect molecules are not only observed for H_2O ice surfaces, and observed in small $(H_2O)_{20}$ clusters.[18] The calculated structures for $(H_2O)_{20}$ clusters are composed of d-H(D), d-O, and S-4 molecules (see Fig. 6; Section I.2.2.1),[25,26] and the IR spectrum of the $(H_2O)_{20}$ clusters qualitatively agree with the IR spectrum of the cubic ice surface (see Fig. 22; Section III.1). So, the surface-defect vibrational modes are observable and comparable for the ice surface and the $(H_2O)_{20}$ clusters. Also, a classical computational study conducted for an ice surface finds that the potential energies of d-H(D), d-O, and S-4 are -19.0, -17.7, and -23.3 Kcal/mol, respectively.[27]

The experimental objective is to obtain IR spectra of the H_2O ice surface. Various experimental equipment and experimental procedures are used to produce an ice

surface that has observable surface-defect vibrational modes. Depositing nanocrystals onto the windows of the static cluster cell (see Fig. 10; Section II.2.2) is (in our opinion) an excellent way to create enough cubic ice surface that is observable in the IR spectrum. Window deposited nanocrystals (WDN) are formed by loading a gaseous sample of 100/1 (N_2/H_2O) molar mixture into the static cluster cell that is precooled to ~70 K, where approximately 5% of the nanocrystals deposit on the IR transparent windows of the cluster cell (see section II.3.1.2). By repeating the loading of the gaseous sample into the precooled cluster cell, a deposit of nanocrystals is created on the surface of the windows. WDN allow the average WDN size to be changed by annealing the sample, and allow pressures between a few torr (from isothermal data; see section IV.4) and an atmosphere of an adsorbing gas. Annealing is used to expose the surface (see section II.3.2), and applying pressure of an adsorbing gas over the WDN allows the collection of isothermal data that are used to calculate thermodynamical values such as ΔH_{ads} (see IV.4). A WDN sample remains good for weeks, and allows good signal-to-noise levels because time does not limit the number of scans that can be taken.

WDN have enough surface area that the d-D surface-defect vibrational mode is observed in the standard unmanipulated IR spectrum. However, there exist a significant contribution from the bulk ice spectrum (see section Fig. 1; Section I.2.1) to the total WDN IR spectrum. Therefore, techniques are devised to expose the surface-defect IR spectrum. This is achieved by using two difference-spectra schemes, which are the annealing difference scheme and the adsorbate-shifted difference scheme.

The annealing difference scheme exposes the IR spectrum of the WDN surface by increasing the average size of the WDN upon annealing to higher temperatures (see II.3.2.1). In the annealing scheme, a WDN sample is annealed at a temperature T_1, and then cooled to a temperature T_2, where a spectrum S_1 is taken. The sample is rewarmed and annealed at a temperature T_3 that is higher than T_1. The sample is then recooled to T_2, and a second spectrum S_2 is taken. The difference spectrum is given by subtracting

S_1 by S_2 (see Fig. 15; Section II.3.2.1). The positive IR bands are due to the surface spectrum, and the negative IR bands correspond to the bulk spectrum, because the WDN in S_2 have more H_2O molecules in the bulk portion of the nanocrystals and less surface area than the WDN in S_1. The adsorbate-shifted difference spectra are obtained by adsorbing molecules onto the ice surface (see section II.3.2.2). A WDN sample is annealed at a temperature T_1 and cooled to temperature T_2. An IR spectrum S_1 of the bare ice surface (an ice surface with no molecules adsorbed on it) is taken. Adsorbate molecules are applied to the ice surface at temperature T_2, and a second IR spectrum S_2 is taken. The difference spectrum is given by subtracting S_2 by S_1 (see Fig. 16; Section II.3.2.2). The positive IR bands are due to the adsorbate-shifted surface-defect vibrational modes, and the negative IR bands are attributed to the surface-defect vibrational modes of the bare surface.

The qualitative agreement between the $(H_2O)_{20}$ IR spectrum[18] and the surface portion of the annealed difference spectrum indicates that the coordination of the H_2O molecules accounts for specific bands in the IR spectrum and is similar from phase-to-phase. One of the earliest assignment of a surface-defect vibrational mode is for the free-OH stretch at ~3700 cm^{-1} (i.e., the d-H(D)).[18] The d-H(D) IR band is observed in the unadjusted standard nanocrystalline IR spectrum at 3692 (2725) cm^{-1}. Also, the d-H(D) band is observed in low density amorphous ice, and in zeolites.[19-22]

The surface portion of an annealed difference spectrum can be resolved into separate IR bands by band fitting (see Fig. 19; Section II.4.3). The initial Gaussian band positions and intensities are obtained from computational and experimental data.[39] The band fit of the surface region allows further assignments of the surface-defect vibrational modes to be made. The out-of-phase vibrational modes for the d-H(D), d-O, and S-4 surface-defect groups are assigned 3692 (2725), 3564 (2640), and 3485 (2564) cm^{-1} (see section III.3), respectively. The in-phase vibrational modes for d-H(D), d-O, and S-4 are tentatively assigned 3150 (2350), 3300 (2450), and 3440 (2490) cm^{-1} (see section III.3),

respectively. The in-phase vibrational mode assignments for d-H(D) and d-O are taken from the calculated frequencies of Buch et al.[72], and the assignment for S-4 is taken from the band fit of the annealed difference spectrum (see Fig. 28; Section III.3). Finally, the surface-defect bending modes for d-H(D) and d-O are assigned 1650 (1215), and 1690 (1235) cm^{-1}. The assignments of the out-of-phase vibrational and bending modes are considered to be correct, because of their agreement with the computational results (see section III.3). However, assignments of the in-phase vibrational modes are not made as confidently as the out-of-phase modes, and are primarily determined from a simulated IR spectrum of the annealed cluster.[72]

Adsorption of various molecules onto the ice surface causes the surface-defect vibrational modes to shift to lower frequencies (red shift). These shifts are observed in the adsorbate-shifted difference spectra and the adsorbate-shifted annealed difference spectra (see sections II.3.2.1 and II.3.2.2), and the magnitudes of the shifts in the d-H(D) and d-O IR bands for different adsorbed molecules are given in Table 7 in section IV.3. The interactive nature of the ice surface is evaluated by applying adsorbate onto the ice surface (see section IV.1). Preferential adsorption of adsorbate molecules onto a particular group of surface-sites is experimentally observed (see section IV.3), and theoretically predicted by *ab initio* calculations of dimer complexes that involve an H_2O molecule interacting with another molecule, such as N_2.[55] The two calculated dimer complexes correspond to adsorption on the d-H(D) and d-O sites (see section IV.4).

Fractional coverage of adsorbed molecules on the WDN surface is determined for a specific group of surface-sites (see section IV.4). An isotherm equation is used to fit the isothermal data that contain the fractional coverage, pressure, and temperature. Values calculated by fitting isotherm equations to the isothermal data are used to calculate values for the ΔH_{ads} (see IV. 4). Isothermal data collected for CO, N_2, and H_2 used the d-D sites to determine fractional coverages. The values of -2.81 and -2.08 Kcal/mol for ΔH_{ads} are calculated for CO (see Fig 39; Section IV.4.1) and N_2 (see Fig.

41; Section IV.4.2) adsorptions on the d-D sites by using values that are determined by the fit of the Langmuir isotherm equation to the isothermal data. The use of the Langmuir isotherm equation requires that the adsorbate-site interaction must be localized. So, CO and N_2 adsorbed molecules interact with d-D sites in a localized manner, and all other interactions, such as the adsorbate-adsorbate interactions, are trivial. A value of -0.664 Kcal/mol for ΔH_{ads} is calculated for H_2 adsorption. However, H_2 isothermal data are fit with an isotherm equation (ANIE) that is used to account for occupied site-unoccupied site interactions (see Fig. 43; Section IV.4.3). Therefore, H_2 molecules adsorbed on the ice surface are not exclusively localized on the d-D sites, but interact with the unoccupied d-D sites while adsorbed on neighboring sites.

V.2. The Simplistic Model of the Ice Surface

Our simplistic model of the ice surface considers the H_2O crystalline ice surface to be a cleaved crystalline ice surface (see Fig. 3; Section I.2.2). The surface-defect groups are identified by the hydrogen-bonded environment that surrounds a surface molecule, and the vibrational modes in the surface IR spectrum are observed for each group. Therefore, the IR bands in the IR surface spectrum correspond to a particular set of surface sites. Any interaction of an adsorbate with the ice surface is evaluated with a site-specific analysis. By following the effect of an adsorbate on the specific sites, the interactive nature of the ice surface (such as the heat of adsorption) can be determined.

V.3. New Experimental Results and Revision of the Simplistic Model

By following the TO-LO (transverse optical and longitudinal optical) splitting in the triply degenerate ν_3 CF_4 vibrational mode, the surface morphology is determined for the nanocrystal surface.[67] The morphology of the nanocrystalline surface is smooth (no

micropores that are found on the surface of the low density amorphous ice), and disordered (does not have evenly and repetitively spaced surface sites). This differs from the cleaved surface structure of the simplistic model that considers the nanocrystal surface as a smooth-ordered structure. Therefore, the model of the ice surface morphology is changed from an ordered cleaved surface to a more disordered surface.

Other results that differ from those reported in this thesis are the assignments for the in-phase D_2O surface-defect vibrational modes of d-D, d-O, and S-4.[68] In this thesis, the in-phase assignments reported for d-O, S-4, and d-D, which are made by band fitting the annealed difference spectrum and by using the simulated IR cluster spectrum, are 2450, 2490, and 2350 cm^{-1}, respectively. The latest assignments for d-O, S-4, and d-D in-phase vibrational modes, which are deduced from adsorbate-shifted difference spectra, are located at 2480, 2430, and 2300 cm^{-1}.[68] This change in the in-phase assignments does not effect the out-of-phase surface-defect vibrational mode assignments. Also, the contribution of the sub-surface (the layers of H_2O molecules that are immediately below the surface bilayer) vibrational modes to the IR surface spectrum are trivialized in this thesis, and are significant contributors to the IR spectrum of the ice surface.[72]

V.4. Further Studies

We believe that the study of the crystalline ice surface, which is reported in this thesis, lays the groundwork for many future experiments. The accessibility to study specific groups of surface-site on a molecular level allows many experiments to be conducted on this surface, but only four experiments that can be done in the future are listed in this thesis.

1. Better assignments for the surface-defect bending modes need to be made for the d-H(D), d-O and S-4. The previous assignments for d-H(D) and d-O bending modes may be correct, but no S-4 bending-mode assignment has been made.

2. We expect formation of clathrate hydrate nanocrystals to exhibit interesting properties such as the increase the order of the surface and sub-surface structures, which can be probed with CF_4 and difference spectra analysis. By annealing WDN under the pressure of a clathrating gas, we believe that clathrates can be formed at temperatures lower than the reported formation temperatures. Clathration occurs when guest molecules (such as CO, or ethylene oxide) are surrounded by an ordered H_2O cage.

3. Crystallization of molecules on the ice surface could force order in the surface and sub-surface structures of the nanocrystals. This is presumably achieved by adsorbing various molecules to the surface of the WDN and warming the sample under a pressure of an adsorbing gas. Once adsorbate crystallization occurs, the sample is cooled to a temperature at which the adsorbate has little or no vapor pressure, and CF_4 is applied to determine the surface morphology. Ordering of the sub-surface could be observed by evaluating difference spectra.

4. Ice is a major component in the upper atmosphere and in interstellar space.[2-9] Many reactions and interactions occur on the surface of "ice" clusters ("ice" may not be solely composed of H_2O molecules).[2-9] The use of the H_2O ice surface that can be used to facilitate low temperature reactions which are similar to those in space is interesting to us. The reactions can be followed for the reactants, products, and the nanocrystal surface-sites. Simple reactions (such as NO dimerizing) could be studied at first, but the study of reactions of interest to astrophysics would be the ultimate goal.

REFERENCES

1. Mumma, M. J., Weissman, P. R., and Stern, S. A. "Comets and the Origin of the Solar System: Reading the Rosetta Stone." Protostars and Planets III, (edited by Levy, E. H., Lunine, J. I., and Matthews, M. S., University of Arizona Press, Tucson) 1992.

2. Tielens A. G. G. M., and Allamandola, L. J. "Evolution of Interstellar Dust." Physical Processes in Interstellar Clouds, (edited by Morfill, G. E. and Scholer, M., Reidel Publishing Company) p.333, 1987.

3. "Ozone Depletion: 20 Years After the Alarm." C&E News, p. 68, Aug. 15, 1994.

4. a.) Zhang, R., Jayne, J. T., and Molina, M. J. "Heterogeneous Interactions of $ClONO_2$ and HCL with Sulfuric Acid Tetrahydrate: Implications for the Stratosphere." J. Phys. Chem., Vol. 98, p. 867, 1994.

   b.) Molina, M. J., Tso, T., Molina, L. T., and Wang, F. C. Y. "Antarctic Stratospheric Chemistry of Chlorine Nitrate, Hydrogen Chloride, and Ice: Release of Active Chlorine." Science, Vol. 238, p. 1253, 1987.

5. a.) Hallett, J. "Progress in Cloud Physics 1979-1982." Reviews of Geophysics and Space Physics, Vol. 21 (5), p.965, 1983

   b.) Gross, G. W. "Role of Relaxation and Contact Times in Charge Separation During Collisions of Precipitation Particles with Ice Targets." J. Geophys. Res., Vol. 87, p. 7170, 1982.

6. Moore, M. H., Donn, B., Khanna, R., and A'Hearn, M. F. "Studies of Proton-Irradiated Cometary-Type Ice Mixtures." Icarus, Vol. 54, p. 388, 1983.

7. Buch, V. "Interstellar Grain Chemistry." Molecular Astrophysics, (edited by , Harhquist T., Cambridge University Press) p.132, 1990.

8. Sandford, S. A., Allamandola, L. J., and Geballe, T. R. "Spectroscopic Detection of Molecular Hydrogen Frozen in Interstellar Ices." Science, Vol. 262, p. 400, 1993.

9. Bush, V. and Devlin, J. P. "Interpretation of the 4141 cm^{-1} (2.415 μm) Interstellar Infrared Absorption Feature." Ap. J., Vol. 431, p. L135, 1994.

10. Thiel, M. V., Becker, E. D., and Pimentel, G. C. "Infrared Studies of Hydrogen Bonding of Water by Matrix Isolation Technique." J. Chem. Phys., Vol. 27, p. 486, 1957.

11. Ayers. G. P. and Pullin, A. D. E. "The I. R. Spectra of Matrix Isolated Water Species - IV. The Configuration of the Water Dimer in Argon Matrices." Spectrochimica Acta., Vol. 32A, p. 1695, 1997.

12. Engdahl, A. and Nelander, B. "Water in Krypton Matrices." J. Mol. Struct., Vol. 193, p. 101, 1989.

13. Coker, D. F., Miller, R. E., and Watts, R. O. "The Infrared Predissociation Spectra of Water Clusters." J. Chem. Phys., Vol. 82, p.3554, 1985.

14. Honegger, E. and Leutwyler, S. "Intramolecular Vibrations of Small Water Clusters." J. Chem. Phys., Vol. 88, p. 2582, 1988.

15. Ritzhaupt, G., Smyrl, N., and Devlin, J. P. "Vibrational Spectra of Glassy Water Aggregates and Thin Films." J. Chem. Phys., Vol. 64, p. 435, 1975.

16. Hagen, W., Tielens, A. G. G. M., and Greenberg, J. M. "Infrared Spectra of Amorphous Solid Water and Ice I_c Between 10 and 14 K." Chem. Phys., Vol. 56, p. 367, 1986.

17. Hagen, W., Tielens, A. G. G. M., and Greenberg, J. M. "Laboratory Study of the Infrared Spectra of Interstellar Ices." Astrophys. Suppl. Ser., Vol. 51, p. 389, 1983.

18. Page, R. H., Vernon, M. F., Shen, Y. R., and Lee, Y. T. "Infrared Vibrational Predissociation Spectra of Large Water Clusters." Chem. Phys. Lett., Vol. 141, p. 1, 1987.

19. Rowland, B. and Devlin, J. P. "Spectra of Dangling OH Groups at Ice Cluster Surfaces and Within Pores of Amorphous Ice." J. Chem. Phys., Vol. 94, p. 812, 1991.

20. Kiricsi, I., Flego, G., Pazzuconi, G., Parker, W. O., Millini, R., Perego, C., and Bellussi, G. "Progress towards Understanding Zeolite *B* Acidity: An IR and ^{27}Al NMR Study." J. Phys. Chem., Vol. 98, p. 4627, 1994.

21. Makarova, M. A., Ojo, A. F., Karim, K., Hunger, M., and Dwyer, J. "FTIR Study of Weak Hydrogen Bonding of Bronsted Hydroxyls in Zeolites and Aluminophosphates." J. Phys. Chem., Vol. 98, p. 3619, 1994.

22. Butanin, K. M., Alexeeve, A. V., Bystrov, D. S., Lavalley, J. C., and Tsyganenko, A. A. "IR Study of Ozone Adsorption on SiO_2." J. Phys. Chem., Vol. 98, p. 5100, 1994.

23. Callen, B. W., Griffiths, K., and Norton, P. R. "Observation of Free Hydroxyl Groups on the Surface of Ultra Thin Ice Layers on Ni (110)." Surface Science Lett., Vol. 261, p. 144, 1992.

24. Materer, N., Starke, U., Barbier, A., Van Hove, M. A., Somorjai, G. A., Kroes, G. J., and Minot, C. "Molecular Surface Structure of a Low-Temperature Ice I (0001) Crystal." J. Phys. Chem., Vol. 99, p. 6267, 1995.

25. Buffey, I. P. and Brown, W. B. "Structure of Water Clusters Computed with the Aid of Molecular Graphics." Chem. Phys. Lett., Vol. 109, p. 59, 1984.

26. Jordan, K. D. and Tsai, C. J. "Theoretical Study of Small Water Clusters: Low-Energy Fused Cubic Structures of $(H_2O)_n$, n = 8, 15, 16, and 20." J. Phys. Chem., Vol. 97, p. 5208, 1993.

27. Buch, V. "Growth and Structure of Amorphous Ice Condensate: A Computational Study. II." J. Chem. Phys., Vol. 96, p. 3814, 1992.

28. Oxtoby, D. W. "Homogeneous Nucleation: Theory and Experiment." J. Phys.: Condens Matter, Vol. 4, p. 7627, 1992.

29. Dissellcamp, R. and Ewing, G. E. "Large CO_2 Clusters Studied by Infrared Spectroscopy and Light Scattering." J. Chem. Phys., Vol. 99, p. 2439, 1993.

30. Miller, R. E. and Dunder, T. "Infrared Spectroscopy and Mie Scattering of Acetylene Aerosols Formed in a Low Temperature Diffusion Cell." J. Chem. Phys., Vol. 93, p. 3693, 1990.

31. Engdahl, A. and Nelander, B. "On the Relative Stabilities of H- and D- bonded water dimers." J. Chem. Phys., Vol. 86, p. 1819, 1987.

32. Somorjai, G. A. and Davy, J. G. "Studies of Vaporization Mechanism of Ice Single Crystals." J. Chem. Phys., Vol. 55, p. 3624, 1971.

33. Yang, C. H. and Qiu, H. "Theory of Homogenous Nucleation: A Chemical Kinetic View." J. Chem. Phys., Vol. 84, p. 416, 1986.

34. Dean, R. B. and Dixon, W. J. "Simplified Statistics for Small Numbers of Observation." Analy. Chem., Vol. 23, p. 636, 1951.

35. Mokomela, T. D., Rencken, I., Yeo, G. A., and Ford, T. A. "Ab Initio Molecular Orbital Calculations of the Infrared Spectra of Interacting Water Molecules Part 2. Complexes of Water with Carbon Monoxide and Nitrogen." J. Mol. Struct., Vol. 275, p. 33, 1992.

36. Rowland, B., Fisher, and M., Devlin, J. P. "Surface-Defect Vibrational Modes of Large Ice Clusters." J. Phys. Chem., Vol. 97, p. 2485, 1993.

37. Knochemuss, K. and Leutwyler, S. "Structures and Vibrational Spectra of Water Clusters in the Self-Consistent-Field Approximation." J. Chem. Phys., Vol. 96, p. 5233, 1992.

38. Ojamae, L. and Hermansson, K. "Ab Initio Study of Coopertativity in Water Chains; Binding Energies and Anharmonic Frequencies." J. Phys. Chem., Vol. 98, p. 4271, 1994.

39. Rowland, B., Kadagathur, N. S., Devlin, J. P., Buch, V., Feldman, T., and Wojcik, M. J. "Infrared Spectra of Ice Surfaces and Assignments of Surface-Localized Modes from Simulated Spectra of Cubic Ice." J. Chem. Phys., Vol. 102, p. 8328, 1995.

40. Xantheas, S. S. "Ab Initio Studies of Cyclic Water Clusters $(H_2O)_n$, n = 1 - 6. II." J. Chem. Phys., Vol. 100, p. 7523, 1994.

41. Hermansson, K., Knuts, S., and Lindgren, J. "The OH Vibrational Spectrum of Liquid Water from Combined Ab Initio and Monte Carlo Calculations." J. Chem. Phys., Vol. 95, p. 7486, 1991.

42. Wojcik, M. J., Buch, V., and Devlin, J. P. "Spectra of Isotopic Ice Mixtures." J. Chem. Phys., Vol. 99, p. 2332, 1993.

43. Makarova, M. A., OjO, A. F., Karim, K., Hunger, M., and Dwyer, J. "FTIR Study of Weak Hydrogen Bonding of Bronsted Hydroxyls in Zeolites and Aluminophosphates." J. Phys. Chem., Vol. 98, p. 3619, 1994.

44. Zilles, B. A. and Person, W. B. "Interpretation of Infrared Intensity Changes on Molecular Complex Formation. I. Water Dimers." J. Chem. Phys., Vol. 79, p. 65, 1983.

45. Hixson, H. G., Wojcik, M. J., Devlin, J. P., and Buch, V. "Experimental and Simulated Vibrational Spectra of H_2 Adsorbed in Amorphous Ice: Surface Structure, Energetics, and Relaxations." J. Chem. Phys., Vol. 97, p. 753, 1992.

46. Devlin, J. P., Silva, S. C., Rowland, B., and Buch, V. "Spectroscopic and Simulated Study of Ice Surfaces: Bare and with Adsorbates." Hydrogen Bond Networks (edited by Bellissen-Funnel, M. C. and Dore, J. C., Kluwer Academic Publishers), p. 373, 1994.

47. Silva, S. C. and Devlin, J. P. "Interactions of Acetylene, Ethylene, and Benzene with the Ice Surface." J. Phys. Chem., Vol. 98, p. 10847, 1994.

48. Devlin, J. P. "Molecular Interactions with Icy Surfaces: Infrared Spectra of CO Absorbed in Microporous Amorphous Ice." J. Phys. Chem., Vol. 96, p. 6185, 1992.

49. Rowland, B., Kadagathur, N. S., and Devlin, J. P. "Infrared Spectra of CF_4 Adsorbed on Ice: Probing Adsorbate Dilution and Phase Separation with the ν_3 Transverse-Longitudinal Splitting." J. Chem. Phys., Vol. 102, p. 13, 1995.

50. Del Bene, J. E. "Molecular Orbital Theory of Hydrogen Bond. Pi Electrons as Proton Acceptors." Chem. Phys. Lett., Vol. 24, p. 203, 1974.

51. Frisch, M. J. and Pople, J. A. "Hydrogen Bonds between First-Row Hydrides and Acetylene." J. Chem. Phys., Vol. 78, p. 4063, 1983.

52. Jonsson, B., Karlstrom, G., and Wennerstrom, H. "Ab Initio Molecular Orbital Calculations on the Water-Carbon Dioxide System: Molecular Complexes." Chem. Phys. Lett., Vol. 30, p. 58, 1975.

53. Chatasinski, G., Szczeniak, M. M., and Scheine, S. "Ab Initio Study of the Intermolecular Potential of Ar-H_2O." J. Chem. Phys., Vol. 94, p. 2807, 1991.

54. Dimitrova, Y. and Peryerimhoff, S. D. "Theoretical Study of Hydrogen-Bonded Formaldehyde-Water complexes." J. Phys. Chem., Vol. 97, p. 12731, 1993.

55. Sadlej, J., Rowland, B., Devlin, J. P., and Buch, V. "Vibrational Spectra of Water Complexes." J. Chem. Phys., Vol. 102, p. 4804, 1995.

56. Dai, D. J. and Ewing, G. E. "Induced Infrared Adsorption of H_2, HD, and D_2 Physisorbed on NaCl Films." J. Chem. Phys., Vol. 98, p.5050, 1993.

57. Richardson, H. H., Baumann, L., and Ewing, G. E. " Infrared Spectroscopy and Thermodynamic Measurements of CO on NaCl Films." Surf. Sci., Vol. 187, p. 15, 1987.

58. Sandford, S. A. and Allamandola, L. J. "H_2 in Interstellar Extragalactic Ices: Infrared Characteristics, Ultraviolet, Production, and Implications." Ap. J., Vol. 409, p. L65, 1993.

59. Sandford, S. A. and Allamandola, L. J. "Condensation and Vaporization Studies of CH_3OH and NH_3 Ices: Major Implications for Astrochemistry." Ap. J., Vol. 417. p. 815, 1993.

60. An Introduction to Statistical Thermodynamics, (edited by Hill, T. C.) Addison-Wesley Publishing Company, Inc., 1960.

61. Statistical Thermodynamics, (edited by Fowler, R. and Guggenheim, E. A.) The Syndics of the Cambridge University Press, 1949.

62. Dunn, S. K. and Ewing, G. E. "Infrared Spectra and Structure of Acetylene on NaCl (100)." J. Phys. Chem., Vol. 96, p. 5284, 1992.

63. Yang, C. "Statistical Mechanical Aspects of Adsorption System Obeying the Temkin Isotherm." J. Phys. Chem., Vol. 97, p. 7097, 1993.

64. Ovchinnikov, M. A. and Wight, C. A. "Infrared Lineshapes of Clusters and Microcrystals: Vibrational Modes Mixed by Dipole Interactions." J. Chem. Phys., Vol. 100, p. 972, 1994.

65. Moore, M. H., Ferante, R. F., Hudson, R. L., Nuth III, J. A., and Donn, B. "Infrared Spectra of Crystalline Phase Ices Condensed on Silicate Smokes at T<20 K." The Astrophysical Journal, Vol. 428, p. L81, 1994.

66. Moore, M. Private Communication

67. Buch, V. Delzeit, L., Blackledge, C., and Devlin, J. P. "Structure of the Ice Nanocrystal Surface of Simulated versus Experimental Spectra of Adsorbed CF_4." submitted and accepted, J. Phys. Chem., spring, 1996.

68. Devlin, J. P. and Buch, V. "FT-IR Spectra of Nanoparticles: Surface and Adsorbate Modes." to be published, Mikrochimica Acta, spring, 1996.

69. Whalley, E. and Klug, D. D. "Origin of the High Integrated Infrared Intensity of the O-H Stretching Vibrations in Ice I Relative to the Vapor." J. Chem. Phys., Vol. 84, p. 4807, 1986.

70. CRC Handbook of Chemistry and Physics, 64th edition, (edited by Weast, R. C., Astle, M. J., and Beyer, W. H.) Chemical Rubber Publishing Company, 1983.

71. Sack, N. J. and Baragiola, R. A. "Sublimation of Vapor-Deposited Water Ice below 170 K, and Its Dependence on Growth Conditions." Phys. Rev. B *condensed matter*, Vol. 48, p. 9973, 1993.

72. Devlin, J. P. and Buch, V. "The Surface of Ice as Viewed from Combined Spectroscopic and Computer Modeling Studies." J. Phys. Chem., submitted and accepted, spring 1996.

APPENDICES

Appendix A.1. Average Size of the Nanocrystal

The average size of nanocrystals is calculated by using well-established physical constants (such as the density of cubic ice) to solve for the average radius of the nanocrystals. The values that are obtained experimentally are the integrated areas of the out-of-phase d-H(D) IR band and the bulk H_2O (D_2O) IR stretching region (see Fig. 18; Section II.4.3). These areas are used to solve for the average radius by using two assumptions. The first assumption is that the d-H(D) surface-defect sites represent half of the defect-sites on the top layer of the surface bilayer (the other half is d-O surface-defect sites), and the second assumption is that the IR band intensity of the bulk OH stretch is 28.4 times greater than the IR band intensity of the d-H(D) band.[69] By using these assumptions, a ratio of (d-H band area)/(bulk H_2O band areas) corresponds to a ratio of the (number of surface molecules)/(number of bulk molecules).

The ratio of band areas is used to calculate the average nanocrystal radius by using

(1) $K=(\#\text{ of surface molecules})/(\#\text{ of bulk molecules})=(4\pi r^2 S)/(4/3\pi r^3 d)$,

where K, S and d are the ratio of the surface-to-bulk molecules, number of H_2O molecules per unit area, and the density of cubic ice, respectively. The density of cubic ice (0.917 g/cm^3) is known,[70] but the surface area density is not available. However, the value for S is approximately determined by using the density of cubic ice in the following manner.

(2) $d=0.917 g/cm^3=30.6522\ H_2O$ molecules/nm^3

(3) 1 H_2O moleule=0.0326241 $nm^3=4/3 \times \pi r^3$

(4) $r=0.1982211$ nm/H_2O

Since the average radius of an H_2O molecule in cubic ice is obtained, the radius is used to calculate S.

(5) $\pi r^2 = 0.1234382\ nm^2/H_2O$

(6) $S=8.10123\ H_2O/nm^2$

If equations 2 and 6 is substituted into equation 1, an equation that relates the radius to the ratio of the surface-to-bulk molecules is

(7) $K=0.7928857nm/r_{nc}$,

where r_{nc} is the average radius of the nanocrystals.

Areas of the d-H(D) and the bulk IR bands correspond to the concentrations of the surface molecules and bulk molecules. Beer's law and the second approximation of this appendix (the IR intensity of the bulk vibrational modes is 28.4 times greater than the d-H(D) band intensity) are used to properly weight the extinction coefficient that equivocally relates the d-H(D) IR absorbance to the bulk IR absorbance. A ratio of (surface molecules)/(bulk molecules) from equation 1 is obtained.

(8) $E_{BH2O}=28.4 \times E_{d\text{-}H}$

(9) $A[d\text{-}H]=E_{d\text{-}H} \times b \times c_{SH2O}$

(10) $A[BH_2O]=28.4 \times E_{d\text{-}H} \times b \times c_{BH2O}$

(11) $c_{SH2O}/c_{BH2O}= (28.4 \times A[d\text{-}H])/A[BH_2O]$

The constants E_{BH2O} and $E_{d\text{-}H}$ are the extinction coefficients for the bulk and d-H(D) IR absorptions. The variable A[d-H] is the band-fitted area of the d-H(D) IR band, $A[BH_2O]$ is the band-fitted area of the bulk IR region, c_{SH2O} represents the concentration of surface H_2O molecules, and c_{BH2O} represents the concentration of the bulk H_2O molecules. The ratio of c_{SH2O}/c_{BH2O} is related to K by the assumption that half of the surface-defect sites within the top layer of the surface bilayer are d-H sites.

(12) $2 \times c_{SH2O}/c_{BH2O}=K$

By substituting 11 into 12, an equation that relates the integrated band areas to K is

(13) $K=2 \times 28.4 \times A[d\text{-}H]/A[BH_2O]$.

By combining equations 7 and 13, an equation that relates the integrated IR band areas to the average radius of the nanocrystal is

(14) r_{nc}=(0.0139 nm) x A[BH_2O] /A[d-H].

Appendix A.2. Annealing

The following derivation uses a quantitative approach used to illustrate the relationship that exists between vapor pressure and cluster size. This derivation is not intended to predict accurate cluster sizes, but the predicted sizes of clusters are within the range of the experimental sizes that are observed for WDN. The purpose of this illustration is to demonstrate that smaller clusters at a given temperature are more unstable than larger clusters. This "vaporization model" is used to explain the annealing process that occurs for WDN.

The free energy expression from the liquid drop nucleation model is used as a starting point to show the cluster size-to-vapor pressure relationship,[33] and is

(1) $\Delta G = -n\,\Delta u + \sigma A$,

where ΔG is the Gibb's free energy for a cluster, n is the number of molecules in the cluster, Δu represents the chemical potential (u(vapor)-u(liquid)), A is surface area of a cluster, and σ represents the surface tension of a cluster. Equations for A, n, Δu, and σ are used to change equation 1 into an equation that is used to relate vapor pressure to cluster size.

(2) $n = \rho(4/3)\pi r^3$

(3) $A = 4\pi r^2$

(4) $\Delta u = kT \ln(P_V/P_{eq})$

The variables T, k, P_V, P_{eq}, and ρ are the temperature in Kelvin, Boltzman constant, vapor pressure, equilibrium vapor pressure of the clusters, and density of cubic ice, respectively. By substituting equations 2, 3, and 4 into equation 1, the following equation is derived:

(5) $\Delta G = -(4/3)\,\pi r^3 \rho(kT \ln(P_V/P_{eq})) + 4\sigma\pi r^2$.

The ΔG is eliminated by evaluating equation 5 at the critical radius of a cluster. The critical radius is when the internal binding-forces that hold the cluster together and the

vaporization forces that destroy the cluster are minimized with respect to the radius (i.e., $\partial\Delta G/\partial r = 0$).

(6) $\partial\Delta G/\partial r = -4\rho\pi r^2(kT \ln(P_V/P_{eq})) + 8\sigma\pi r = 0$

By rearranging equation 6 and solving for P_V/P_{eq}, the relationship between pressure and cluster size is

(7) $P_V/P_{eq} = e^{(2/\rho k)(\sigma/(Tr))}$,

(8) $W = 2/\rho k$,

(9) $P_V/P_{eq} = e^{W(\sigma/(Tr))}$,

Where r is in units of nanometers.

For a particular phase, the term $2/\rho k$ is a constant that is calculated from the density, and Boltzman constant.

The largest approximation that is used to derive the cluster size-to-vapor pressure relationship is calculating a value for σ. The surface tension is determined by fitting a reverse sigmodal function to known surface tensions (see Fig. 47A).[70] The function is used to determine the surface tension at temperatures lower than 256 K. The calculated surface tensions are 94.063, 92.764, and 90.401 g/s at 100, 120, and 150 K, respectively. This seems to be an unreasonable way to determine σ for clusters because 'liquid' phase H_2O clusters do not exist at 100 K. However, the cluster sizes that are predicted by using this assumption are within the range of experimental sizes for WDN (~25-70 nm).

Equation 9 gives the relationship between pressure and radius, but the equilibrium vapor pressure must be determined to allow the calculation of approximate vapor pressures for each cluster size. By using vapor pressure data that is obtained from reference 71, P_{eq} is approximated by using

(10) $P_{eq} = c\Phi$,

where Φ is the flux off the surface of crystalline cubic ice. The flux is obtained by fitting a 4th-order polynomial to the experimental data presented in reference 71 (see Fig. 47B).

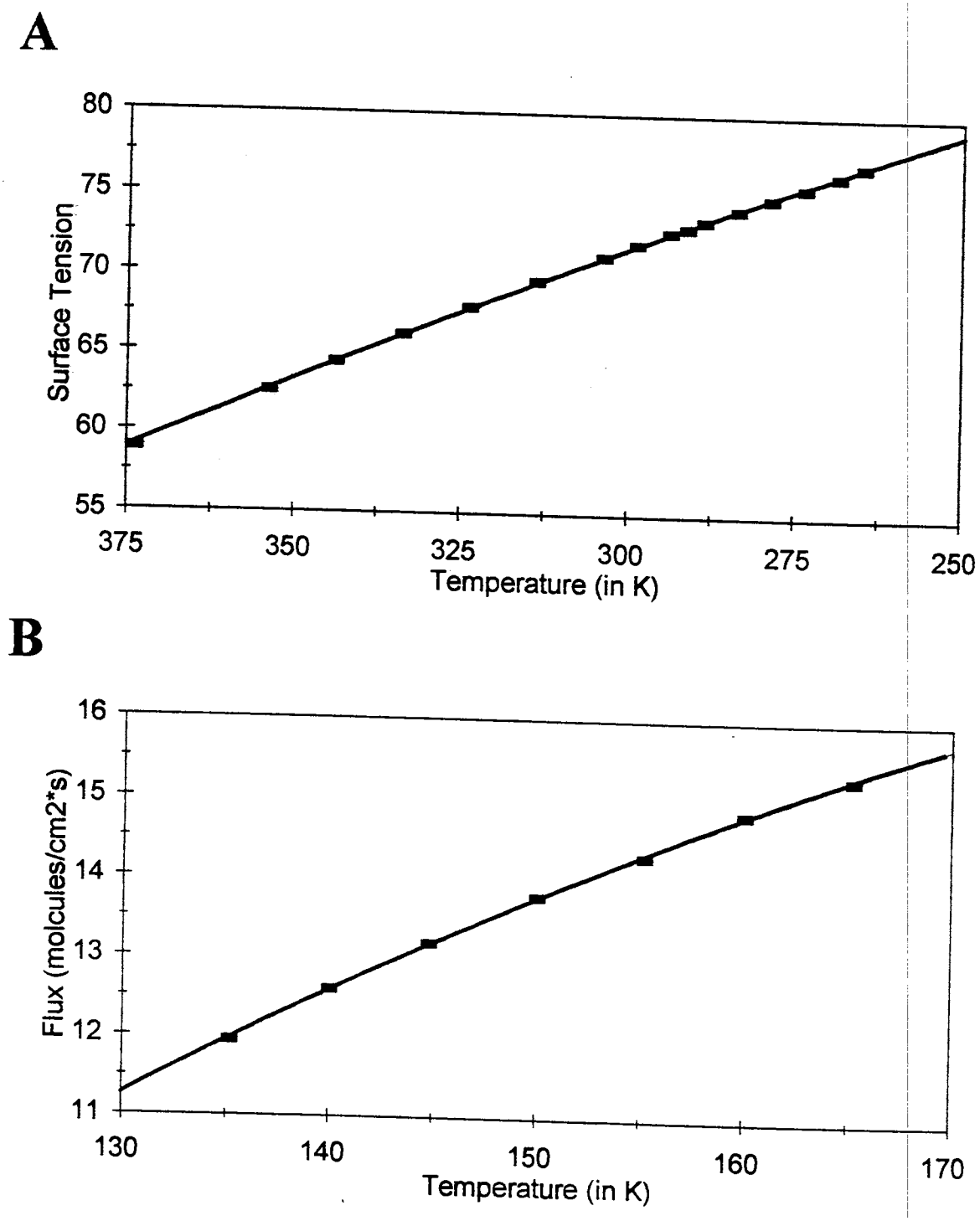

Figure 47. The fitted plots of the surface tension (A) and flux (B) versus temperature

This allows the equilibrium vapor pressures to be determined for particular temperatures below the reported temperature in reference 71. Values extrapolated for Φ at 100, 120, and 150 K are 4.0667, 9.618, and 13.650 molecules/(cm^2 s), respectively. The mean molecular speed of the vaporized H_2O molecules is represented by c.[71] By substituting equation 10 into equation 9, the equation that relates the cluster size to vapor pressure is given by

(11) $P_V = [e^{W(\sigma/Tr)}]_c \Phi$.

A plot of equation 11 for the temperatures of 100, 120, and 150 K (common annealing temperatures for WDN) is given in Figure 48 . The dependence of the vapor pressure on the cluster size is demonstrated at the different temperatures. Also, larger clusters are shown to be more stable than smaller clusters because of the rise in vapor pressure (above the equilibrium vapor pressure) as the cluster sizes decrease, and larger clusters vaporize as the annealing temperatures increase (due to the increase in P_V). This is the reason that larger clusters are formed upon annealing at increasing temperatures.

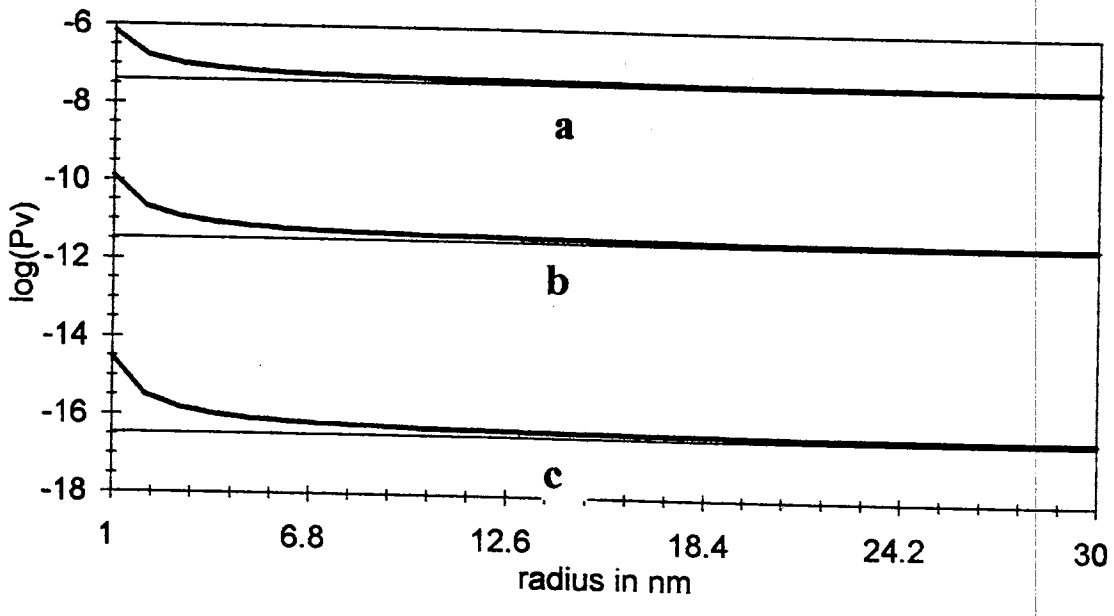

Figure 48. The plot of vapor pressure versus nanocrystal radius for 150 K (a), 120 K (b), and 100 K (c)

Appendix A.3. The Adsorbate-Neighbor Isotherm Equation (ANIE)

The structure of the crystalline ice surface consists of a bilayer of surface-defect groups. This bilayer is composed of 3-coordinate dangling-D and dangling-O H_2O molecules that are connected by surface 4-coordinate molecules (see Fig. 3; Section I.2.2). The approximate ratio between the d-H(D), d-O, and S-4 sites is 1:1:2 for the cleaved crystalline ice surface. Therefore, a fourth of the surface sites are d-H(D) or d-O, and half of the surface sites are S-4. We assume that this is the average surface site arrangement which is used to derive the following isotherm equation. For the cleaved ice-surface model, a d-H(D) site is surrounded (on average) by three S-4 molecules at 2.8 A° (oxygen-to-oxygen distance), and is also surrounded by three d-H(D) and three d-O sites at 4.5 A° (oxygen-to-oxygen distance). Molecules adsorbed on sites that are within 4.5 A° from unoccupied d-D sites are considered to interact with the d-D sites, and are important in the derivation of the adsorbate-neighbor isotherm equation (ANIE)..

A symbolic representation of adsorbed molecules that are localized on the surface sites is presented in Figure 49A. Symbols A_B, A_C, and A_D represent adsorbing molecules on the B, C, and D sites, respectively. The B, C, and D sites represent the d-H(D), d-O, and the S-4 surface sites in their assumed ratios, respectively. The total number of adsorbed molecules is

(1) $N_t = N_b + N_c + N_d$,

where N_t, N_b, N_c, and N_d are the total number of occupied surface sites, and the number of occupied d-H(D), d-O, and S-4 sites, respectively. By applying the postulated ratios between surface sites, equation 1 is becomes

(2) $N_t = 4N_b$.

The molecules that are adsorbed on the ice surface interact with neighboring unoccupied surface-sites while adsorbed on other surface sites as displayed in Figure 49B. The total number of adsorbate-empty site interactions is

A

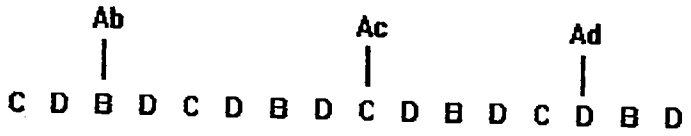

B

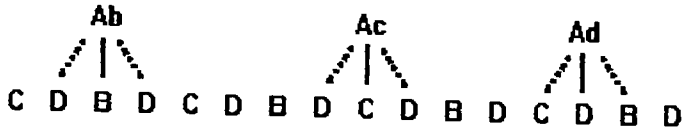

C

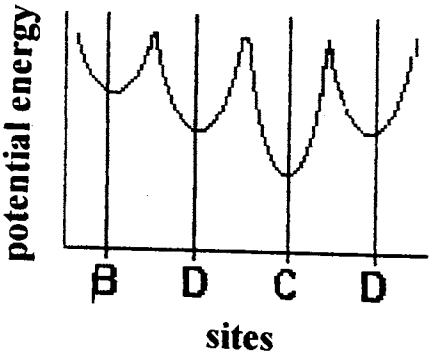

Figure 49. Symbolic representation of localized adsorption (A), adsorption + near neighbor interactions (B), and an arbitrary potential energy plot for adsorption (C)

(3) $N_{A0} = N_{b0} + N_{c0} + N_{d0}$,

where N_{b0}, N_{c0}, N_{d0}, and are the number of molecules adsorbed on the d-H(D), d-O, and S-4 sites that interact with unoccupied sites, and N_{A0} represents the total number of adsorbate-to-empty site interactions. The number of interactions that involve the occupied d-H(D) sites with neighboring empty sites is $N_{A0}/4$. If all the possible combinations of occupied site-empty site interactions are evaluated (using the ratio of 1 d-H(D): 1 d-O: 2 S-4), the number of occupied sites that interact with bare d-H(D) sites is also $N_{A0}/4$. Therefore, the number of occupied site-empty site interactions that involve the d-H(D) sites is $N_{A0}/2$. The determination of the number of interactions that involve d-H(D) sites is given in Figure 50.

The adsorbed-to-empty site interactions are important in developing an isotherm equation that is used to fit the H_2 isothermal data. A pictorial representation of the adsorbed-to-empty site interaction is displayed in Figure 49B. Also, an arbitrary potential-energy plot to illustrate the potential-energy wells of the surface is displayed for the symbolic surface (see Fig. 49C). We assume that the wells are localized on the surface sites and the equation for the potential is

(4) $U = u[A_B; B] + u[A_C; C] + u[A_D; D]$,

where U, $u[A_B; B]$, $u[A_C; C]$, and $u[A_D; D]$ represent the total localized potential energy of the surface sites, and the potential energies for adsorbed molecules that have localized interactions on the B, C, and D sites, respectively. The interaction energy that accounts for the adsorbed-to-empty site interactions is expressed as

(5) $W = \Sigma w[A_B; C, D] + \Sigma w[A_C; B, D] + \Sigma w[A_D; B, C]$,

where W is the total interaction energy, and Σw is the summation of the interaction energies for molecules adsorbed on one surface sites interacting with the other sites.

By following the out-of-phase d-H(D) IR band during adsorption, fractional coverages are determined for the d-H(D) surface-defect sites only. This eliminates the potential-energy terms for the d-O and S-4 surface-defect groups, and simplifies the

There are three sites in a 1:1:2 ratio

B D_1 C D_2

The possible interaction pairs (excluding a site pairing with itself) are

B-D_1 D_1-B C-B D_2-B
B-C D_1-C C-D_1 D_2-D_1
B-D_2 D2-D_1 C-D_2 D_2-C

The number of pairs that are involved with B is 6 (1/2 of the total pairs)

B-D_1, D_1-B, C-B, D_2-B, B-D_2, B-C

The number of pairs that are involves with sites interacting with B is 3 (1/4 of the total pairs)

D_1-B, C-B, D_2-B

Figure 50. Determination of the fraction of occupied-unoccupied site interactions

derivation to only account for localization on the d-H(D) sites. Therefore, equation 4 simplifies to

(6) $U = u[A_B; B]$.

The interaction energies are simplified by determining the fractional coverage for the d-H(D) sites. All interaction-energy terms are ignored, except the average number of occupied sites that interact with unoccupied d-H(D) sites. This average number of adsorbed-unoccupied d-H(D) interactions is represented by $avg[N_{A0}/4]$, and reduces equation 5 to

(7) $W_{0B} = avg[N_{A0}/4]\ W$.

The partition function for an adsorbed diatomic molecule on a d-H(D) site is given by

(8) $q_{ads} = q_x\ q_y\ q_z\ q_{H\text{-}H}\ q_{r,n}\ e^{(u[AB; B])}$,

where q_{ads}, q_x, q_y, q_z, $q_{H\text{-}H}$, and $q_{r,n}$ correspond to the partition functions of the surface adsorbed molecule, "rattling" (vibration of the trapped (adsorbed) adsorbate molecule in the potential well of the surface) in the x direction, "rattling" in the y direction, "rattling" in the z direction, diatomic vibration, and rotational with the nuclear spin accounted for, respectively. Rattling in the x and y directions is degenerate, so, equation eight is further reduce to

(9) $q_{ads} = q_x^2\ q_z\ q_{H\text{-}H}\ q_{r,n}\ e^{(u[AB; B]}$.

The canonical partition function is

(10) $Q_{ads} = \Sigma g(N_b, N_B)\ (q_{ads})^{Nb}\ e^{(-avg(NAO/4)\ W/(zkT))}$,

where N_b, and N_B are the number of occupied d-H(D) sites and the total number of d-H(D) sites, respectively. The total number of ways that the d-H(D) sites can be occupied is represented by $\Sigma g(N_b, N_B)$, and z represents the number of neighbor sites that surround a d-H(D) site.

The term $\Sigma g(N_b, N_B)$ is expressed as

(11) $\Sigma g(N_b, N_B) = N_B!/(N_b!\ (N_B\text{-}N_b)!)$.

By substituting equation 11 into equation 10, the canonical partition function is given by

(12) $Q_{ads} = N_B!/(N_b!\ (N_B\text{-}N_b)!)\ (q_{ads})^{Nb}\ e^{(-avg(NAO/4)\ W/(zkT))}$.

The average number of occupied site-empty d-H(D) site interactions ($avg(N_{AO}/4)$) must be expressed in terms of N_b and N_B. The method that is chosen to solve the $avg(N_{AO}/4)$ is called the "crude approximation method", and is outlined in reference 61.

The following relationships (found in reference 61) are used to solve $avg(N_{AO}/4)$ for N_b and N_B. These equations are

(13a) $2\ avg(N_{AA}) + avg(N_{A0}) = z\ N_A$,

(14a) $2\ avg(N_{00}) + avg(N_{A0}) = z\ (N_S\text{-}N_A)$,

and (for a system with randomly occupied sites)

(15a) $2\ (avg(N_{AA}))\ 2\ (avg(N_{00})) = (avg(N_{A0}))^2$,

where N_A and N_S represent the total number of occupied sites and the total number of sites, respectively. By adding equations 13a and 14a, an equation for the total number of sites is

(16a) $2\ avg(N_{AA}) + 2\ avg(N_{00}) + 2\ avg(N_{A0}) = z\ N_S$.

Equations 13a-to-16a are changed into equations that incorporate of N_b and N_B. This is accomplished by relating N_{AA}, N_{A0}, and N_{00} to the d-H(D) sites. So, equations 13a-16a become

(13b) $2\ avg(N_{AA}/2) + avg(N_{A0}/4) = z\ N_b$,

(14b) $2\ avg(N_{00}/2) + avg(N_{A0}/4) = z\ (N_B\text{-}N_b)$,

(15b) $2\ (avg(N_{AA}/2))\ 2\ (avg(N_{00}/4)) = (avg(N_{A0}/4))^2$,

and

(16b) $2\ avg(N_{A0}/2) + 2\ avg(N_{00}/4) + 2\ avg(N_{A0}/2) = z\ N_B$.

By rearranging equations 13b and 15b, and substituting them into equation 16b, the $avg(N_{A0}/4)$ is given by

(17) $avg(N_{A0}/4) = z\ (N_b\text{-}N_b^2/N_B)$.

If equation 17 is substituted into equation 12, the canonical partition function for molecules adsorbed onto the d-H(D) sites is changed to

(18) $Q_{ads} = N_B!/(N_b!\ (N_B\text{-}N_b)!)\ (q_{ads})^{Nb}\ e(\text{-}(Nb\text{-}Nb\ Nb/NB)\ W/(kT))$.

The above equations must be changed to a common isothermal relationship that uses pressure and fractional coverage. To do this, an equation is used to relate Helmholt's free energy to the chemical potential, and is given by

(19) $A = -\Phi M + u N$,

where A, Φ, M, u, and N are the Helmholt's free energy, surface area, spreading coefficient, chemical potential, and the number of occupied sites, respectively. An equation that corresponds Helmholt's free energy to the canonical partition function for adsorbed molecules is

(20) $A = -kT \ln(Q_{ads})$.

If equation 19 and 20 (with equation 18 substituted into equation 20) are set equal to each other, the resulting equation is

(21) $-\Phi M + u N_b = -kT \ln[N_B!/(N_b!\ (N_B\text{-}N_b)!)] - kT\ N_b \ln(q_{ads}) + (N_b\text{-}N_b^2/N_B)\ W$.

The chemical potential is solved by applying the Sterling's approximation to equation 21 and then taking the derivative of equation 21 with respect to the number of occupied sites (N_b). Once these operations are performed on equation 21, an equation that gives the chemical potential in terms of N_b, N_B, and q_{ads} is

(22) $u/(kT) = \ln[N_b/((N_B - N_b)\ q_{ads})] - (N_b/N_B - 1)\ W/(kT)$,

Equation 22 is simplified by using the definition of

(23) $\theta \equiv N_b/N_B$,

and becomes

(24) $u/(kT) = \ln[\theta/((1 - \theta)\ q_{ads})] - (\theta - 1)\ W/(kT)$.

Adsorbed molecules on d-H(D) sites are in an equilibrium with adsorbate molecules in the gas phase. The chemical potential is related to the partition function of gas-phase molecules through

(25) $u/(kT) = 1/(kT)\,(\partial A/\partial N_b) = \partial/\partial N_b\,(-\ln(Q_{gas}))$,

(26) $Q_{gas} = (q_{trans}\, q_{H\text{-}H}\, q_{r,n})^{Nb}$,

where Q_{gas}, q_{trans}, $q_{H\text{-}H}$, and $q_{r,n}$ are the canonical partition function for gas-phase molecules, translational partition function, vibrational partition function, and the rotational-nuclear spin partition function, respectively. By using the standard form of the translational partition function[60,61] and substituting it into equation 26, Q_{gas} is given by

(27) $Q_{gas} = [((2\pi mkT/h^2)^{3/2}\, kT/p)\, q_{H\text{-}H}\, q_{r,n}]^{Nb}$,

where p, h, and m represent the pressure, Plank's constant, and molecular mass, respectively. By substituting equation 27 into 25 and rearranging, an equation that relates the chemical potential to the pressure is

(28) $u/(kT) = \ln(p) - \ln(q'(p))$,

where q'(p) represents the pressure related gas-phase partition function, and is

(29) $q'(p) = ((2\pi mkT/h^2)^{3/2}\, kT)\, q_{H\text{-}H}\, q_{r,n}$.

The equation that is used to fit the H_2 isothermal data in chapter 4 is obtained by combining and rearranging equations 24 and 28 to obtain

(30) $p = (q'(p)/q_{ads})\,(\theta/(1 - \theta))\, e^{(-(\theta - 1)\, W/(kT))}$.

The ratio of the partition functions ($q'(p)/q_{ads}$) and the interaction energy (W) are obtained by fitting equation 30 to the isothermal data (see Fig. 43; Section IV.4.3). Values that are used to calculate ΔHads are calculated by fitting an equation for q'(p)/qads to the experimental ratios of partition functions (see Fig. 44; Section IV.4.3). The equation for the ratio of the partition functions is obtained by dividing equation 29 with equation 8, and is given by

(31) $q'(p)/q_{ads} = [((2\pi mkT/h^2)^{3/2}\, kT)/(q_x^2\, q_z)]\, e^{(-u[AB;\, B])}$.

The rotational and vibrational partition functions for gas-phase and adsorbed molecules council out in the ratio of $q'(p)/q_{ads}$.

The partition functions of q_x^2 and q_z is evaluated to determine the heat of adsorption (ΔH_{ads}). These partition functions are described as the "rattling" of trapped diatomic molecules in the d-H(D) potential well. The partition functions are of the standard vibrational partition-function form[60,61], and are

(32) $q_x^2 = [1/(1 - e^{(-h\nu x/(kT))})]^2$,

(33) $q_z = [1/(1 - e^{(-h\nu z/(kT))})]$,

where ν_x and ν_z represent the rattling frequencies in the x and z directions, respectively. If equations 32 and 33 are substituted into equation 31, an equation that is used to fit the experimental ratios of the partition functions at different temperatures is

(34) $q'(p)/qads = [((2\pi mkT/h^2)^{3/2}\ kT)\ (1-e^{(-A/T)})]\ [(1-e^{(-B/T)})]^2\ e^{(-u[AB;\ B])}$,

(35) $A = h\nu_z/k$, and $B = h\nu_x/k$.

The goal of this derivation is to calculate the thermodynamic value of ΔH_{ads}. Assumptions. which are made in this derivation, are that the four surface-defect sites have the set ratio of 1 (d-H(D)): 1 (d-O): 2 (S-4), that the surface-sites are occupied randomly upon adsorption, and that the adsorbate-adsorbate interactions are trivial and can be ignored. The ratios of the partition functions are obtained by fitting equation 30 to the isothermal data. The ratios of the partition functions are then fit with equation 34, and yield values that are used to calculate ΔH_{ads}. By using the Clausius-Clapeyron equation, ΔH_{ads} is calculated by

(36) $-\Delta H_{ads}/(RT^2) = (\partial \ln(p)/\partial T)_\theta = \partial[\ln(q'(p)/qads) + \ln(\theta/(1-\theta))-(\theta-1)\ w/(kT)]/\partial T$,

where R represents the gas law constant. By substituting equation 34 into 36 and performing the derivative with respect to temperature, The equation that is used to calculate the ΔH_{ads} is

(37) $\Delta H_{ads} = -5/2\ RT + RT\ [e^{(-A/T)}\ (A/T)/(1-e^{(-A/T)})] + 2\ RT\ [e^{(-B/T)}\ (B/T)/(1-e^{(-B/T)}) - u[AB;\ B] + W/2$.

The important equations that are used in this thesis are the adsorbate-neighbor isotherm equation (ANIE), the ratio of the partition functions, and the equation that is used to calculate the ΔH_{ads}, which are given by

(30) $p = (q'(p)/qads)\,(\theta/(1-\theta))\,e^{(-(\theta-1)\,W/(kT))}$,
(34) $q'(p)/qads = [((2\pi mkT/h^2)^{3/2}\,kT)\,(1-e^{(-A/T)})]\,[(1-e^{(-B/T)})]^2\,e^{(-u[AB;\,B])}$,
(37) $\Delta H_{ads} = -5/2\,RT + RT\,[e^{(-A/T)}\,(A/T)/(1-e^{(-A/T)})] + 2\,RT\,[e^{(-B/T)}\,(B/T)/(1-e^{(-B/T)}) - u[AB;\,B] + W/2$.

2

VITA

James Bradly Rowland

Candidate for the Degree of

Doctor of Philosophy

Thesis: FT-IR STUDY OF THE H_2O CRYSTALLINE ICE SURFACE

Major Field: Chemistry

Biographical:

Personal Data: Born in Durant, Oklahoma, on August, 26, 1968, the son of James and Glenda Rowland; married Suzette Rollor in Milburn, Oklahoma, on May 25, 1991

Education: Graduated from Milburn High School, Milburn, Oklahoma in May 1986; received Bachelor of Science degree in Chemistry and Mathematics from Southeastern Oklahoma State University, Durant, Oklahoma in May 1990. Completed the requirements for the Doctor of Philosophy degree at Oklahoma State University in December 1995.

Experience: Raised on a ranch near Milburn, Oklahoma; employed as a ranch hand; owned hay hauling and welding businesses; employed by Southeastern Oklahoma State University Departments of Mathematics and Chemistry as a math tutor and a chemistry teaching assistant; employed by USDA-ARS as a undergraduate research assistant; employed by Oklahoma State University Department of Chemistry as a teaching and graduated research assistant; Oklahoma State University, Department of Chemistry, 1990 to present.

Professional Memberships: American Chemical Society